# MEG studies of visual cortical processing during eye movements

Konstantinos Nasiotis



Integrated Program in Neuroscience

Department of Neurology & Neurosurgery

McGill University, Montreal

2019

A thesis submitted to McGill University in partial fulfillment of the requirements of the degree of Doctor of Philosophy (Neuroscience)

## Acknowledgements

I would first like to thank my supervisor Dr. Christopher Pack for his guidance and mentorship throughout all these years of my PhD work and for always been available to discuss any matter, scientific or not. His absolute dedication to research and scientific curiosity have been truly inspiring and I consider myself extremely fortunate to have him as my supervisor. It was a privilege to work with him and none of this work would have been possible without his help.

Although not officially my supervisor, Dr. Sylvain Baillet acted like one. He guided me through every step of my journey and showed immense appreciation for the work we performed.

I would also like to extend my thanks to the member of my advisory committee Dr. Dan Guitton. He provided a fertile environment for academic and personal improvement and he always had his door open for me.

A special mention goes to Dr. Theodoros Zanos who has been my mentor during my initial steps in research. Our collaboration and friendship have given me the necessary foundation for scientific growth.

I would also like to thank Dr. Matthew Krause for all his help through every project I worked on.

Matt was always available for endless scientific conversations and continuously eager to help.

Also, my lab members that have created an ideal environment for exchanging ideas and promoting knowledge: Dr. Shahab Bakhtiari, Dr. Pedro Vieira, Nardin Nakhla, Yavar Korkian, Dr. Kuwook Cha, Bennett Csorba, Dr. Sujaya Neupane, Dr. Dave Liu, Frederic Simard and Pooya Lameraad.

Special thanks go to Naomi Takeda for always finding the solution to perplex administrative issues, Elizabeth Bock for teaching me everything about the MEG system and Julie Coursol for valuable help during my initial training involving work on non-human primates.

On a more personal note, I would like to thank my mother for her unconditional support and the countless video-calls we had through all these years. Although she was thousands of kilometers away, I always felt her close to me.

Also, Lawrence for all the late-night conversations and thought-provoking stimulations that I needed. It is largely thanks to her encouragement that this thesis is coming to a completion. In addition, Gerry, Anna, Adam and Andrea for making me feel that I have a second family away from home.

Finally, my humble praise and gratitude goes to the most important person in my life, my partner Amanda. She has always pushed me to be a better person and I could not complete this PhD without her unconditional support. I cannot but only look up to her as a partner, as a professional and as a well-rounded person. I am grateful for having her by my side and I could not ask for a more loving, supportive, understanding and inspiring partner.

This thesis is dedicated to my mother.

### **Abstract**

Exploration of the visual scene is comprised of periods of fixation on specific objects in our environment, interrupted by abrupt eye movements that bring new objects in our visual field. Whenever we perform an eye movement, a chaotic smearing of the visual world is introduced on the retina from the input displacement. However, our perception of our environment remains stable. In order to achieve this, our brain must have a compensation mechanism for these shifts. Since eye-movements last for a very brief period of time, it is imperative to make use of a modality that is able to capture the transient characteristics of this compensatory phenomenon.

This thesis is a compiled series of findings that utilize magnetoencephalography (MEG) for studying the areas involved in encoding the visual input in human subjects, during fixation and around eye movements. The advantage that MEG provides is coverage of the entire cortical surface with submillisecond precision.

The visual cortex during fixation has been extensively studied for decades (with invasive and imaging modalities), showing spatial and feature selectivity in individual visual areas. However, retinal mapping on the cortical surface was crudely presented with MEG, making it an unfavourable modality for studying neural mechanisms that rely on visual spatial selectivity. Chapter 2 of this thesis demonstrates a novel approach for MEG in creating high-resolution retinotopic maps on the primary visual cortex, with results comparable to the golden standard fMRI. Moreover, by utilizing these maps, the spatial resolution of MEG is quantified, showing that with proper stimulation and brain curvature, MEG can achieve spatial resolution comparable to that of fMRI.

Chapter 3 contains the results from the studies investigating visual remapping, which is one of the mechanisms that our brain uses for achieving visual stability around eye movements. In remapping, visual neurons respond to stimuli outside of their classical receptive field, but only if there is an imminent eye movement. This study supports the modulatory effect of attention on remapping and shows the spectral and temporal engagement of the superior parietal and visual cortices in this mechanism. Moreover, two different types of remapping with unique temporal and

spatial signatures are shown in the human cortex, further reconciling the controversy about the mechanistic role of remapping.

MEG techniques rely on high sampling of cortical signals from hundreds of sensors. The amount of data that is created through every session can provide challenges in the management and efficiency of the analysis. Imaging studies in general benefit from high quality software that provide tractable and efficient analysis pipelines. However, although invasive neurophysiology methods are constantly evolving in recent years, especially by using dense electrode arrays – generating a vast amount of data, most labs rely on developing their own analysis techniques, with error-prone verification and poor documentation. Chapter 4 of this thesis provides a novel approach to invasive neurophysiology analysis, by introducing a new research resource, that bridges across recording scales (from slices to behaving animals) and delivers a unifying analytical environment to the broadest research community in neurophysiology. Overall, this chapter contributes to reproducibility, standardization and transparency in science.

### Résumé

L'exploration de la scène visuelle comprend des périodes de fixation sur des objets spécifiques de notre environnement, interrompues par des mouvements oculaires brusques qui apportent de nouveaux objets dans notre champ visuel. Chaque fois que nous effectuons un mouvement oculaire, une tache chaotique du monde visuel est introduite sur la rétine du déplacement d'entrée. Cependant, notre perception de notre environnement reste stable. Pour y parvenir, notre cerveau doit disposer d'un mécanisme de compensation pour ces changements. Étant donné que les mouvements oculaires durent très peu de temps, il est impératif de recourir à une modalité capable de saisir les caractéristiques transitoires de ce phénomène compensatoire.

Cette thèse est une série de résultats compilés qui utilise la magnétoencéphalographie (MEG) pour étudier les zones impliquées dans le codage de l'entrée visuelle chez des sujets humains, pendant la fixation et autour des mouvements oculaires. L'avantage que MEG fournit, est la couverture de toute la surface corticale avec une précision sous-milliseconde.

Le cortex visuel lors de fixation a été étudié de manière approfondie pendant des décennies (avec des modalités invasives et d'imagerie), montrant une sélectivité spatiale et caractéristique dans les zones visuelles individuelles. Cependant, la cartographie rétinienne sur la surface corticale a été grossièrement présentée avec MEG, ce qui en fait une modalité défavorable pour étudier les mécanismes neuronaux qui reposent sur la sélectivité spatiale visuelle. Le chapitre 2 de cette thèse démontre une nouvelle approche pour MEG dans la création de cartes rétinotopiques à haute résolution sur le cortex visuel primaire, avec des résultats comparables à l'étalon d'or - l'IRMf. De plus, en utilisant ces cartes, la résolution spatiale de MEG est quantifiée, montrant qu'avec une stimulation et une courbure cérébrales appropriées, MEG peut atteindre une résolution spatiale comparable à celle de l'IRMf.

Le chapitre 3 contient les résultats des études portant sur le remappage visual, l'un des mécanismes que notre cerveau utilise pour atteindre la stabilité visuelle autour des mouvements oculaires. Lors du remappage, les neurones visuels répondent à des stimuli en dehors de leur champ récepteur classique, mais uniquement en cas de mouvement oculaire imminent. Cette

étude soutient l'effet modulateur de l'attention sur le remappage et montre l'engagement spectral et temporel des cortex pariétaux et visuels supérieurs dans ce mécanisme. De plus, deux types différents de remappage avec des signatures temporelles et spatiales uniques sont présentés dans le cortex humain, ce qui réconcilie davantage la controverse sur le rôle mécaniste du remappage. Les techniques MEG reposent sur un échantillonnage élevé des signaux corticaux provenant de centaines de capteurs. La quantité de données qui est créée à chaque session peut poser des défis dans la gestion et l'efficacité de l'analyse. Les études d'imagerie bénéficient en général de logiciels de haute qualité qui fournissent des pipelines d'analyse faciles à manier et efficaces. Cependant, bien que les méthodes de neurophysiologie invasive évoluent constamment au cours des dernières années, en particulier en utilisant des réseaux d'électrodes denses générant une grande quantité de données, la plupart des laboratoires s'appuient sur le développement de leurs propres techniques d'analyse, avec une vérification sujette aux erreurs et une mauvaise documentation. Le chapitre 4 de cette thèse propose une nouvelle approche de l'analyse de la neurophysiologie invasive, en fournissant une nouvelle ressource de recherche, qui fait le pont entre les échelles d'enregistrement (des tranches aux animaux qui se comportent) et offre un environnement analytique unificateur à la communauté de recherche la plus large en neurophysiologie. Dans l'ensemble, ce chapitre contribue à la reproductibilité, à la normalisation et à la transparence de la science.

## Contributions of Authors

This thesis is composed of five chapters. Chapter 1 (Introduction), Chapter 3, and Chapter 5 (Discussion) were written by me. Chapters 2 and 4 are original peer-reviewed research articles, that were published in NeuroImage and Nature Scientific Data respectively. Chapter 3 is in preparation and will be submitted for potential publication.

All experiments and data analysis were performed by me.

The studies for chapter 2 were conceived by me and C.C.P.. S.C. performed the fMRI experiments. The manuscript was prepared by me, C.C.P. and S.B..

The studies for chapter 3 were conceived by me and C.C.P.. S.N. and S.Bakhtiari provided input on the experimental design. S.Baillet provided input to the analysis.

Chapter 4 software was designed and coded by me. The manuscript was prepared by me, S.B. and C.C.P.

## Table of contents

ACKNOWLEDGEMENTS	
ABSTRACT	IV
CONTRIBUTIONS OF AUTHORS	VIII
TABLE OF CONTENTS	IX
CHAPTER 1: INTRODUCTION	1
1.1 Vision as part of consciousness	1
1.2 Encoding during fixation	2
1.2.1 Receptive field	4
1.2.2 Visual hierarchy	5
1.2.3 Retinotopy	7
1.3 Eye movement circuitry	8
1.4 Visual stability	11
1.4.1 Remapping	11
1.4.2 Remapping as a mechanism for visual stability or as a	
mechanism for attentional pointers?	13
1.4.3 Receptive field expansion during remapping?	
1.5 Magnetoencephalography	15
1.5.1 Retinotopy in MEG	17
1.5.2 Remapping in MEG	
1.6 Open science	19

1.6.1 Open source – software for invasive neurophysiology	19
CHAPTER 2 - HIGH-RESOLUTION RETINOTOPIC MAPS ESTIMATED W MAGNETOENCEPHALOGRAPHY	
2.1 Abstract	22
2.2 Introduction	22
2.3 Materials and Methods	23
2.3.1 Participants	23
2.3.2 Structural MRI	24
2.3.3 fMRI Retinotopic Experiment	24
2.3.4 MEG Data Collection	25
2.3.5 Regions of interest	27
2.3.6 MEG data analysis	
<b>2.3.7</b> Software	33
2.4 Results	34
2.4.1 Visual receptive fields estimated from individual occipital	
sources	34
2.4.2 Retinotopic maps estimated with MEG	35
2.4.3 Estimate of cortical magnification factor with MEG	39
2.4.4 Comparison with fMRI	41
2.4.5 Spatial resolution of MEG	41
2.5 Discussion	44
2.5.1 Brief summary of results	44
2.5.2 Comparison to previous work	44
2.5.3 Limitations of current results	46
2.5.4 MEG usage is beneficial in areas were the fMRI signal gets	
distorted due to large blood vessels	47
2 5 5 Resolution	17

<b>2.5.6</b> Conclusion	48
2.6 Acknowledgements	49
2.7 References	49
2.8 Supplementary Figures - Appendix	56
2.8.1 Efficiency of receptive field estimation with MEG	57
CHAPTER 3 - TRANSIENT SHIFTING OF ATTENTIONAL ENCODING	
MEASURED WITH MAGNETOENCEPHALOGRAPHY	61
3.1 Abstract	61
3.2 Introduction	62
3.3 Methods	63
3.3.1 Participants	63
3.3.2 Structural MRI	64
3.3.3 MEG Data Collection	64
3.3.4 Stimulus	64
3.3.5 Artifact Removal	66
3.3.6 Time-segments of interest	67
3.3.7 MEG data analysis	68
3.3.8 Statistical analysis	69
3.3.9 Time-Frequency analysis	69
3.3.10 Regions of interest for information flow	69
3.3.11 Computation of information flow	70
3.3.12 Software	71
3.4 Results	72
3.4.1 Time Frequency – ERSD	72
3.4.2 Statistical significance of remapped responses	74

3.4.3 Information flow	76
3.5 Discussion	78
3.5.1 Brief summary of results	78
3.5.2 Previous work	78
3.5.3 Where we expected to see remapping with MEG	80
3.5.4 Experimental Design	81
3.5.5 Two types of remapping	
3.5.6 Remapping information flow	84
3.5.7 Why we didn't see remapping in all expected areas	84
3.5.8 Future research	86
3.6 Conclusion	87
3.7 Acknowledgements	87
3.8 References	88
CHAPTER 4 - INTEGRATED OPEN-SOURCE SOFTWARE FOR	
MULTISCALE ELECTROPHYSIOLOGY	96
4.1 Abstract	96
4.2 Introduction	97
4.3 Results	99
4.3.1 Importing, reviewing and pre-processing raw data	100
4.3.2 Spike detection and spike sorting	101
4.3.3 Extraction of local field potentials	103
4.3.4 Epoching	104
4.3.5 Analysis of individual LFP signals	104
4.3.6 Analysis of individual neuron spiking activity	106
4.3.7 Spike-spike analysis: Noise correlations	107

4.3.8 Spike-LFP analysis	108
4.3.9 Statistical inference and machine learning	110
4.3.10 Additional features	110
4.4 Discussion	112
4.5 Methods	113
4.5.1 Code availability	
4.6 Data Availability	113
4.7 Acknowledgements	114
4.8 Author Contributions	114
4.9 Competing Interests	114
4.10 References	115
4.11 Figures	120
CHAPTER 5: DISCUSSION	130
5.1 Summary of results and contribution to original knowledge	130
5.1.1 Retinotopy in MEG	130
5.1.2 Remapping in MEG	131
5.1.3 Invasive neurophysiology analysis	133
5.2 Future development	134
REFERENCES	136

## Chapter 1: Introduction

#### 1.1 Vision as part of consciousness

Whenever an artist paints a painting, they try to capture a still image of the environment they had in front of them. Every stroke slowly contributes to different attributes of all the characteristics of the objects that laid before their eyes: luminance, edges, shape, color, size, depth etc. A compendium of these characteristics, each with a different level of importance, create a vivid recreation of what the artist was experiencing, and the artist's personal touch on the finished artwork. This procedure is performed for every position of the environment that is finally depicted in the painting. Breaking down the steps that ultimately contributed to the finished painting: the artist was constantly looking around their environment, sequentially used different brushes and colors to make a representation of their environment, and finally they created a still image of their environment.

Analogous steps apply to the brain when it encodes the visual information of the visual scene. Our perception of the outside world relies on the effortless communication between several brain regions which contribute to encoding different aspects of our environment. Vision plays a crucial role in our awareness and is of no surprise that a substantial portion of the brain is dedicated to vision (Felleman and Van Essen, 1991), with a plethora of areas specializing in specific attributes of the visual scene. However, although there are many cortical and subcortical areas collaboratively contributing to the creation of an internal representation of the outside world, this is achieved in a surprisingly brief period of time (information is encoded even at images presented as briefly as ~13ms (Potter et al., 2014)).

The exploration of the visual scene is comprised of fixation periods, followed by brief periods of eye-movements where the high-resolution part of the eye (the fovea) is focused on the point of interest. Although the eye-movements are performed around 3 times per second while we explore different objects in our environment, we don't perceive a chaotic scene but rather a stable one, just like the finished painting that was described in the analogy earlier.

An explanation for this observation is that the brain needs to have compensation mechanisms that contribute to visual stability around eye-movements. Studying such a phenomenon, dictates the usage of a modality that is able to capture its transient characteristics.

This thesis studies the processes that take place during fixation (Chapter 2) and around eye-movements (Chapter 3), in real-time, non-invasively, in human subjects. Moreover, Chapter 4 introduces a unifying framework for performing invasive neurophysiology analysis across any recording scale (from cells to whole brain).

#### 1.2 Encoding during fixation

Vision has been a field of study among scientists and philosophers for centuries. The encoding of the visual information starts the moment that the light reflections of our environment reach the retina and is followed by a series of sequential processing from several different areas as the signal propagates through the brain.

An analogy that vision acts as a camera can be accurate up to the point that they both receive light as their input, but that is about it. Even for this oversimplification though, anyone who has some experience with photography can appreciate the challenges in capturing a crisp picture of the environment, especially when the conditions are not ideal: e.g. in low lighting conditions, or when there is small movement in the frame.

However, the mechanisms that allow us to ultimately perceive individual objects in our surroundings from just the light input is, as (Gregory, 1966) put it: "no short of a miracle".

Mammalian eyes have evolved to have a high-resolution part which is located at the center of the retina (fovea) that provides detailed processing of the target. Anatomically, this differentiation of spatial sampling in the retina is attributed to the non-homogeneous density of two different types of photoreceptors along the retina: rods and cones. The rods are extremely sensitive to luminance (they can be activated by a single photon) and are prevalent around the outer ring of the retina. In contrary, the cones need a brighter source of light to be activated and are sensitive to the

wavelength of the light source. The distribution of the cones is larger close to the fovea and decreases along the eccentricity of the eye.

Based on the characteristics of these 2 types of photoreceptors, there is a trade-off between luminance sensitivity and visual acuity.

The photoreceptors pass the information to retinoganglion cells that utilize their long axons to ultimately propagate the visual signals to cortical and subcortical structures. The visual field is separated to two visual hemifields (left - right) and the connections from each eye follow an orderly separation in the optic chiasm. The axons of the retinoganglion cells form the optic nerve up to the optic chiasm. After the optic chiasm, the axons that carry information from each hemifield, bundle together to form the optic tract and reach the lateral geniculate nucleus (LGN) in the thalamus, on the contralateral hemisphere. This arrangement dictates that the entire processing of each visual field (from low level to high level) will be conducted on the contralateral hemisphere. Projections from the LGN finally reach the primary visual cortex. These afferent fibers create a neural mapping of the visual scene to the cortical surface of the primary visual cortex (V1). The arrangement of these afferent fibers on the cortex is called the optic radiation.

Since the center of gaze consists of higher resolution encoding, is it expected that the fibers that reach the primary (striate cortex) and extrastriate visual cortex would have a bigger representation of the fovea on the cortex relative to the periphery. There is a substantially greater portion of the cortex designated to the visual area around the point of fixation compared to the more peripheral elements of the visual scene. This cortical arrangement is called cortical magnification and is biologically justified by the importance of the locus where the animal/human focuses their gaze upon. This arrangement will be revisited later at the section about retinotopy.

The anatomical connectivity that was described above, is depicted in Figure 1.1.

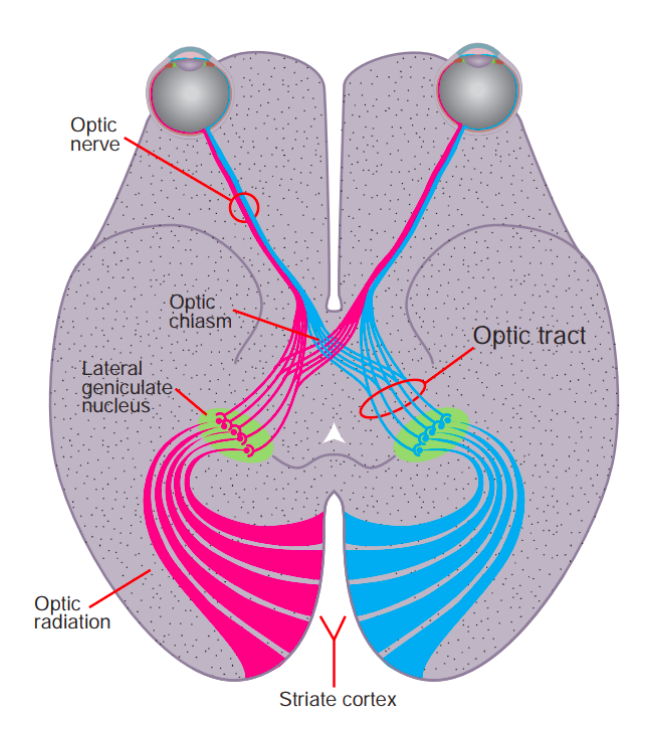


Figure 1.1 Visual information travels from the retina to the primary visual cortex through an organized fiber network. Adapted from (Polyak, 1941)

#### 1.2.1 Receptive field

Neurons in the sensory areas are selective to a subspace of their encoding sensory space and this subspace is termed the receptive field (RF) of those neurons. The term was first introduced in the tactile domain by Sherrington (1906) in his analysis of the scratch withdrawal reflex. Visual receptive fields were first investigated by (Hartline, 1938, 1940) in the frog, where the discovered that retinal light stimulations could elicit excitatory responses on isolated optic nerve fibers. (Kuffler, 1953) discovered the antagonistic center-surround organization of the cat RFs and this work was later extended to stimulus size (Barlow et al., 1957). The most famous work on receptive fields was performed by Hubel and Wiesel where they recorder on the visual cortex of the cat and the monkey and found RF selectivity in shape, orientation and position of the stimulus in the anaesthetised paralysed cat (Hubel and Wiesel, 1959, 1962) and later in the monkey (Hubel and Wiesel, 1968).

#### 1.2.2 Visual hierarchy

Early 20<sup>th</sup> century anatomical research paved the road to cerebral segregation (Brodmann, 2006). Brodmann used anatomical criteria (size, shape, density of neuronal populations) to create a map of individual areas in the brain. Later work that was concentrated in the visual cortex, discovered a few dozens of visual areas that contributed to different visual processing (Felleman and Van Essen, 1991). The most important outcome from these studies, is the amount of cortical "real estate" that is assigned to vision.

The anatomical distinction of visual areas provides valuable information about the existence of separate areas but doesn't explicitly inform us of the role of each area. Invasive neurophysiological studies in the past century have been invaluable to our understanding of the role of each area. Most importantly, the location of the receptive fields, and the selectivity in particular stimuli have built a fully functional map of the visual cortex.

Neuronal selectivity and anatomical connectivity in visual areas has led to two different hierarchical pathways to emerge: the ventral and dorsal pathways (Figure 1.2). The ventral pathway is involved in object recognition (what) and the dorsal pathway is involved in visual information in guiding movements (where). The ventral pathway starts from the primary visual cortex and continues all the way to the temporal lobe. An example from the ventral pathway would be neurons in inferotemporal cortex (IT), which exhibit poor spatial selectivity, but can discriminate between specific semantic categories (e.g., face vs. non-face stimuli) and even between different instances of those categories (e.g., specific people). In contrary, the dorsal pathway accumulates information about movement. It extends from the primary visual cortex to the parietal cortex, an area that specializes in integrating visuomotor information.

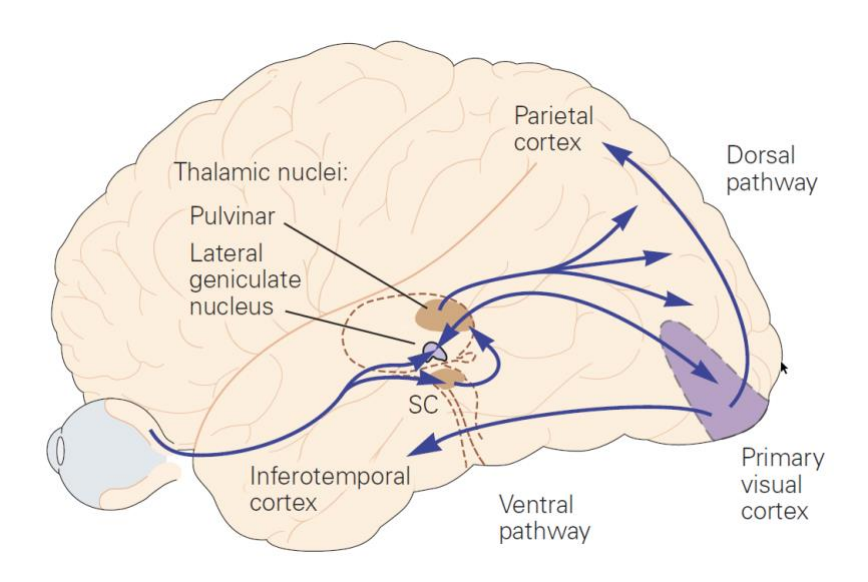


Figure 1.2 Dorsal and ventral pathways. Adapted from (Mack et al., 2013)

As mentioned before, both pathways follow a hierarchical model. The complexity of the stimuli that the areas encode follow the order of the visual hierarchy. For example, the retina would be at the bottom of the visual hierarchy since neurons in it can only differentiate between different light stimulations, and the neurons in area IT described before would be much higher. (Felleman and Van Essen, 1991) suggested that the hierarchical organization of the visual system constructs the new features of each area through a pooling system. Every stage of the hierarchy is responsible for selectively pooling their inputs according to what each area encodes, and ultimately creating a more and more complex selectivity in their features.

Moreover, the size of the receptive fields varies based on the neuron's eccentricity (how far from the fovea lies the location of the encoding visual field) and the position of the neuron in the visual hierarchy. Receptive field size follows the order of the visual hierarchy and increases along the eccentricity. This is true for all the successive stages of visual processing (from photoreceptors, bipolar cells, ganglion cells, through neurons in multiple visual cortical).

A summary of these two points are depicted in Figure 1.3 for visual areas V1, V2, and V4 (Adapted from (Freeman and Simoncelli, 2011)):

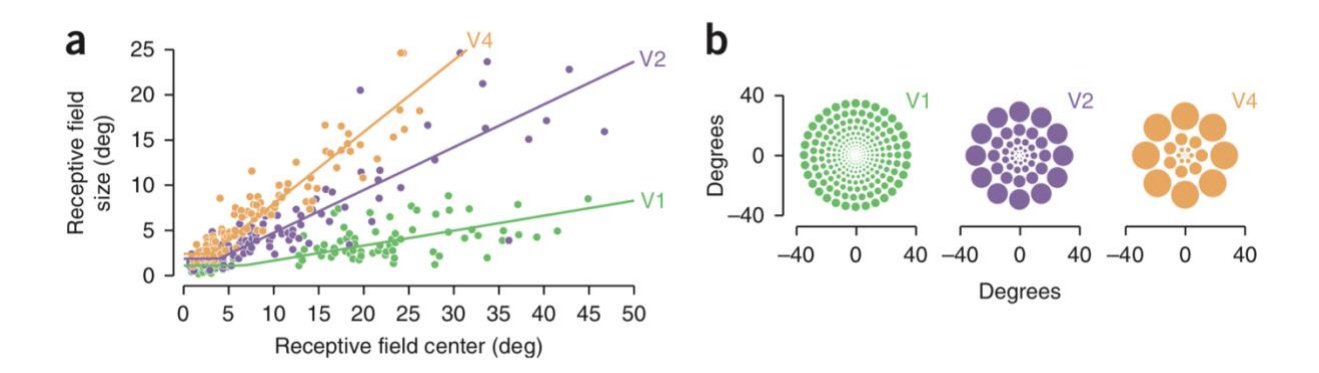


Figure 1.3 Physiological measurements of receptive field size in macaque monkey in several visual areas, across various eccentricities.

#### 1.2.3 Retinotopy

The visual cortex is organized into visual maps, so that nearby neurons encode nearby regions of visual space. In other words, for a given change in the cortical location, we can expect a corresponding change in the retinal position that is encoded by that location (Dumoulin and Wandell, 2008; Engel et al., 1997; Holmes, 1945; Horton JC and Hoyt WF, 1991; Sereno et al., 1995). This organization on the visual cortex is termed retinotopy.

Foveal representation is encoded in the most caudal part of the occipital cortex and eccentricity increases more rostrally.

Over half of the neocortex in non-human primates is occupied by visual areas. Most of them have been studied by a collection of micro-electrode, histological staining and tracing techniques. Extensive mapping of the characteristics of each visual area can be tedious with these techniques. More importantly, studying human visual areas invasively is impractical, and most early knowledge of the human retinotopic organization was from soldier wounds.

The development of fMRI revolutionized retinotopic mapping. Researchers were able to reveal unprecedented functional cortical details from a variety of visual areas. Traditional experiments were comprised of a moving wedge or expanding and contracting circles around a central fixation

point (Figure 1.4). The use of mapping techniques to identify individual cortical visual areas has allowed hierarchical processing and functional specialisation to be investigated much more directly.

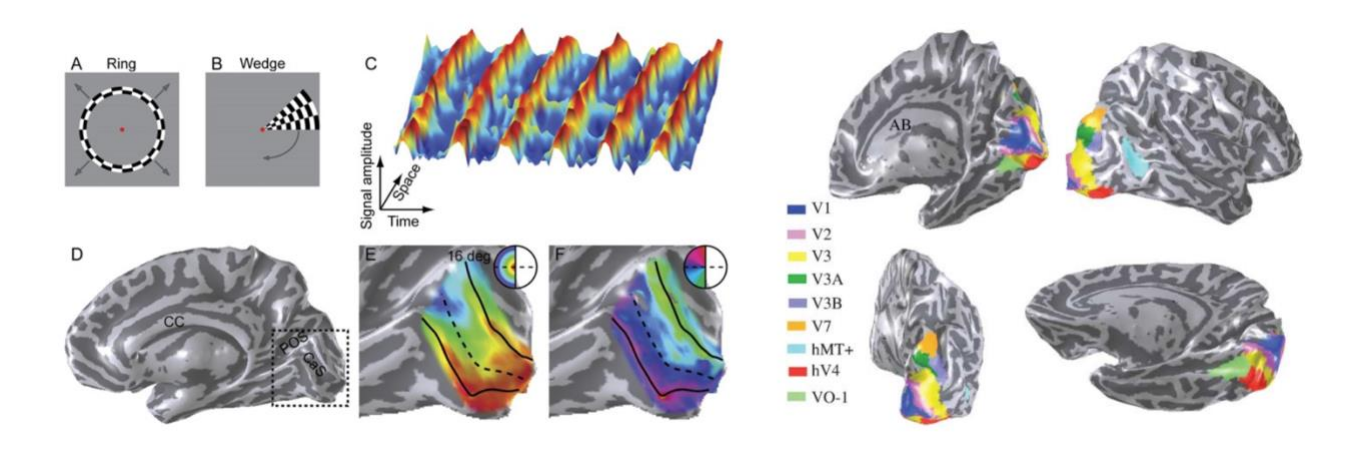


Figure 1.4. Travelling wave retinotopic paradigm for mapping visual areas in the human visual cortex. Adapted from (Wandell et al., 2007).

#### 1.3 Eye movement circuitry

The previous sections described how the visual system deconstructs a still visual scene into specialized features in each visual area: from low level features such as orientation lines, all the way to more complex features like objects and faces.

However, in realistic conditions, our eyes are never really lying still, but rather continuously explore the environment. Eye movements bring the high resolution part of the eye, the fovea, to the point of interest, exploiting the high density of photoreceptors that are localized around that area. This heterogeneity of the human retina is dictating that gaze can be directed to only one object at a time.

Eye tracking during the exploration of the visual scene reveals trajectory patterns that are associated with informative features of the visual scene that capture our attention. In other words, attention can be considered an information-processing filter. A series of studies (Itti and Koch,

2000; Tatler and Vincent, 2008; Tatler et al., 2005) have proposed that gaze is influenced by physically salient visual features, in a bottom-up manner, where low level features of the images provide an "objective" focus of attention, in models for feature integration theory (Treisman and Gelade, 1980), guided search (Wolfe, 1998) and attentional engagement theory (Duncan and Humphreys, 1992, 1989). On the other hand, top-down approaches of gaze control are based on semantics, working memory and the demands of the behavioral task (Castelhano et al., 2009; Fischer et al., 2013; Mills et al., 2011; Tatler and Vincent, 2008; Yarbus, 1967). Art exploration for example, is a complex process where multiple low and high level features can affect the eye's trajectory. It has been shown that the viewer's art expertise and familiarity or interest in a specific work of art, influence the exploration process (Nodine et al., 1993). Moreover, the viewing behavior during the time-course of the scene exploration appears to be influenced initially by bottom-up saliency features, followed by late top-down control characteristics (Castelhano et al., 2009; Helo et al., 2014; Mills et al., 2011; Tatler and Vincent, 2008).

Our understanding of the circuitry that is responsible for the saccadic generation comes both from human and animal experiments. Human experiments typically involve study of patient groups that have suffered a lesion in isolated areas, or from non-invasive imaging techniques. Animal models provide information of the saccadic involvement of an area through microstimulation or from activation-deactivation of neurons through the usage of substances. A series of studies have isolated critical nodes in the saccadic-generation network in the brainstem, superior colliculus, the thalamus, basal ganglia, parietal and frontal regions (Hikosaka et al., 2000; Leigh and Zee, 1991; Moschovakis, 1996; Scudder et al., 2002; Wurtz and Goldberg, 1989). Eye-ball rotation control is believed to be produced by a network of neurons that provide a burst generator in the brainstem (see detailed review Scudder et al., 2002). However, brainstem is controlled by the superior colliculus and the frontal eye fields, operating in a recurrent network through the basal ganglia and the thalamus (Chalupa & Werner, 2004). Figure 1.5 represents the nodes that interact for the production of eye movements.

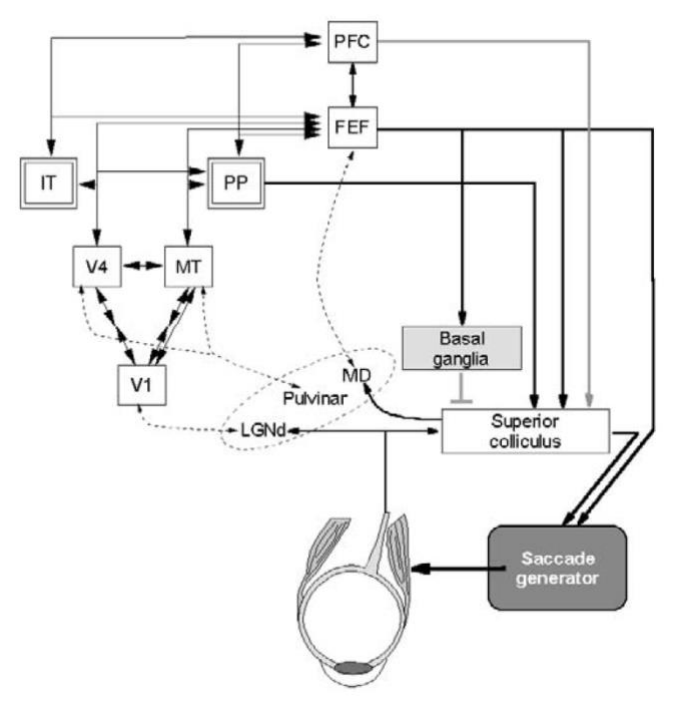


Figure 1.5. Circuitry for saccadic generation. Adapted from "The visual Neurosciences (2004)".

The superior colliculus is connected directly to the retina, the ventral and dorsal pathways, but also the prefrontal cortex (Fries, 1984). The visual inputs that is has create a retinotopic map on its superficial layers. Additionally, the intermediate layers of the superior colliculus, functionally create a topographic map of the saccade direction and amplitude. However, the receptive or movement field of each neuron is larger than the precision of each saccade, therefore in order to produce a specific saccade, a combinatorial activation of several neurons leads to the summation to the appropriate saccadic vector (Lee et al., 1988; Van Gisbergen et al., 1987).

The circuitry that is depicted in the previous figure, support the theory that saccadic eye movements can both be influenced by a bottom-up but also a top down mechanism: the visual inputs from the dorsal and ventral streams can provide a saliency map based on visual/object features, whereas inputs from the prefrontal cortex to the superior colliculus can add a higher-order/contextual cognitive selection of the target.

#### 1.4 Visual stability

When we explore the visual scene, we make 2-3 saccades every second while our eyes jump abruptly through each object around us. The exploration can be broken down to two parts: fixation periods that last a few hundred ms, and eye displacements that are much shorter (~40-50 ms). The eye movements can be formulated by the initiation point during each fixation, and a vector that corresponds to the visual field translation caused by the saccade.

Early studies assumed that a cancellation signal was sent to the visual eye-movement centers that canceled the effect of the displacement. It was initially termed as "effort of will" (Helmholtz, 1896) and later as a corollary discharge (Sperry, 1950), but both represented the same principle idea: a representation of the vector of the imminent movement is sent to multiple areas of the cortex.

The corollary discharge is considered to contribute to several distinct mechanisms that provide visual stability, such as saccadic omission and saccadic suppression, but these mechanisms are outside of the scope of this thesis.

#### 1.4.1 Remapping

The visual information encoding during fixation was described in a previous section. During fixation, the retina receives input from a fraction of the environment and transmits this information to the visual areas for specialized feature extraction. The spatial selectivity of each neuron is determined during the early stages of development and maintained throughout the individual's life.

However, the receptive fields of neurons in several visual areas have been shown to demonstrate transient shifts around the brief timing of a saccade. It has been hypothesized that this is a neuronal mechanism that the brain uses to compensate for the visual field displacements, and ultimately contribute to visual stability (Colby and Goldberg, 1999). This mechanism is termed remapping. Remapping relies on a corollary discharge to get the information of the source and the target of the neural population connected by the saccade vector, in order to exchange information about the visual input (Sommer and Wurtz, 2006).

The first demonstration of visual remapping was performed in the lateral parietal cortex (LIP) (Duhamel et al., 1992) — Figure 1.6. In this study, the experimenters first identified the classic receptive fields of LIP neurons (this was termed the current field or CF) while the animal fixated on a target. Then they briefly flashed a probe right before the saccade, at the location that the receptive field of each neuron would occupy right after the saccade (this was termed the future field, or FF), and the neurons still elicited responses. In other words, neurons revealed anticipatory access to information from what was going to fall in their receptive field in the future after the completion of the saccade, acting in a sense as neuronal "fortune tellers". The access that neurons have to spatial information both from the CF and the FF around the timing of the saccade, is one of the mechanisms that is believed to enable smooth perceptual transition.

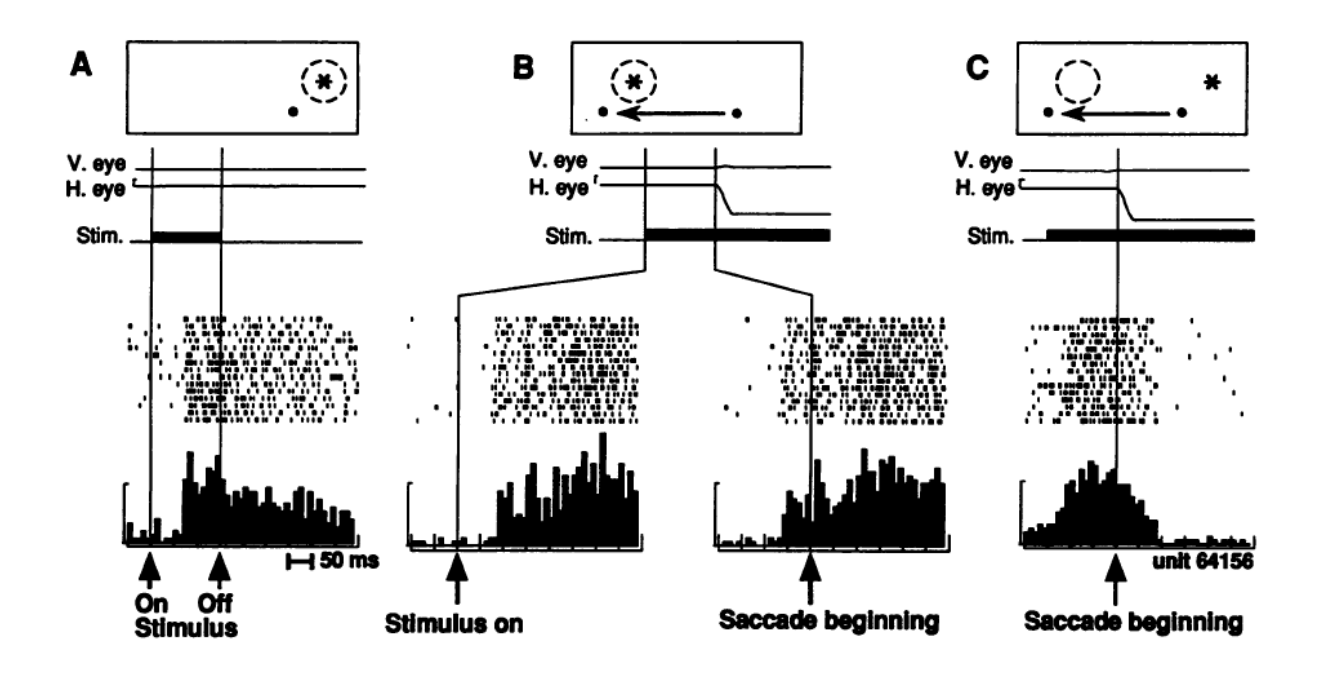


Figure 1.6. First demonstration of the remapping mechanism. Adapted from (Duhamel et al., 1992)

These experiments paved the way for a series of studies that investigated the neuronal mechanism that leads to this shift of the location of receptive fields. The LIP anatomical connectivity to SC and FEF, and the engagement of specific areas during eye-movements, indicated potential candidate areas for finding the same predictive mechanism. Remapping has been observed using electrophysiology in several brain regions; Superior Colliculus: (Churan et al., 2011; Walker et al., 1995), Frontal Eye Fields (FEF): (Umeno and Goldberg, 1997), Lateral Intraparietal Area (LIP): (Duhamel et al., 1992; Wang et al., 2016; Kusunoki and Goldberg, 2003), V4: (Neupane et al., 2016a; Tolias et al., 2001a). Early areas in the visual hierarchy have shown less evidence of the effect, with decreasing presence of remapping for earlier areas (Nakamura and Colby, 2002). Additionally, fMRI studies have shown remapping effects on the parietal cortex, and on the extrastriate and striate cortex (Merriam and Colby, 2005; Merriam et al., 2007).

Remapping has been shown to be dependent on a corollary discharge that originates in the SC and is mediated through the mediodorsal thalamus to FEF. Deactivation of the mediodorsal thalamus with muscimol impaired the ability of monkeys to perform a double step saccade and also remapping activity in FEF diminished (Sommer and Wurtz, 2002, 2006).

## 1.4.2 Remapping as a mechanism for visual stability or as a mechanism for attentional pointers?

The early remapping experiments showed that a neuron that exhibits remapping can be activated from a probe that is presented at a location that corresponds to the translation of the neurons' receptive field by the saccade vector. However, a series of studies (Zirnsak and Moore, 2014) in FEF and (Tolias et al., 2001a) in V4, showed that neurons in those areas could exhibit remapping at shifted locations of the FF towards the saccade target (convergent, or saccade target remapping). This result is contradictory to the hypothesis that remapping is contributing to visual stability since it is more consistent with a role in emphasizing visual information around the saccade target. However, (Neupane et al., 2016a) showed that both types of remapping can be monitored within visual area V4. The important differentiation between the two types of remapping that was shown in this study was that remapping associated with perceptual constancy occurred

for saccades in all directions, while attentional shifts mainly occurred for neurons that their receptive fields were located in the same hemifield as the saccade target.

The approach of remapping solely as a mechanism for spatial constancy becomes problematic when we consider that a plethora of inter- and intra-areal connections need to be established to account for every possible saccade vector movement. A line of thought that emerged to account for this problem was to consider that visual compensation during eye-movements could be restricted to salient or task-relevenat objects, selected by spatial attention (Cavanagh et al., 2010; Rolfs and Szinte, 2016; Szinte et al., 2018). Psychophysical experiments have shown the influence of anticipatory spatial attention to the location that the visual stimulus will occupy after the saccade (Jonikaitis and Theeuwes, 2013; Rolfs et al., 2011a; Szinte et al., 2016). Additionally, MT neuronal recordings showed that attention plays a crucial role in the strength of remapping (Yao et al., 2016). However, in contrast to this "infinite connectivity" paradox, (Neupane et al., 2017) showed selective connectivity between neurons that encode the CF and the FF through communication by coherence.

Moreover, there have been indications that remapping is influenced from a top down mechanism when monitoring the latency and strength of remapping in the visual cortex in humans with fMRI (Merriam et al., 2007) and in the monkey (Nakamura and Colby, 2002). However, the link to the strength of remapping in the visual cortex is not linked to attention per se, but rather to the density of connections from FEF (Nakamura and Colby, 2002; Schall et al., 1995; Stanton et al., 1995) or LIP to early visual areas.

#### 1.4.3 Receptive field expansion during remapping?

When an object is flashed close to the timing of a saccade, it has been shown that subjects mislocalize their position (Dassonville et al., 1992; Honda, 1989; Jeffries et al., 2007; Ross et al., 1997). A series of studies tried to investigate a link between remapping and this mislocalization by monitoring the intermediate retinal positions that connect the current field to the future field. By projecting stimuli along the vector that connects the two receptive field locations, (Wang et al., 2016) showed in LIP that "there is a spread of activity from caudal to rostral, such that neurons with movement fields successively closer to the center of gaze fire later". This wave-like activity propagation showed that there is an expansion of the receptive fields around the timing of the saccade. However, this finding came in contrast to a previous study (Sommer and

Wurtz, 2006) that investigated the same kind of expansion in FEF that couldn't find expansion and concluded that there is a "jump" of the remapped responses from the CF, straight to the FF. One explanation could be difference in the stimulation positions as discussed in (Wang et al., 2016) or area discriminations.

#### 1.5 Magnetoencephalography

When a current flows along a wire, a magnetic field is induced around it (Orsted, 1819). Moreover, an electrical dipole is always surrounded by a magnetic field, and the polarity of the field is influenced by the direction that the current is flowing. This electromagnetic property is also present in the neuronal "wiring". Pyramidal neurons with their long apical dendrites that are perpendicular to the cortical surface create a tractable magnetic field that with the usage of extremely sensitive sensors can be monitored from a distance (Buzsáki et al., 2012). Although the magnetic field produced by a single neuron is extremely small, synchronized post-synaptic currents flowing across multiple neurons can summate to a detectable signal.

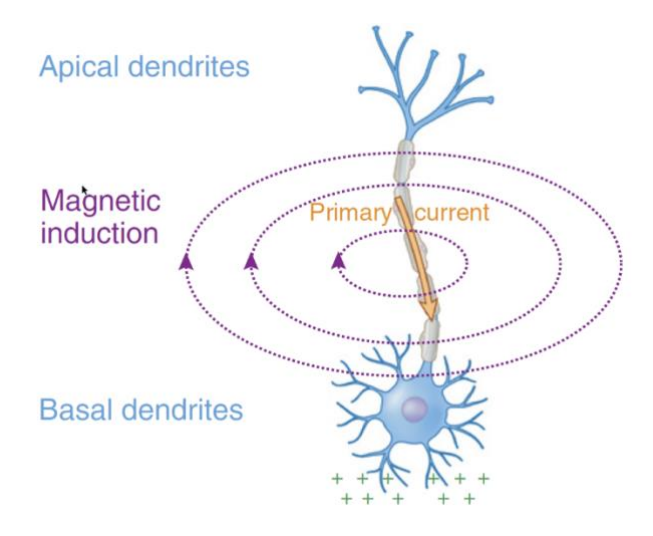


Figure 1.7 Cellular origin of MEG signals. Adapted from (Baillet, 2017).

Magnetoencephalography (MEG) is a non-invasive neurophysiological technique that measures the magnetic fields generated by the neuronal activity of the brain. MEG has the ability to monitor the entire cortical surface simultaneously with excellent temporal resolution (Baillet, 2017). A typical MEG system consists of a few hundred sensors that are located within a magnetically shielded room.

MEG faces the challenge that the signal to noise ratio decreases with source depth; the deeper a neural generator is relative to the MEG sensors, the more attenuated the magnetic signal is (in proportion to distance squared); however, there have been reports of localization of deep structures: amygdala (Balderston et al., 2014; Cornwell et al., 2008; Dumas et al., 2013), hippocampus (Cornwell et al., 2012) and brainstem (Coffey et al., 2016a; Parkkonen et al., 2009). Signal attenuation is also reported within sulci (Goldenholz et al., 2009).

More importantly, since the MEG utilizes an array of sensors that are far from the cortical sources, it ultimately becomes a modeling problem to correctly allocate the active sources. Several methods have been proposed to solve this problem, each with a different set of assumptions needed to reach to a unique solution (Baillet et al., 2001; Hämäläinen and Ilmoniemi, 1994; Hämäläinen et al., 1993; Pascual-Marqui et al., 1994; Sarvas, 1987, Gramfort et al., 2013a). Traditionally, there are two approaches for modeling the brain activity with MEG: the dipole methods and the imaging methods. Dipole methods place a set number of dipoles on the cortical surface with a given orientation, and then fit the modeling to the data. The localization accuracy of these methods can be perfect, but it can be problematic when more sources are actually active than the assumed on the model, or when a larger area is activated (Benbadis et al., 2010; Darvas et al., 2004). On the other hand, the imaging methods place a distributed network of sources (typically a few hundreds of thousands) along the cortical surface (traditionally, the MRI of the subject is also acquired for these methods), and although the resolution becomes much coarser, multiple sources are monitored much better. The sources are oriented perpendicularly to the cortical surface, effectively following the cortical manifold to resemble the pyramidal cells.

The spatial resolution of MEG is often assumed to be poor because of the ill-posed nature of the MEG sources, but a quantitative analysis was seldom performed. Chapter 2 of this thesis utilizes a retinotopic paradigm that takes into account the modeling and physical properties of neuronal populations along the cortical surface in order to monitor the spatial resolution of MEG. This study concluded that there is an interplay between distance between sources and cortical curvature that affects the resolution; resolving MEG sources can be separated by as little as 0.5mm of cortex, with an average resolution on the order of 2-3mm. This study showed that the spatial resolution of MEG, in same convoluted areas, can even exceed the spatial resolution of fMRI. It is important to note here that these values were computed for responses elicited in the primary visual cortex, that has very high spatial specificity. Areas that encode high resolution sensory stimuli (e.g. primary auditory cortex) would be expected to show equally precise resolution if stimulated properly. It would be interesting to measure the trade-off between specificity and spatial resolution in different cortical areas, but this study focused on the absolute limit of MEG's spatial resolution.

#### 1.5.1 Retinotopy in MEG

Although single cell recordings and fMRI techniques have revealed retinal inputs to the cortex for decades now, a cortical representation of the visual field with MEG hadn't been demonstrated. Previous studies in the visual cortex with MEG showed temporal discrimination between entire visual areas (Cottereau et al., 2011; Hagler et al., 2009), or used a small number (4-8) of stimuli to perform coarse retinotopic mapping (Brookes et al., 2010; Moradi et al., 2003; Poghosyan and loannides, 2007; Sharon et al., 2007). Moreover, the traditional experimental paradigm for retinotopy in fMRI (rotating wedge), yielded an inconsistent trajectory with V1 anatomy (Perry et al., 2011). Spatial localization comparison studies have shown 3-5 mm localization error to fMRI in V1 (Moradi et al., 2003) and 2mm from activation simulation centers (Poghosyan and Ioannides, 2007).

Chapter 2 demonstrates a novel technique for characterizing the spatial distribution of MEG signals across the primary visual cortex. We showcase confined receptive fields of the visual input

computed from sources located within the primary visual cortex (visual area V1). Having access to the mapping of which sources encode which part of the visual scene can be detrimental for certain studies; remapping is an ideal example, since it relies on the receptive fields before and after the saccade. The MEG results were compared with fMRI performed on the same subjects and the retinotopic maps showed surprising resemblance.

#### 1.5.2 Remapping in MEG

As explained in previous sections, remapping is a complex mechanism that involves several brain regions. The transient character of remapping dictates that monitoring of the neuronal signals in real-time is crucial. Therefore, MEG is an ideal candidate for studying the fast mechanisms of remapping. However, to my knowledge, no MEG study has attempted to study remapping with the traditional approaches that were described in the section regarding remapping.

(Moon et al., 2007; Werf et al., 2008) investigated the sensorimotor transformation in FEF and LIP during saccades and anti-saccades, but didn't demonstrate the selective spatial neuronal shift. (Medendorp et al., 2007) investigated single and double step saccades but the temporal delay used in their paradigm allowed them to investigate the memory aspect of the parietal cortex involvement in the saccades, rather than spatial remapping intrinsically.

Chapter 3 of this thesis takes into account the modulatory effect that attention has on remapping and we show remapping activity in the superior parietal and early visual cortices. Moreover, we showcase the two different types of remapping that was shown in (Neupane et al., 2016b) – forward and saccade target remapping.

#### 1.6 Open science

Science moves forward by corroboration. Researchers need to verify each other's results and replicate them since "replication is the cornerstone of science" (Moonesinghe et al., 2007). However, there is growing alarm about results that cannot be reproduced; "Reproducibility crisis" was a term that emerged through disappointing replication results in various medical, life and behavioural sciences in the last decade (Open Science Collaboration, 2015). Moreover, Nature reported in 2016: "More than 70% of researchers have tried and failed to reproduce another scientist's experiments, and more than half have failed to reproduce their own experiments" (Baker, 2016).

A line of defense against this problem, is the establishment of standardized methods that are common among researchers. Several scientific communities e.g., in genetics, astrophysics or neuroimaging, have approached the issue by developing and supporting open and well-documented software platforms for verified, reproducible and shareable approaches to mass-data handling and analytics. However, although neuro-electrophysiology has evolved tremendously over the recent years, with a growing emphasis on recording from dense and distributed electrode arrays, most labs rely on developing their own analysis techniques, with error prone verification and poor documentation.

Moreover, due to the high sampling rate of neurophysiological techniques, the inflation in data volumes and dimensions redefines the frontiers of analytical approaches in the field. This also raises new challenges in terms of data management and transparency of increasingly complex analytical pipelines.

#### 1.6.1 Open source – software for invasive neurophysiology

Invasive neurophysiology has benefited from software tools for specific segments of the analysis workflow, such as spike-detection, sorting and time series analysis (Fee et al., 1996; Hazan et al., 2006; Hill et al., 2011; Mitra and Bokil, 2007; Oostenveld et al., 2011; Pachitariu et al., 2016a;

Quiroga et al., 2004; Siegle et al., 2017). However, they remain relatively specialized, some with limited support and documentation and most with restricted interoperability with other tools.

Chapter 5 in this thesis is dedicated to an analytical solution that can help tackle reproducibility crisis in invasive neurophysiology. In the spirit of open neuroscience, the software platform incorporates and interoperates with existing prominent open-source resources such as Brainstorm for scalp electrophysiology, a collection of spike-sorting tools (WaveClus, Kilosort, UltraMegaSort2000), the open Neurodata Without Borders format (NWB - (Rübel et al., 2019; Teeters et al., 2015)) etc. Additionally, the integrated app also provides a practical solution to data organization and annotation via the Brain Imaging Data Structure (BIDS) harmonization grassroot effort (Gorgolewski and Poldrack, 2016; Gorgolewski et al., 2016).

The app features an intuitive graphical user interface to access the most varied possibilities in data reviewing and analyses and advanced 3-D visualization and registration with anatomical imaging — all with no coding knowledge. A vast library of tools is also accessible via scripts that users can produce directly or generate with an assembly-block logic also from the graphical interface. The app is extensively documented online and supported by a user forum. Our manuscript features the tools with array recordings and MRI structural data from non-human primates, augmented with a step-by-step online tutorial, as companion material provided to readers.

This new research resource bridges across recording scales (from cells to whole-brain) and data modalities, registers neurophysiology with structural anatomy, and thereby delivers a unifying analytical environment to the broadest research community in neurophysiology.

Chapter 2 contains the results from the study undertaken during the PhD work to investigate the risual selectivity of individual MEG sources. It provides evidence of high-resolution retinotopic maps estimated within the primary visual cortex and an estimation of the spatial resolution of the
MEG. This work was published in Neuroimage (Nasiotis et al. 2017).

## Chapter 2 - High-resolution retinotopic maps estimated with magnetoencephalography

Konstantinos Nasiotis<sup>a,\*</sup>, Simon Clavagnier<sup>b</sup>, Sylvain Baillet<sup>a</sup>, and Christopher C. Pack<sup>a,\*</sup>

<sup>a</sup> Montreal Neurological Institute, 3801 University Street, Montreal, H3A 2B4, QC, Canada

<sup>b</sup> Montreal General Hospital, 1650 Av. Cedar, Montreal H3G 1A4, QC, Canada

\*Correspondence: konstantinos.nasiotis@mail.mcgill.ca, christopher.pack@mcgill.ca.

#### 2.1 Abstract

Magnetoencephalography (MEG) is used in clinical and fundamental studies of brain functions, primarily for the excellent temporal resolution it provides. The spatial resolution is often assumed to be poor, because of the ill-posed nature of MEG source modeling. However, the question of spatial resolution in MEG has seldom been studied in quantitative detail. Here we use the well-known retinotopic organization of the primary visual cortex (V1) as a benchmark for estimating the spatial resolution of MEG source imaging. Using a standard visual stimulation paradigm in human subjects, we find that individual MEG sources exhibit well-delineated visual receptive fields that collectively follow the known mapping of the retinal surface onto the cortex. Based on the size of these receptive fields and the variability of the signal, we are able to resolve MEG signals separated by approximately 7 mm in smooth regions of cortex and less than 1 mm for signals near curved gyri. The maximum resolution is thus comparable to that of the spacing of hypercolumns in human visual cortex. Overall, our results suggest that the spatial resolution of MEG can approach or in some cases exceed that of fMRI.

#### 2.2 Introduction

Among the various methods for non-invasive imaging, magnetoencephalography (MEG) source imaging is known to provide outstanding temporal resolution, while it is typically assumed to have modest spatial resolution (Darvas et al., 2004; Hämäläinen et al., 1993). Consequently MEG imaging is most often used in experiments aimed at measuring temporal fluctuations in neural

signals for which the assignment of a precise anatomical source is not critical. Although recent reports have raised the possibility of extracting rich spatial signals from MEG (Cichy et al., 2015), a quantitative estimate of the resolution that can be attained with this imaging modality is lacking.

Here we have examined the capacity of MEG to resolve the well-known retinotopic organization of the primary visual cortex (V1). This representation provides a useful benchmark, because it has been thoroughly and quantitatively characterized using a variety of methods, including electrophysiology (Das and Gilbert, 1995; Hubel and Wiesel, 1977), PET (Fox et al., 1987), optical imaging (White and Culver, 2010) and fMRI (Engel et al., 1997). These approaches have demonstrated a smooth change in the locus of cortical activation for corresponding changes in the position of the retinal stimulus (Dumoulin and Wandell, 2008; Engel et al., 1997; Sereno et al., 1995). Thus to the extent that an imaging modality has high spatial resolution, it should be able to differentiate responses to visual stimuli in different locations. The smallest shift in the locus of cortical activation that can be detected serves as a measure of resolution.

Here we have obtained retinotopic maps from human subjects using MEG in combination with a standard visual stimulation paradigm. We show that surprisingly high spatial resolution maps can be obtained with appropriate choices of visual stimulation and source modeling. In particular, we are able to reliably detect distinct MEG responses emanating from sources separated by 7.0 mm along smooth cortical surfaces and less than 1 mm along the arched gyri.

#### 2.3 Materials and Methods

#### 2.3.1 Participants

Data were recorded from two healthy, right-handed male subjects (one author, one naïve), both of whom had normal or corrected to normal vision. Both subjects gave written consent prior to participation in three sessions, involving structural MRI, functional MRI, and MEG recordings. All experimental protocols were approved by the Research Ethics Board of the Montreal Neurological Institute.

#### 2.3.2 Structural MRI

For the MRI scans, each subject was positioned on his back with a 32 channel surface coil centered over the occipital pole. Three-dimensional T1-weighted anatomical MR image volumes covering the entire brain were acquired on a Siemens TIM Trio scanner, prior to the functional scans (3D-MPRAGE, TR/TE= 2300/2.98 ms, TI = 900 ms, 176 sagittally oriented slices, slice thickness = 1 mm,  $256 \times 240$  acquisition matrix).

fMRI data from Subject 1 (S1) and Subject 2 (S2) were originally collected for independent studies. A multi-slice T2\*-weighted Gradient-echo echo-planar imaging (GE-EPI) sequence with slightly different parameters was used for S1 (TR/TE = 1940/30 ms, flip angle = 76 degrees, slice number = 32 with no gap, slice thickness = 2 mm; 128 x 128 acquisition matrix, a 256 x 256 mm rectangular field of view (FOV) and GRAPPA (acceleration factor along Phase Encoding direction (PE) = 3, reference lines = 33) and S2 (TR/TE = 2000/30 ms, flip angle = 76 deg, slice number = 37 with no gap, slice thickness = 3 mm; 64 x 64 acquisition matrix, 192 x 192 mm rectangular FOV and GRAPPA. The slices were pseudo-coronally oriented perpendicular to the calcarine sulcus and covered the entire occipital lobe.

#### 2.3.3 fMRI Retinotopic Experiment

The visual stimuli were generated with the Psychophysics Toolbox (Brainard, 1997; Pelli, 1997) and were back-projected on a screen outside of the bore at a viewing distance of 140 cm.

For S1, the stimulus consisted of a checkerboard pattern (100% contrast) visible through apertures of various orientations, as previously used for neuronal population receptive field (pRF) mapping (Clavagnier et al., 2015; Dumoulin and Wandell, 2008). The stimuli were viewed monocularly, with the dominant or the non-dominant eye being covered by a black patch alternatively on each run.

For S2, the stimuli consisted of 8 wedges (each subtending 45°) and 8 rings (each with a width of 1.38°) of a high-contrast moving dartboard pattern (Dumoulin and Wandell, 2008; Engel et al., 1997; Sereno et al., 1995). The 8 wedges and the 8 rings were successively presented for 2 seconds. The wedges were presented in a clockwise predictable order, and the rings of different eccentricities were sequentially presented in the expanding direction. The presentation followed

a periodic pattern and completed a full cycle in 16 seconds with a total of 8 cycles per scanning run. The maximum stimulus radius was 11°, and all stimuli were viewed under binocular conditions.

In both cases, eye position was controlled by means of a fixation task (colored dot at the center of the visual field). The volunteer had to report, via a button press, the occurrence of a color change of the fixation target (from red to green or green to red). Each fMRI time series consisted of 106 (S1) or 60 (S2) measurements. Eight (S1) or four (S2) fMRI scans per eye were collected.

#### 2.3.4 MEG Data Collection

Data were recorded using a 275-channel (axial gradiometers) whole-head MEG system (CTF MEG International Services Ltd.). Each subject's head was digitized (typically 200 points) with a 6 degree-of-freedom digitizer (Patriot - Polhemus) prior to MEG data collection. This was used to mark the scalp, eyebrows and nose, and to optimize co-registration with the anatomical MRI. Three head positioning coils were attached to fiducial anatomical locations (nasion, left/right preauricular points) to track head movement inside the MEG. Eye movements and blinks were recorded using 2 bipolar electro-oculographic (EOG) channels. EOG leads were placed above and below one eye (vertical channel) and the second channel was placed laterally to the two eyes (horizontal channel). Heart activity was recorded with one channel (ECG), with electrical reference at the opposite clavicle, for subsequent MEG artifact detection and removal. All data were sampled at 2400 Hz.

Visual stimuli were presented onto a screen placed in front of the subjects at a viewing distance of 45 cm, which permitted visual stimulation up to 25x20 degrees of eccentricity. The display system consisted of a projector (Sanyo PLC-XP57L) located outside the magnetically shielded room and two reflecting mirrors that directed images to the screen. The refresh rate of the projector was 60 Hz with a resolution of 1280x1024 pixels.

Subjects were seated in a dimly illuminated room (0.13 cd/m²) and asked to fixate a red dot of 0.1 degree radius; the fixation point remained visible throughout the experiment. While the subject fixated, we presented stimuli comprised of multiple square probes positioned randomly within the central 20 degrees of the visual field (Figure 1). Probe stimuli on each frame were comprised of 5-15 squares (34.59 cd/m²) displayed at maximum contrast against the background (0.94 cd/m²). The width of each square was set to 30% of its distance from the fixation point, with the exception of those located at eccentricities less than 1 degree, which were forced to have a size of 0.3 degrees. This scaling was chosen to approximate the size of receptive fields for neurons

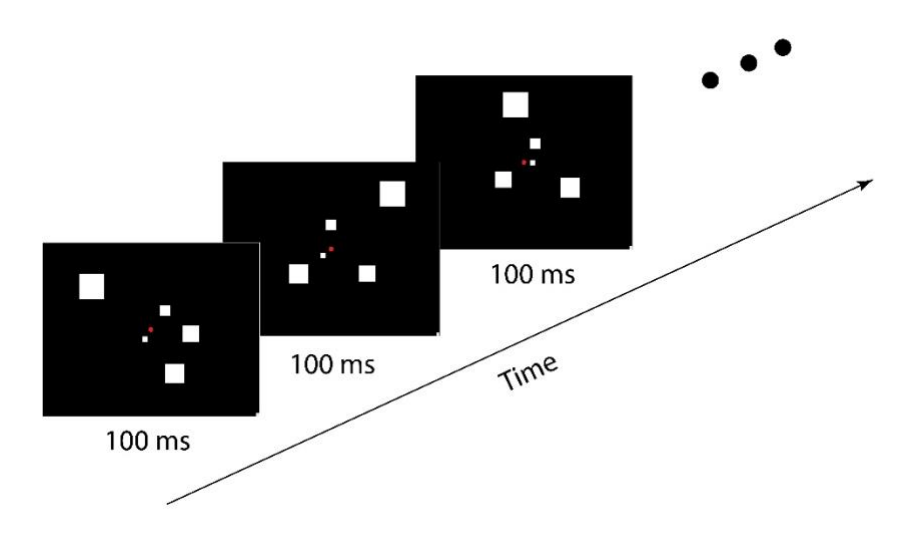


Figure 1 Stimulus presented to the subjects to elicit visual responses. Squares with sizes scaled according to retinal eccentricity were presented in random positions that changed on each frame presented. Each frame was presented for 100 ms, and each run lasted 10 minutes.

in V1 and V2 (Gattass et al., 1987; R Gattass, 1981). When a square overlapped with the fixation point, the latter was always presented over it, so the effective stimulation of that square was less than its area. Regions in which two squares overlapped were shown at the same luminance as individual squares. Each frame was presented for 100 ms with no time gap between frames. Since the screen's refresh rate was 60Hz, each frame was presented for 6 monitor cycles.

Each subject participated in a single MEG session, comprised of 6 runs that lasted 10 minutes each. The sequence of stimulus frames was random within and across runs. Subjects were given a short break between runs.

To measure the actual timing of each stimulus presentation with respect to MEG data collection, we presented a small square at the bottom right corner of each frame. The luminance of the square changed on successive frames, and a photodiode was used to identify the exact time of occurrence of each stimulus frame, relative to the MEG signal.

#### 2.3.5 Regions of interest

The primary visual cortex (V1) has the finest visual resolution among the visual areas in the occipital cortex, since its receptive fields are the smallest for each eccentricity (Burkhalter and Essen, 1986; Felleman and Essen, 1987; Gattass et al., 1987; R Gattass, 1981; Smith et al., 2001; Zeki, 1978). This makes V1 an ideal candidate for evaluating the resolution of MEG, since only a small part of the V1 cortex is expected to be activated with every localized stimulus on the visual field.

From the fMRI experiment, the cortical area of V1 was estimated and imported into the MEG data processing environment as a surface-based anatomical region of interest. Constraints on the visual stimulation available inside the MRI magnet led to limited coverage of the V1 maps for both hemispheres in both subjects. Given previous work showing that higher eccentricities are represented more anteriorly along the calcarine sulcus (Dougherty et al., 2003; Dumoulin and Wandell, 2008; Engel et al., 1997; Sereno et al., 1995), we manually extrapolated our V1-fMRI maps anteriorly by including additional sources until the parieto-occipital fissure. The V1 maps, along with the extrapolated area, were selected as a region of interest for MEG source analysis.

#### **2.3.6** MEG data analysis

MEG forward modeling was completed with the overlapping spheres approach (Huang et al., 1999). This method fits a sphere to the scalp surface under each sensor. A sphere can be used as a simplified model, since the magnetic fields are virtually undistorted by the skull (Barth et al., 1986; Okada et al., 1999).

Noise covariance across MEG sensors was estimated from a 2-minute empty-room recording prior to the experiments. Weighted Minimum Norm Estimates (wMNE) (Lin et al., 2006a) of cortically constrained, distributed sources were obtained using Brainstorm's default

parameters (Depth weighting: 0.5, Regularize noise covariance: 0.1, Whitening: PCA / SNR: 3). Source orientations were constrained to be perpendicular to the cortical surface.

A high-resolution cortical tessellation (150,000 sources) was used from each subject's individual anatomy for creating the source model (Dale and Sereno, 1993). This approach caused sources to have, in most cases, less than a millimeter distance from their closest neighbors, providing the possibility of detecting variations in the MEG signal on small spatial scales.

The inverse modeling transforms the signals from 275 sensor-signals, to 150,000 sources-signals. This leads to a vast amount of data. In order to decrease the volume of data, the signals were down-sampled to 600 Hz, and only the time-series from the sources located inside the V1 regions of interest (as described above) were considered for further analysis (4,890 sources for S1 and 5,311 sources for S2). The signal of each source was epoched into 1-minute bins, and the baseline (time average) of each epoch was subtracted. In order to reduce the contribution of heartbeat artifacts, signal space projection (Tesche et al., 1995; Uusitalo and Ilmoniemi, 1997) was applied to the MEG signals prior to source modeling.

#### 2.3.6.1 Estimation of visual receptive fields

The epoched time-series from the sources located in the region of interest were band-pass filtered (4<sup>th</sup> order Butterworth filter) in the 1-12Hz range (Figure 2). This range was chosen from analysis of pilot data from our lab showing strong, evoked visual responses in this frequency range from sources located in V1 (Appendix 1). Within this range, evoked visual responses were almost always biphasic (Appendix 2, (Aine and Stephen, 2003; Kaoru Seki, 1996; Nakamura et al., 2000; Stephen et al., 2002), with the leading phase varying across sources.

In order to identify the responses associated with individual stimulus frames, we set a threshold of three standard deviations below the mean response of each epoch (Figure 2, green line). The negative polarity of the response was chosen arbitrarily; using the positive phase of the response yielded results that were nearly identical to those reported here. On average ~3% of the total frames presented during the experiment led to threshold crossings in the filtered single-trial MEG responses for both subjects.

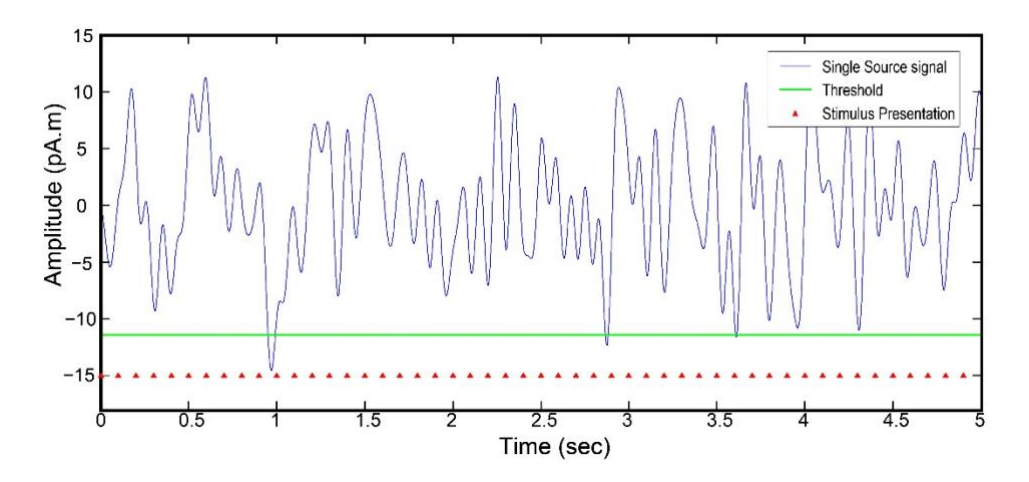


Figure 2. Example of a 5 second segment of signal from an occipital source, filtered between 1 and 12 Hz. The line in green indicates the threshold of 3 standard deviations below the mean of the filtered signal that was used for detection of selective visual responses. The red triangles indicate the time points at which the stimulus was updated.

For each significant response that crossed the threshold on a given source, we took the average value of each pixel on the screen during the preceding two frames (200 ms). This procedure is equivalent to the reverse correlation analysis commonly used to study receptive fields in individual neurons (de Boer and Kuyper, 1968; DeAngelis et al., 1995; Livingstone et al., 2001; Marmarelis and Marmarelis, 1978; Mineault et al., 2013; Pack et al., 2006). The resulting spatial maps were then summed across all significant responses for the same source, to yield that source's receptive field map. This map was then normalized by the frequency with which each pixel was activated during the experiment. Because the most peripheral pixels were activated very infrequently, this normalization introduced discontinuities near the edges of the display screen. We therefore cropped each response-triggered average at ~16 degrees of eccentricity. The analysis was performed for every source individually. In order to avoid artifactual responses, we rejected epochs in which blinks were detected in the EOG.

#### 2.3.6.2 Statistical significance of receptive fields

An anisotropic 2D Gaussian function was fit to each source's responses, to estimate the center of the receptive field and its spread along the two visual field axes:

$$f(x,y) = A * \exp(-(a(x - x_0)^2 - 2b(x - x_0)(y - y_0) + c(y - y_0)^2)), \quad (1)$$

where 
$$=\frac{\cos^2\theta}{2\sigma_x^2}+\frac{\sin^2\theta}{2\sigma_y^2}$$
,  $b=-\frac{\sin2\theta}{4\sigma_x^2}+\frac{\sin2\theta}{4\sigma_y^2}$ ,  $c=\frac{\sin^2\theta}{2\sigma_x^2}+\frac{\cos^2\theta}{2\sigma_y^2}$ 

Here A is the amplitude,  $x_0, y_0$  represent the center, and  $\sigma_x, \sigma_y$  the standard spread of the Gaussian kernel. The angle  $\vartheta$  denotes the clockwise rotation applied to the elliptical function to fit the data.

In order to verify that receptive fields were not due to random signal fluctuations, we compared the amplitude (A) of the Gaussian fit to a threshold that was defined through a permutation test (Pack et al., 2006). We used the same number of frames that were averaged to create the receptive field, but shuffled the order of the stimuli. The resulting receptive field was fit again to a 2D Gaussian function, and the amplitude of this Gaussian was compared to the one that was computed from the experimental data. This procedure was repeated 1000 times. Significant receptive fields were considered as those that had higher amplitude than 95% of those calculated through the permutation.

The distance between the fixation point and the center of the Gaussian fit provided the eccentricity of each source's receptive field. For the sources that demonstrated significant receptive fields, the value of their eccentricity was assigned to each source's cortical location. For display purposes, the eccentricities were grouped into 3 different ranges: 0-2, 2-5, 5-11 and were color-coded for projection onto the cortical surface.

#### 2.3.6.3 Comparison of MEG with fMRI results

For comparing the receptive fields that were obtained from the two modalities, for each hemisphere of the two subjects, we selected a line along the upper lip of the calcarine sulcus, thus sampling a wide range of eccentricities (Engel et al., 1997). For the MEG data points, only the sources that belonged on this line and demonstrated significant receptive fields were taken into account for the comparison. In order to generate a representation of the change of the visual field representation on the cortical surface, a source of 5.8° of eccentricity was selected as the reference. This eccentricity was selected as a reference because all lines from the 4 hemispheres demonstrated a source at 5.8° with significant receptive fields. The eccentricity of each source on those lines was plotted relative to the geodesic distance between the references and every other source. The geodesic distance was computed with the fast-marching algorithm (Sethian, 1996). The fast marching algorithm is very similar to the Dijkstra algorithm (Dijkstra, 1959) that is used in graph theory to find the shortest paths on graphs.

The fMRI points were computed on 2-dimensional, flattened representations of the cortical manifold centered on the foveal confluence and subtending 100 mm of diameter. Linear ROIs were manually drawn within V1 to match as closely as possible those already determined on the MEG-based data, one per each hemisphere. The linear ROI was made of equidistant (on the flat maps) cortical bins that were assigned the average of the eccentricity values of the voxels they contained. The numbers of bins depended on the length of the line. Linear cortical magnification factor was estimated after calculating the geodesic cumulative distance between the bins (with the origin arbitrary set at 5.8°) and plotting them against their main eccentricity.

#### 2.3.6.4 Spatial resolution

For the calculation of spatial resolution, we used data comprised of the threshold crossing of each individual source that demonstrated a significant receptive field. The total number of frames in the experiment was 36,000, and a binary vector ( $1 \times 36,000$ ) was created for each source indicating on which frame the source response passed the threshold. Consequently, for any two sources with significant receptive fields, we formed a  $2 \times 36,000$  matrix. For two sources with identical visual responses, the two rows of this matrix would be identical, which would in turn imply that we were unable to resolve signals at the corresponding inter-source distance.

To quantify resolution, we therefore performed a singular value decomposition (SVD) on that binary matrix and obtained 2 singular values ( $s_1$  and  $s_2$ ) that expressed the separability between the two vectors. When the two vectors are identical, only the first singular value is representative of the matrix,

and the second value is zero. This would correspond to an inability to resolve differences between the two sources. On the other extreme, when the two vectors have their values completely non-overlapping, the two singular values are equal. The separability index (SI), given by  $SI = \frac{s_1^2}{s_1^2 + s_2^2}$ , is therefore indicative of the degree of overlap between the two binary vectors and representative of the correlation among sources. The SI thus ranges from 0.5, when responses are completely independent, to 1.0, when responses are identical. The advantage of using the singular values ratio, compared to the dot product between the two vectors, is that the former is affected by instances when only one of the two sources crosses the threshold, which was often the case in our data.

In order to establish the SI values that would be expected based on pure noise, we described the probability of having concurrent threshold crossings for every pair of sources. This probability is based on the number of frames to which each source showed selectivity and the total number of frames presented. We estimated the cumulative probability of concurrent threshold crossings and included in the plot only the data points that were above the 95% distribution, which was set as the noise level.

The probability of having  $\alpha$  concurrent threshold crossings based on chance is defined by a hypergeometric distribution:

noise distribution = 
$$\frac{\binom{v_1}{\alpha} * \binom{TF - v_1}{v_2 - \alpha}}{\binom{TF}{v_2}}$$
(2)

where  $v_1$  and  $v_2$  are the number of frames on which the first and the second source surpassed the frame selectivity threshold respectively, TF is the total number of frames (36,000), and  $\alpha$  is the number of concurrent threshold crossings ( $\alpha \in [0, \min(v_1, v_2)]$ ). From this distribution we calculated the cumulative distribution for setting the noise threshold at 95%.

For each combination of sources with significant receptive fields in the same hemisphere, we plotted the SI relative to their geodesic distance and their relative orientation, creating a 3 dimensional plot. The data points were binned into 1 mm by 2° bins, extending from 0 - 80 mm and 0 - 180°, for the observed geodesic distance and orientation values respectively. Since not all bins had the same number of data points, we fit the data-points to a 2-dimensional exponential function, weighted by an inverse multivariate kernel density estimator (Hwang et al., 1994):

$$f(d,\theta) = \alpha_0 + ae^{(bD+c\Theta)}$$
 (3)

Here D is the geodesic distance between sources, and  $\Theta$  the relative orientation between the sources.  $\mathbb{Z}_0$  is a constant that captures the baseline (0.5) and common noise among sources,  $\alpha$  is the amplitude and b and c are constants that capture the decay of the exponential function for the distance and orientation axes.

The threshold for defining the resolution is based on the decay constant of the exponential function that was used to fit the data points. Since the exponential is 2-dimensional, the threshold is a line that relates geodesic distance and relative orientation between sources. The decay constant shows the spaceangle combinations that are needed for the correlation to drop to 1/e (36.8%) of its maximum value. The line that defines this threshold can be interpreted as the point where the responses of the two sources are 63.2% separable. The threshold is given by the equation:

$$-1 = bD + c\Theta \tag{4}$$

The placement of the sources on the cortical surface, and therefore the geodesic distance and the relative orientation between them, is affected by the curvature of the surface. For examining the possible placements for given curvatures, we assumed for simplicity that the local cortical surface could be approximated by an osculating sphere with radius: R = 1/curvature (DoCarmo, 1976). The combinations of the orientation and perimetric distance of sources that can be placed on a sphere form a line that follows:

$$d = \frac{2\pi\theta}{360 * Curv} \tag{5}$$

where d is the distance between the two dipoles along the curve of the osculating sphere,  $\theta$  is the relative angle between the dipole sources, and Curv is the curvature of the sphere (1/Radius of the sphere). By solving the linear system of equations (4) and (5), we can derive the maximum resolution that MEG can achieve for surfaces with given curvatures.

#### 2.3.7 Software

MEG data analysis was performed with Brainstorm(Tadel et al., 2011). Cortical reconstruction and volumetric segmentation were performed with the Freesurfer image analysis suite (http://surfer.nmr.mgh.harvard.edu/) (Dale et al., 1999; Fischl et al., 1999, 2001).

#### 2.4 Results

We studied the spatial properties of MEG signals emanating from the visual cortex in two human subjects. We elicited visual responses by presenting images comprised of a small number of squares flashed simultaneously on a computer monitor. In this section we analyze the relationship between the positions of individual stimulus squares and MEG source responses, as well as the distribution of these receptive fields across the cortical surface; we use these data to derive an estimate of the overall resolution of MEG source imaging.

#### **2.4.1** Visual receptive fields estimated from individual occipital sources

Based on the stimulation procedure illustrated in Figure 1, we were able to recover discrete visual receptive fields for individual MEG sources. These receptive fields were obtained by reverse correlating (de Boer and Kuyper, 1968; Ringach and Shapley, 2004) the source responses and the stimuli (see Methods). The results described below were based on receptive field estimates obtained with 60 minutes of data collection, although comparable results can be obtained with far less data (Appendix 3).

Figure 3 illustrates the receptive field that was calculated for a single source located in the right hemisphere in area V1 of subject 1. The origin of this plot corresponds to the position of the fixation point. For this source there was a well-localized receptive field located at a retinal eccentricity of 4.3 degrees; as expected from a source located in the right hemisphere, its receptive field was in the left visual field. The radius of the receptive field for this source was 1.4 degrees, which is about 10 times bigger than what previous studies have demonstrated for individual V1 neurons (Gattass et al., 1987; R Gattass, 1981; Van Essen et al., 1984) and about 2 times bigger than V1 population receptive fields obtained with fMRI (Dumoulin and Wandell, 2008). This suggests that the spatial resolution of MEG, while somewhat coarse, can be comparable to that of other imaging modalities. However, as shown below, MEG spatial resolution varies substantially with source orientation.

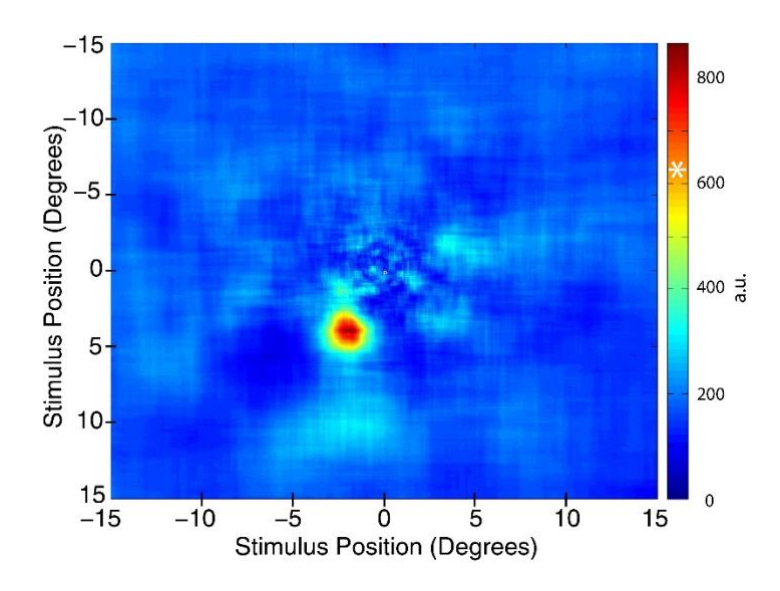


Figure 3 Example of a receptive field calculated from a single cortical source. This source belonged to the right hemisphere and was located above the calcarine sulcus in the primary visual cortex. The white star on the color bar defines the limit, above which the receptive field was deemed significant.

#### 2.4.2 Retinotopic maps estimated with MEG

The visual cortex is organized into visual maps, so that nearby neurons encode nearby regions of visual space(Dumoulin and Wandell, 2008; Engel et al., 1997; Holmes, 1945; Horton JC and Hoyt WF, 1991; Sereno et al., 1995). That is, for a given change in cortical location, one finds a predictable change in the retinal position encoded by that location. In order to estimate this relationship in our MEG data, we calculated the physical location and the retinal eccentricity associated with each MEG source.

The physical location of each source was estimated from structural MRI images for each subject, from which we created cortical surface reconstructions (Dale and Sereno, 1993). The calculation of the receptive fields was performed only on the sources that were located inside the regions of interest. Within these regions we computed 4,890 receptive fields for subject 1 and 5,311 for subject 2. For every computed receptive field, a 2-D Gaussian function was fit to the data and significance testing was conducted (see Methods).

For both hemispheres in both subjects, there was a fairly smooth gradation of the eccentricities of the significant receptive fields along the upper lip of the calcarine sulcus in area V1. The sources that had foveal responses were clustered at the most posterior part of the cortex, and those with higher eccentricity were located more anteriorly, as expected from known retinotopic organization (Wandell et al., 2007).

Figures 4 and 5 depict the individual MEG retinotopic maps based on eccentricity. The eccentricity values were binned into 3 categories, and an example receptive field from one source from each eccentricity category is displayed next to the maps for each hemisphere for both subjects. The figures also show the occipital eccentricity maps that were calculated from the subjects' fMRI data. Separate maps that show the polar angle are depicted in Appendix 4 and 5.

The individual receptive fields for the example sources indicate localized spatial selectivity in the positions and sizes of the receptive fields. The foveal sources exhibited clear receptive fields at eccentricities as small as 0.34 degrees; this was the smallest eccentricity for which receptive fields could be reliably estimated, given the 0.15° extent of the fixation point. The maps also indicate a precise mapping of visual inputs to the contralateral hemisphere, with very little spread of receptive fields across the vertical meridian (Jeffreys and Axford, 1972). As expected, the receptive fields were larger for more peripheral sources.

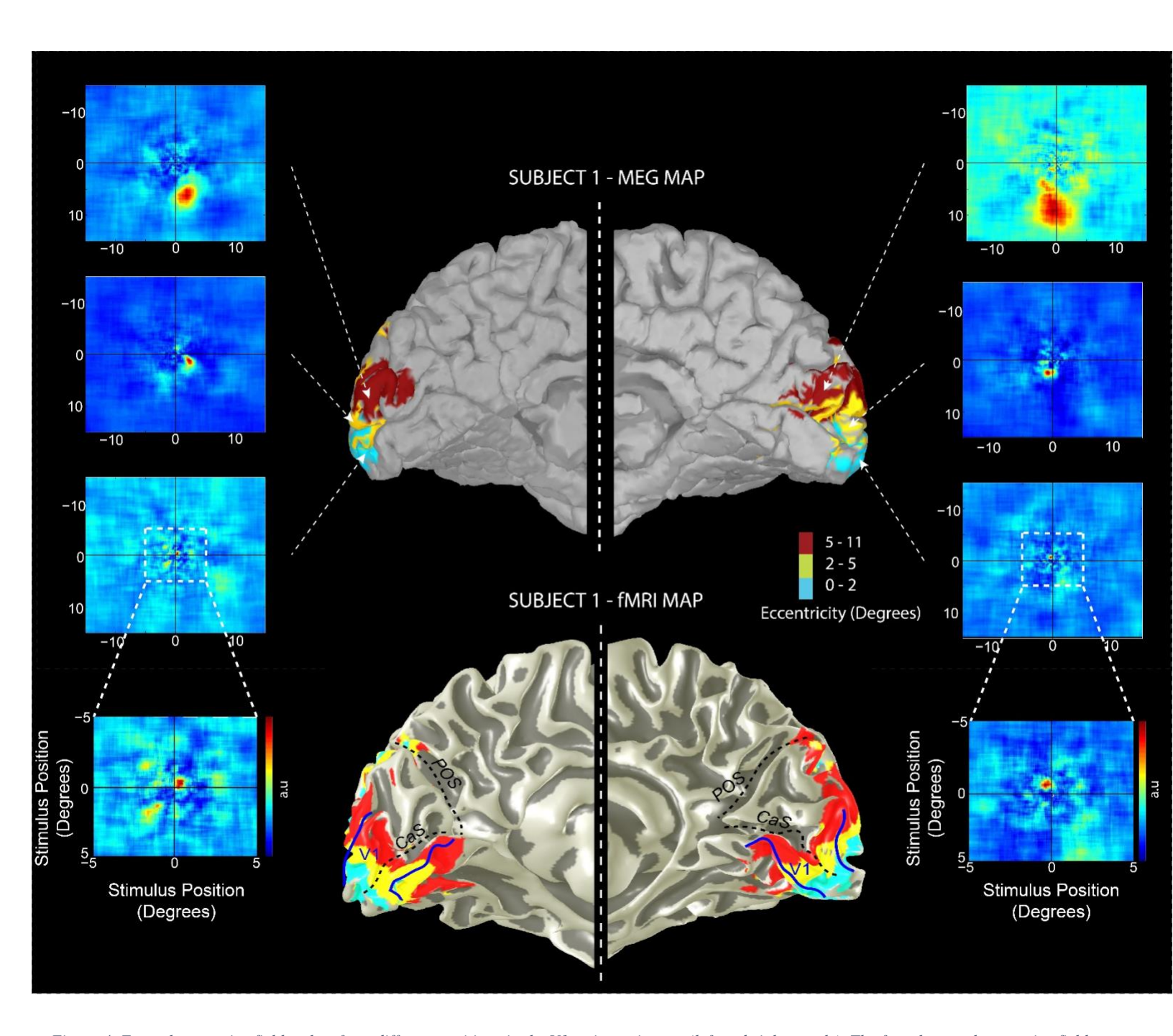


Figure 4. Example receptive fields taken from different positions in the V1 retinotopic map (left and right panels). The foveal example receptive fields are expanded for better visualization. Full retinotopic maps are shown for MEG (top) and fMRI (bottom) for subject 1. Only sources that formed a cluster of 3 or more sources and all of them demonstrated receptive fields are projected.

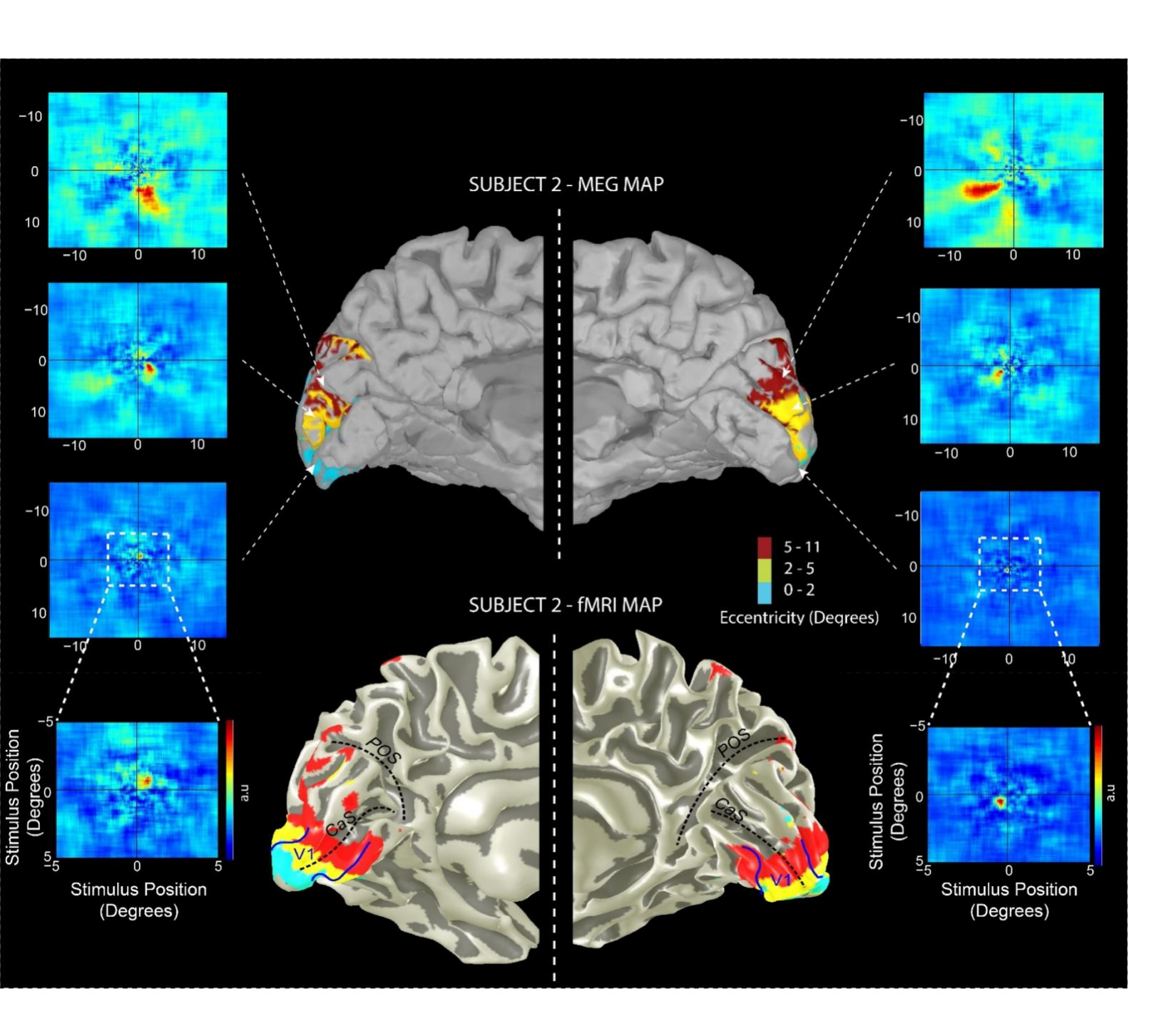


Figure 5. Same as Figure 4, but for subject 2

#### 2.4.3 Estimate of cortical magnification factor with MEG

In order to draw a more quantitative comparison between the maps obtained with MEG and those obtained with other methods, we computed the cortical magnification factor for V1 in each individual hemisphere, using the full 60 minutes of data for each experiment. Cortical magnification corresponds to the amount of cortical space devoted to a given portion of the retinal input: Notably, previous work has shown that the central visual field is represented by a larger area compared to periphery (Daniel and Whitteridge, 1961).

To quantify cortical magnification across the retinotopic maps recovered previously, we selected sources located on a line running along the upper lip of the calcarine sulcus for all 4 hemispheres of the two subjects (Engel et al., 1997). The line was chosen to sample the range of eccentricities shown in Figures 4 and 5.

Figure 6A plots the location of each receptive field as a function of the position of the corresponding source. Here position is referenced to a single source with a receptive field at an eccentricity of 5.8° (Engel et al., 1997 used 10°). Relative to more foveal sites, stimulation at 5.8° activates a small portion of the visual cortex, which facilitates more accurate alignment across subjects and across hemispheres.

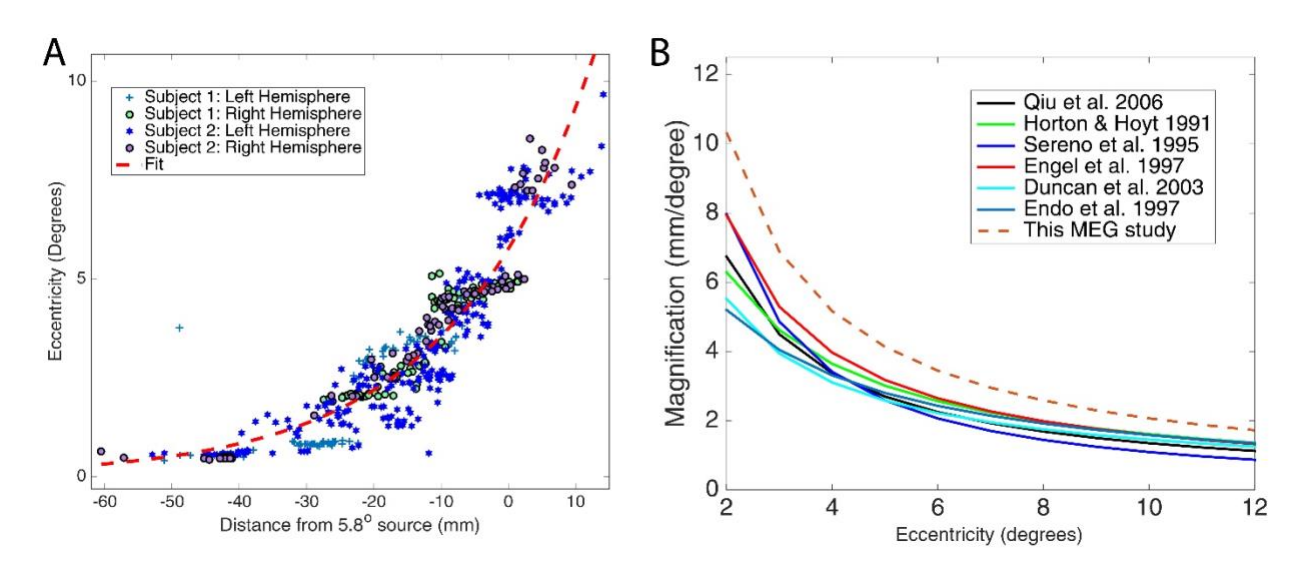


Figure 6. (A) Visual field eccentricity as a function of distance from the 5.80 source in VI for all 4 four hemispheres of the two subjects. The sources were selected from a line that runs along the upper lip of the calcarine sulcus. The different shapes and colors of the data points indicate the hemisphere to which they belong. The dashed red line represents the fit to the data. (B) Comparison of the cortical magnification factor among the present and previous studies.

Each point in Figure 6A corresponds to a source with a significant receptive field. Negative values on the x-axis correspond to sources located posterior to the 5.8° eccentricity point, and positive values indicate more anterior sources. The x-axis of the plot represents geodesic distances between the sources on the cortical surface.

The results indicate a consistent trend across hemispheres and across subjects. Near the posterior end of the occipital cortex (leftmost points in Figure 6A), changes in cortical location yield very small changes in the retinal location of the corresponding receptive fields; in other words, the central region of the retina is represented by a relatively large amount of cortical space, as reported with other methods (Duncan and Boynton, 2003; Endo et al., 1997; Engel et al., 1997; Horton JC and Hoyt WF, 1991; Qiu et al., 2006; Sereno et al., 1995). In contrast, sources located more anteriorly (rightmost points in Figure 6A) are associated with less cortical tissue; small changes in retinal position yield large changes in cortical position.

These trends can be captured parametrically by an exponential function that relates increases in retinal eccentricity distances on the cortical surface. To explore this relationship, we fit a function of the form:  $\theta = e^{c(d+d_0)}$  (6) (Engel et al., 1997), where  $\theta$  is the eccentricity of the receptive field for the source, d the cortical distance, and c and d<sub>0</sub> are parameters that scale and shift the exponential relationship. The mean values of the parameters obtained were:  $\theta = e^{0.04*(d+40.01)}$ . From these values we obtained the linear magnification factor, which has units of millimeters of cortex per degree of visual angle:  $M(\theta) = \left(\frac{1}{c}\right)\theta^{-1}$  (Qiu et al., 2006). From our data, the corresponding relationship is  $M(\theta) = 21.14\theta^{-1}$  mm/degree. These values are plotted in Figure 6B (Brown dashed line), along with analogous functions from previous studies.

The shape of *M* found from our data is similar, although with a clear upward shift with respect to that obtained with fMRI and PET(Duncan and Boynton, 2003; Engel et al., 1997; Horton JC and Hoyt WF, 1991; Qiu et al., 2006; Sereno et al., 1995).

#### 2.4.4 Comparison with fMRI

To compare the results that we obtained from the MEG analysis to those obtained in the same subjects with fMRI, we selected the same lines along the calcarine sulcus that were selected for creating Figure 6A for each of the 4 hemispheres. These are overlaid with the data points from the fMRI results in Figure 7. Only the data points for MEG sources with significant receptive fields were included on the plot. Overall the results indicate a close correspondence between the retinotopic organization obtained with MEG (red dots) and with fMRI (blue stars) in all hemispheres.

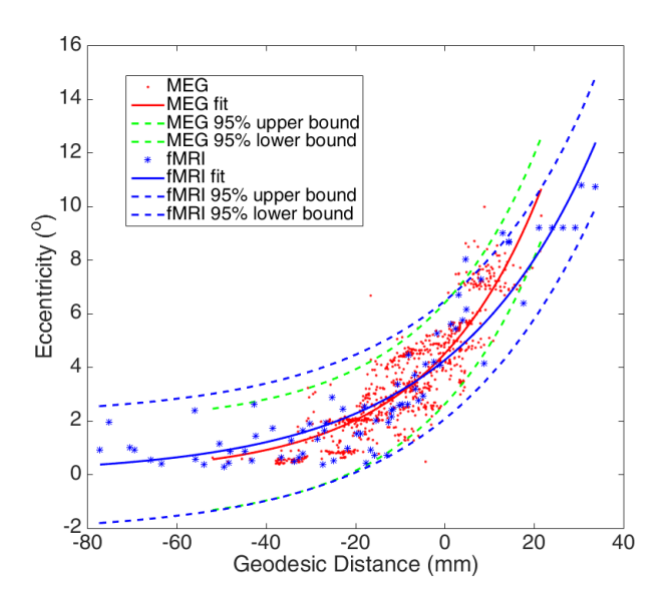


Figure 7. Comparison between MEG (red dots) and fMRI (blue stars) data for the 4 hemispheres. Data points were selected along linear regions of interest that run along the upper lip of the calcarine sulcus. The green and blue dashed lines correspond to the 95% significance bounds for MEG and fMRI exponential fits respectively.

#### 2.4.5 Spatial resolution of MEG

We used the pattern of visual responses and source locations described above to estimate the spatial resolution of MEG. Conceptually one can characterize spatial resolution as the minimum physical separation of sources that reliably yields different visual responses. Given the convoluted nature of the cortex, we expect this measure of resolution to differ depending on the position of each source relative to individual sulci and gyri. We therefore estimated spatial resolution separately for sources of different orientations. For this analysis, we considered all sources for which statistically significant receptive fields could be recovered (see Methods).

We developed a metric of correlation (SI; see Methods) that takes into account the responses of each source to each frame of the visual stimulus presentation. This metric takes values near 1.0 for sources that have identical responses across all stimuli to 0.5 for sources that respond completely independently. We estimated this correlation for all pairs of sources, combining data for sources separated by similar geodesic distances and relative orientations.

The pairwise value of this correlation is plotted in Figure 8A, as a function of geodesic proximity and relative orientation between sources. As expected, the responses of nearby sources with similar orientation are highly correlated, and this correlation decreases with increasing differences in spatial position or orientation. In the limit, the pairs of sources are nearly completely independent, as sources that are physically far apart respond to stimuli that are widely separated in retinal space.

We estimated the spatial resolution of MEG as the decay constant of an exponential fit to the correlation functions obtained in our data (see Methods and Figure 8A) (Adjusted R<sup>2</sup>: 0.68). The results show that for sources with the same orientation (i.e. cortical regions along a relatively flat region of a sulcus), responses can be reliably differentiated when they are separated by approximately 7.0 mm. For regions of greater curvature (i.e. near a gyrus), resolution can be considerably greater. The red line in Figure 8B indicates that the decay constant is reached at smaller physical separations for dipoles of increasing relative orientations. Assuming a maximum curvature of 1.5 mm<sup>-1</sup> that can be measured before reaching the noise level of the MRI measurement on an 1x1mm isotropic space (Pienaar et al., 2008), this calculation yielded a maximum MEG resolution of 0.49 mm (blue line). For regions with more modest curvature (green and yellow lines in Figure 8B), resolution was on the order of 2 to 4 mm.

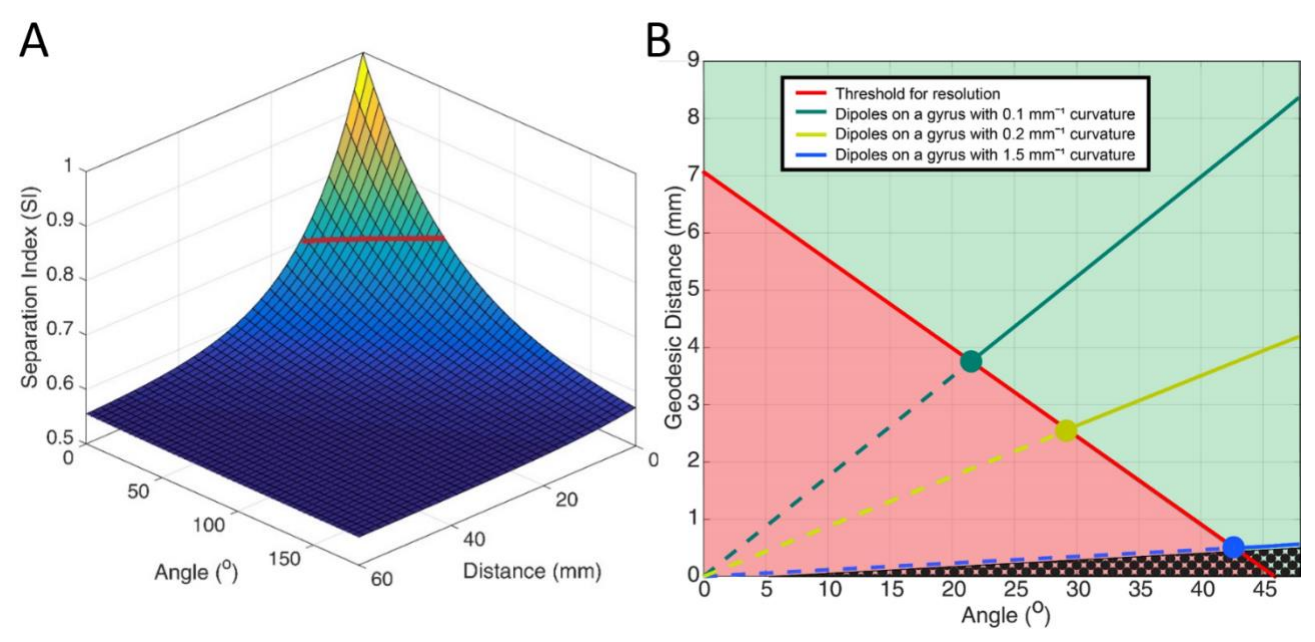


Figure 8. (A) 2-dimensional exponential fit of the separation index (SI) as a function of spatial separation and relative orientation of pairs of sources. The correlation decreases along both dimensions, and the decay constant (red line) is taken as a measure of resolution. (B) Different combinations of geodesic distance and relative orientation between sources influence the separability among responses. The red line represents the red line in figure 8A. The area marked in red represents the combinations that are beyond the resolution of MEG, and the green area the combinations that MEG can resolve. The dark patterned area represents observations that are within the noise level of the MRI tessellations. The other colored lines represent resolution for dipoles placed near gyri with different curvatures. The blue line shows the combinations on a gyrus with the maximum curvature typically found in human brains; this therefore represents the limit of MEG resolution.

Of course, any estimate of resolution will depend on various experimental and analytical choices. Although we did not explore these factors exhaustively, we performed one additional analysis to explore the influence of response threshold (see Methods). A lower threshold (2 standard deviations below the mean) admitted far more responses into our receptive field measurements, but lowered the resolution significantly, yielding values of 41.3mm and 105.0 degrees for the space and orientation constants. By comparison, a threshold of 4 standard deviations yielded a space constant of 3.6mm, and an orientation constant of 52.5 degrees. Although this resolution was slightly better than what we obtained with the 3 standard deviations threshold, it led us to reject 97% of the data that was used in the 3 std threshold condition. Thus the higher threshold might be warranted for experiments with rich data records, if extra resolution is necessary.

#### 2.5 Discussion

#### 2.5.1 Brief summary of results

In this study we have demonstrated the capacity of individual MEG sources to show selectivity for specific areas of the visual field. We showed that localized visual receptive fields for individual sources (Figure 3) can be obtained from modest amounts of data (Appendix 3), and that the ensembles of these receptive fields form orderly maps within the occipital lobe (Figures 4 and 5). These maps are well matched to those obtained with fMRI (Figure 7). Analysis of correlated responses between pairs of sources suggest a reliable resolution on the order of a few millimeters, with the precise number depending on local brain curvature (Figure 8).

#### **2.5.2** Comparison to previous work

The resolution of any imaging modality depends on a combination of the instrument and the analysis methods. For MEG, an important aspect of data analysis is the set of assumptions needed to reach a unique solution (Baillet et al., 2001; Hämäläinen and Ilmoniemi, 1994; Hämäläinen et al., 1993; Pascual-Marqui et al., 1994; Sarvas, 1987) to the electromagnetic inverse problem (Helmholtz, 1853). These require a method for modeling the source of MEG signals.

Traditionally, two approaches for modeling brain activity have been used: dipole methods, and imaging methods. Dipole methods make use of a small number of dipoles to explain the cortical activity in the simplest possible way. Although they achieve seemingly point-like localization, these models are restrictive, and an imaging method is preferred when the number of active regions cannot be predicted or large areas are activated (Benbadis et al., 2010; Darvas et al., 2004). An imaging method with distributed sources along the cortex is generally expected to provide coarse resolution due to the largely underdetermined character of the inverse problem: the model transforms the signals from a few hundred sensors to tens of thousands of sources on the cortex. Nevertheless, imaging methods provide a more realistic representation of the cortex and are more suitable to account for spatially extended cortical activations. When the activated areas are in close cortical proximity, the localization of the sources becomes problematic, resulting

in crosstalk between nearby sources (Liu et al., 2002). The minimum distance required to overcome this crosstalk provides one estimate of the spatial resolution of MEG.

Previous studies focused on the localization accuracy of MEG, which is the cortical distance between a "ground truth" cortical location, and the center of mass or peak of the MEG activation. The cortical points that are selected as the true origin of the activity are usually cortex locations that show increased activation in equivalent fMRI experiments (Moradi et al., 2003; Poghosyan and Ioannides, 2007; Sharon et al., 2007), locations that have been chosen in simulations (Liu et al., 2002), dipole localization in phantom studies (Leahy et al., 1998; Sutherling et al., 2001) or even dipoles that were placed inside a cadaver head (Barth et al., 1986).

Although previous MEG studies have examined the visual cortex, none to our knowledge has attempted to recover detailed retinotopic maps. Two previous studies demonstrated differentiation in response timing across entire visual areas(Cottereau et al., 2011; Hagler et al., 2009), while another study (Sharon et al., 2007) used several inverse methods to compare localization of fMRI and MEG+EEG from only 4 visual field stimuli positions. Cicmil et al. (2014) used 3 different inverse problems (MNE, Beamformers and Multiple Sparse Priors) with quadrant checkerboards and rings of 3 different eccentricities, and concluded that significant improvement could be achieved by using MNE on eccentricity stimuli confined to one visual field quadrant. Another study (Brookes et al., 2010) used a retinotopic experiment of 5 wedges and investigated the effect of data averaging from a retinotopic experiment on the spatial specificity of MEG. Moradi et al. (2003) compared MEG early activation with fMRI in V1 and achieved localization errors on the order of just 3-5 mm. Perry et al. (2011) used a rotating checkerboard stimulus and examined the elicited power at gamma frequencies, which did not yield a trajectory consistent with V1 anatomy. Poghosyan and Ioannides (2007) displayed circular checkerboards in 8 positions of the visual field and achieved localization in each visual cortex area to within 2mm of a simulated activation center.

Several previous MEG tonotopy studies have used sharp responses (namely the M100) for detecting selectivity (Cansino et al., 1994; Langner et al., 1997; Pantev et al., 1988, 1994, 1995). It would be interesting to use the method described in this paper to retrieve the tonotopic organization of the auditory cortex.

#### 2.5.3 Limitations of current results

The method for computing the receptive fields that was described in this paper led to the creation of retinotopic maps that follow the known retinotopic organization of the primary visual cortex, on the upper lip of the calcarine sulcus. However, this technique was unable to capture many sources with significant receptive fields in the upper visual field (see Appendix 4 and 5); these are located below the calcarine sulcus. One reason for this might be the fact that every stimulus frame was comprised of several squares that were projected onto both the upper and lower visual field. Since it has been reported (Fylan et al., 1997; Perry et al., 2011; Poghosyan and Ioannides, 2007; Portin and Hari, 1999) that the signals from upper visual field stimulation are weaker than those from the lower visual field, it might be that their event related responses were not strong enough to cross the amplitude threshold.

A second limitation is that our retinotopic maps detected few significant receptive fields inside the sulci. This becomes evident when we project the maps onto an inflated cortex (Appendix 6). This leads to the appearance of discontinuities on the gradient of the eccentricity map for both subjects. These results are consistent with previous work showing reduced signal strength for sources located inside sulci (Goldenholz et al., 2009). Consistent with this idea, we found in pilot studies that the ratios of the peak z-scored signal fluctuations relative to pre-stimulus baseline (Appendices 1-3) were higher in the upper lip of the calcarine sulcus (1.18) than in the lower lip (1.05) or the inside the sulcus (1.00). Since the method for estimating receptive fields is solely based on amplitude thresholding, the lack of significant results in the upper visual field is likely due to relatively poorer signal strength in the corresponding cortical space.

Another limitation was that significant receptive fields were mostly recovered in the primary visual cortex, and our attempts to recover retinotopic maps in extrastriate areas were less successful. We also did not detect the borders between areas V1, V2, and V3 that typically appear as inversions of the angle of visual field selectivity (Dougherty et al., 2003; Sereno et al., 1995; Wandell et al., 2007). One possible explanation is that we filtered our data (Figure 2) at frequencies specifically chosen to optimize V1 responses. This filtering might have been optimal for capturing large signal fluctuations on V1 sources but not necessarily for others. Similarly, we optimized our stimuli based on estimates of receptive field sizes in early visual areas (Freeman and Simoncelli,

2011). Presumably, for any visual area, using larger stimuli would yield poorer resolution, while smaller stimuli would yield weaker responses, although we have not explored this trade-off experimentally.

# **2.5.4** MEG usage is beneficial in areas were the fMRI signal gets distorted due to large blood vessels

The fMRI signal can be affected by the presence of large blood vessels in certain areas due to the inflow effect (Gao and Liu, 2012). Consequently retinotopic maps in our fMRI experiment had small patches in which the signal could not be resolved reliably. Those areas were located on the most posterior part of the cortex for both subjects. Nearby voxels showed selectivity for stimuli presented at eccentricities less than one degree, suggesting that the missing patches also represented the central part of the visual field. Because MEG measures neuronal activity directly, it is not perturbed by large vessels, and thus we were able to resolve cortical activity in these regions (Figures 4 and 5). This suggests that MEG can provide information that is complementary to that obtained with fMRI.

#### 2.5.5 Resolution

Our results show that the resolution is affected by both the distance and relative orientation among sources (Figure 8). Thus we expect spatial resolution to be quite different for sources located around gyri, within the sulci (see above), and in flatter areas. Given optimal brain curvature and sensory stimulation, MEG can detect differential selectivity between sources that are physically very close. However, for flatter regions of cortex, the resolution is likely to be substantially worse than that of fMRI. Therefore smoothing of the retinotopic maps obtained with MEG is helpful for comparing between the two modalities.

Findings of differential selectivity for sources in very close proximity have been reported recently (Cichy et al., 2015), in a study in which the authors investigated the ability of MEG to discriminate between distributed simulated patterns of cortical activity differing on the macro-

column scale. Moreover, a recent study investigated the ability to differentiate cortical laminae with the use of different MEG models and a head-cast for minimizing head-movements (Troebinger et al., 2014). Therefore, a combination of an appropriate model at the appropriate cortical geometry can yield surprisingly good results.

Importantly, any estimate of MEG resolution will be influenced by the forward and inverse modeling required to transform the signals from the sensor level to the source level. Continuous head position recordings or even the usage of a head-casket or bite-bars is expected to improve the co-registration with the head-points and therefore the quality of the data recorded. Our results regarding the effect of dipole orientation on resolution highlight the importance of using each subject's fMRI data to place the dipoles. If the anatomy used is based on an atlas, it is expected that the sources' placements will not be ideal and therefore the localization will be affected.

Although we used standard Brainstorm parameters in our modeling, other choices would likely have led to different conclusions about the level of crosstalk and point spread (Liu et al., 2002) shared by nearby sources. Similarly, our conclusions about resolution were determined by the assumption that the dipoles orientations were normal to the cortical surface and followed cortical curvature along the gyri and sulci. Moreover, the analysis that was performed in this study, reflects the resolution that can be achieved with a specific selection of methods; namely, the threshold applied to the signal amplitude and the stimulus that was projected.

#### 2.5.6 Conclusion

MEG has traditionally been used in applications requiring excellent temporal resolution. However, its spatial resolution is most often considered to be coarse. We have shown that MEG can recover retinotopic maps with similar shape to those obtained with fMRI, and in some areas with comparable spatial resolution.

## 2.6 Acknowledgements

We would like to thank Elizabeth Bock for MEG training and help in data acquisition, François Tadel for valuable suggestions in using Brainstorm and Drs. Matthew Krause and Theodore Zanos for their comments on the data analysis and Dr. Reza Farivar-Mohseni for his help with fMRI surface rendering. This work was funded by a Molson Neuro-Engineering and a Gerry Sklavounos - MNA Laurier-Dorion Scholarship to K.N., and by a grant from NSERC (341534-12) to C.C.P. S.B. was supported by the Killam Foundation, a Senior-Researcher grant from the Fonds de Recherche du Québec - Santé, a Discovery Grant from the National Science and Engineering Research Council of Canada and the NIH (2R01EB009048-05).

#### 2.7 References

Aine, C.J., and Stephen, J.M. (2003). Chapter 5 - MEG Studies of Visual Processing. In The Cognitive Electrophysiology of Mind and Brain, A.Z.M.P.I. Posner, ed. (San Diego: Academic Press), pp. 93–142.

Baillet, S., Mosher, J.C., and Leahy, R.M. (2001). Electromagnetic brain mapping. IEEE Signal Process. Mag. 18, 14–30.

Barth, D.S., Sutherling, W., Broffman, J., and Beatty, J. (1986). Magnetic localization of a dipolar current source implanted in a sphere and a human cranium. Electroencephalogr. Clin. Neurophysiol. 63, 260–273.

Benbadis, S.R., Beran, R.G., Berg, A.T., Jr, J.E., Galanopoulou, A.S., Kaplan, P.W., Koutroumanidis, M., Moshe, S.L., Jr, D.R.N., Serratosa, J.M., et al. (2010). Atlas of Epilepsies (Springer Science & Business Media).

de Boer, R., and Kuyper, P. (1968). Triggered correlation. IEEE Trans. Biomed. Eng. 15, 169–179.

Brainard, D.H. (1997). The Psychophysics Toolbox. Spat. Vis. 10, 433–436.

Brookes, M.J., Zumer, J.M., Stevenson, C.M., Hale, J.R., Barnes, G.R., Vrba, J., and Morris, P.G. (2010). Investigating spatial specificity and data averaging in MEG. NeuroImage 49, 525–538.

Burkhalter, A., and Essen, D.V. (1986). Processing of color, form and disparity information in visual areas VP and V2 of ventral extrastriate cortex in the macaque monkey. J. Neurosci. 6, 2327–2351.

Cansino, S., Williamson, S.J., and Karron, D. (1994). Tonotopic organization of human auditory association cortex. Brain Res. 663, 38–50.

Cichy, R.M., Ramirez, F.M., and Pantazis, D. (2015). Can visual information encoded in cortical columns be decoded from magnetoencephalography data in humans? NeuroImage 121, 193–204.

Cicmil, N., Bridge, H., Parker, A.J., Woolrich, M.W., and Krug, K. (2014). Localization of MEG human brain responses to retinotopic visual stimuli with contrasting source reconstruction approaches. Brain Imaging Methods 8, 127.

Clavagnier, S., Dumoulin, S.O., and Hess, R.F. (2015). Is the Cortical Deficit in Amblyopia Due to Reduced Cortical Magnification, Loss of Neural Resolution, or Neural Disorganization? J. Neurosci. 35, 14740–14755.

Cottereau, B., Lorenceau, J., Gramfort, A., Clerc, M., Thirion, B., and Baillet, S. (2011). Phase delays within visual cortex shape the response to steady-state visual stimulation. NeuroImage 54, 1919–1929.

Dale, A.M., and Sereno, M.I. (1993). Improved Localizadon of Cortical Activity by Combining EEG and MEG with MRI Cortical Surface Reconstruction: A Linear Approach. J. Cogn. Neurosci. 5, 162–176.

Dale, A.M., Fischl, B., and Sereno, M.I. (1999). Cortical Surface-Based Analysis: I. Segmentation and Surface Reconstruction. NeuroImage 9, 179–194.

Daniel, P.M., and Whitteridge, D. (1961). The representation of the visual field on the cerebral cortex in monkeys. J. Physiol. 159, 203–221.

Darvas, F., Pantazis, D., Kucukaltun-Yildirim, E., and Leahy, R.M. (2004). Mapping human brain function with MEG and EEG: methods and validation. NeuroImage 23, Supplement 1, S289–S299.

Das, A., and Gilbert, C.D. (1995). Long-range horizontal connections and their role in cortical reorganization revealed by optical recording of cat primary visual cortex. Nature 375, 780–784.

DeAngelis, G.C., Ohzawa, I., and Freeman, R.D. (1995). Receptive-field dynamics in the central visual pathways. Trends Neurosci. 18, 451–458.

Dijkstra, E.W. (1959). A Note on Two Problems in Connexion with Graphs. Numer Math 1, 269–271.

DoCarmo, M. (1976). Differential Geometry of Curves and Surfaces (Englewood Cliffs, N.J: Pearson).

Dougherty, R.F., Koch, V.M., Brewer, A.A., Fischer, B., Modersitzki, J., and Wandell, B.A. (2003). Visual field representations and locations of visual areas V1/2/3 in human visual cortex. J. Vis. 3, 586–598.

Dumoulin, S.O., and Wandell, B.A. (2008). Population receptive field estimates in human visual cortex. NeuroImage 39, 647–660.

Duncan, R.O., and Boynton, G.M. (2003). Cortical Magnification within Human Primary Visual Cortex Correlates with Acuity Thresholds. Neuron 38, 659–671.

Endo, S., Toyama, H., Kimura, Y., Ishii, K., Senda, M., Kiyosawa, M., and Uchiyama, A. (1997). Mapping visual field with positron emission tomography by mathematical modeling of the retinotopic organization in the calcarine cortex. IEEE Trans. Med. Imaging 16, 252–260.

Engel, S.A., Glover, G.H., and Wandell, B.A. (1997). Retinotopic organization in human visual cortex and the spatial precision of functional MRI. Cereb. Cortex 7, 181–192.

Felleman, D.J., and Essen, D.C.V. (1987). Receptive field properties of neurons in area V3 of macaque monkey extrastriate cortex. J. Neurophysiol. 57, 889–920.

Fischl, B., Sereno, M.I., and Dale, A.M. (1999). Cortical Surface-Based Analysis: II: Inflation, Flattening, and a Surface-Based Coordinate System. NeuroImage 9, 195–207.

Fischl, B., Liu, A., and Dale, A.M. (2001). Automated manifold surgery: constructing geometrically accurate and topologically correct models of the human cerebral cortex. IEEE Trans. Med. Imaging 20, 70–80.

Fox, P.T., Miezin, F.M., Allman, J.M., Essen, D.V., and Raichle, M.E. (1987). Retinotopic organization of human visual cortex mapped with positron-emission tomography. J. Neurosci. 7, 913–922.

Fylan, F., Holliday, I.E., Singh, K.D., Anderson, S.J., and Harding, G.F.A. (1997). Magnetoencephalographic Investigation of Human Cortical Area V1 Using Color Stimuli. NeuroImage 6, 47–57.

Gao, J.-H., and Liu, H.-L. (2012). Inflow effects on functional MRI. NeuroImage 62, 1035–1039.

Gattass, R., Sousa, A.P.B., and Rosa, M.G.P. (1987). Visual topography of V1 in the Cebus monkey. J. Comp. Neurol. 259, 529–548.

Goldenholz, D.M., Ahlfors, S.P., Hämäläinen, M.S., Sharon, D., Ishitobi, M., Vaina, L.M., and Stufflebeam, S.M. (2009). Mapping the signal-to-noise-ratios of cortical sources in magnetoencephalography and electroencephalography. Hum. Brain Mapp. 30, 1077–1086.

Gross, J., Baillet, S., Barnes, G.R., Henson, R.N., Hillebrand, A., Jensen, O., Jerbi, K., Litvak, V., Maess, B., Oostenveld, R., et al. (2013). Good practice for conducting and reporting MEG research. NeuroImage 65, 349–363.

Hagler, D.J., Halgren, E., Martinez, A., Huang, M., Hillyard, S.A., and Dale, A.M. (2009). Source estimates for MEG/EEG visual evoked responses constrained by multiple, retinotopically-mapped stimulus locations. Hum. Brain Mapp. 30, 1290–1309.

Hämäläinen, M.S., and Ilmoniemi, R.J. (1994). Interpreting magnetic fields of the brain: minimum norm estimates. Med. Biol. Eng. Comput. 32, 35–42.

Hämäläinen, M., Hari, R., Ilmoniemi, R.J., Knuutila, J., and Lounasmaa, O.V. (1993). Magnetoencephalography\char22{}theory, instrumentation, and applications to noninvasive studies of the working human brain. Rev. Mod. Phys. 65, 413–497.

Helmholtz, H. (1853). Ueber einige Gesetze der Vertheilung elektrischer Ströme in körperlichen Leitern mit Anwendung auf die thierisch-elektrischen Versuche. Ann. Phys. 165, 211–233.

Holmes, G. (1945). Ferrier Lecture: The Organization of the Visual Cortex in Man. Proc. R. Soc. Lond. B Biol. Sci. 132, 348–361.

Horton JC, and Hoyt WF (1991). The representation of the visual field in human striate cortex: A revision of the classic holmes map. Arch. Ophthalmol. 109, 816–824.

Huang, M.X., Mosher, J.C., and Leahy, R.M. (1999). A sensor-weighted overlapping-sphere head model and exhaustive head model comparison for MEG. Phys. Med. Biol. 44, 423.

Hubel, D.H., and Wiesel, T.N. (1977). Ferrier Lecture: Functional Architecture of Macaque Monkey Visual Cortex. Proc. R. Soc. Lond. B Biol. Sci. 198, 1–59.

Hwang, J.-N., Lay, S.-R., and Lippman, A. (1994). Nonparametric multivariate density estimation: a comparative study. IEEE Trans. Signal Process. 42, 2795–2810.

Kaoru Seki, N.N. (1996). Neuromagnetic evidence that the P100 component of the pattern reversal visual evoked response originates in the bottom of the calcarine fissure. Electroencephalogr. Clin. Neurophysiol. 100, 436–442.

Langner, G., Sams, M., Heil, P., and Schulze, H. (1997). Frequency and periodicity are represented in orthogonal maps in the human auditory cortex: evidence from magnetoencephalography. J. Comp. Physiol. A 181, 665–676.

Leahy, R.M., Mosher, J.C., Spencer, M.E., Huang, M.X., Lewine, J.D., Leahy, R.M., and D, P. (1998). A study of dipole localization accuracy for MEG and EEG using a human skull phantom.

Lin, F.-H., Witzel, T., Ahlfors, S.P., Stufflebeam, S.M., Belliveau, J.W., and Hämäläinen, M.S. (2006). Assessing and improving the spatial accuracy in MEG source localization by depth-weighted minimum-norm estimates. NeuroImage 31, 160–171.

Liu, A.K., Dale, A.M., and Belliveau, J.W. (2002). Monte Carlo simulation studies of EEG and MEG localization accuracy. Hum. Brain Mapp. 16, 47–62.

Livingstone, M.S., Pack, C.C., and Born, R.T. (2001). Two-Dimensional Substructure of MT Receptive Fields. Neuron 30, 781–793.

Marmarelis, P.Z., and Marmarelis, V.Z. (1978). The White-Noise Method in System Identification. In Analysis of Physiological Systems, (Springer US), pp. 131–180.

Mineault, P.J., Zanos, T.P., and Pack, C.C. (2013). Local field potentials reflect multiple spatial scales in V4. Front. Comput. Neurosci. 7, 21.

Moradi, F., Liu, L.C., Cheng, K., Waggoner, R.A., Tanaka, K., and Ioannides, A.A. (2003). Consistent and precise localization of brain activity in human primary visual cortex by MEG and fMRI. NeuroImage 18, 595–609.

Nakamura, M., Kakigi, R., Okusa, T., Hoshiyama, M., and Watanabe, K. (2000). Effects of check size on pattern reversal visual evoked magnetic field and potential. Brain Res. 872, 77–86.

Okada, Y.C., Lahteenmäki, A., and Xu, C. (1999). Experimental analysis of distortion of magnetoencephalography signals by the skull. Clin. Neurophysiol. 110, 230–238.

Pack, C.C., Conway, B.R., Born, R.T., and Livingstone, M.S. (2006). Spatiotemporal Structure of Nonlinear Subunits in Macaque Visual Cortex. J. Neurosci. 26, 893–907.

Pantev, C., Hoke, M., Lehnertz, K., Lütkenhöner, B., Anogianakis, G., and Wittkowski, W. (1988). Tonotopic organization of the human auditory cortex revealed by transient auditory evoked magnetic fields. Electroencephalogr. Clin. Neurophysiol. 69, 160–170.

Pantev, C., Eulitz, C., Elbert, T., and Hoke, M. (1994). The auditory evoked sustained field: origin and frequency dependence. Electroencephalogr. Clin. Neurophysiol. 90, 82–90.

Pantev, C., Bertrand, O., Eulitz, C., Verkindt, C., Hampson, S., Schuierer, G., and Elbert, T. (1995). Specific tonotopic organizations of different areas of the human auditory cortex revealed by simultaneous magnetic and electric recordings. Electroencephalogr. Clin. Neurophysiol. 94, 26–40.

Pascual-Marqui, R.D., Michel, C.M., and Lehmann, D. (1994). Low resolution electromagnetic tomography: a new method for localizing electrical activity in the brain. Int. J. Psychophysiol. 18, 49–65.

Pelli, D.G. (1997). The VideoToolbox software for visual psychophysics: transforming numbers into movies. Spat. Vis. 10, 437–442.

Perry, G., Adjamian, P., Thai, N.J., Holliday, I.E., Hillebrand, A., and Barnes, G.R. (2011). Retinotopic mapping of the primary visual cortex – a challenge for MEG imaging of the human cortex. Eur. J. Neurosci. 34, 652–661.

Pienaar, R., FISCHL, B., CAVINESS, V., MAKRIS, N., and GRANT, P.E. (2008). A methodology for analyzing curvature in the developing brain from preterm to adult. Int. J. Imaging Syst. Technol. 18, 42–68.

Poghosyan, V., and Ioannides, A.A. (2007). Precise mapping of early visual responses in space and time. NeuroImage 35, 759–770.

Portin, K., and Hari, R. (1999). Human parieto-occipital visual cortex: lack of retinotopy and foveal magnification. Proc. R. Soc. B Biol. Sci. 266, 981–985.

Qiu, A., Rosenau, B.J., Greenberg, A.S., Hurdal, M.K., Barta, P., Yantis, S., and Miller, M.I. (2006). Estimating linear cortical magnification in human primary visual cortex via dynamic programming. NeuroImage 31, 125–138.

R Gattass, C.G.G. (1981). Visual topography of V2 in the Macaque. J. Comp. Neurol. 201, 519–539.

Ringach, D., and Shapley, R. (2004). Reverse correlation in neurophysiology. Cogn. Sci. 28, 147–166.

Sarvas, J. (1987). Basic mathematical and electromagnetic concepts of the biomagnetic inverse problem. Phys. Med. Biol. 32, 11.

Sereno, M.I., Dale, A.M., Reppas, J.B., Kwong, K.K., Belliveau, J.W., Brady, T.J., Rosen, B.R., and Tootell, R.B. (1995). Borders of multiple visual areas in humans revealed by functional magnetic resonance imaging. Science 268, 889–893.

Sethian, J.A. (1996). A fast marching level set method for monotonically advancing fronts. Proc. Natl. Acad. Sci. U. S. A. 93, 1591–1595.

Sharon, D., Hämäläinen, M.S., Tootell, R.B.H., Halgren, E., and Belliveau, J.W. (2007). The advantage of combining MEG and EEG: Comparison to fMRI in focally stimulated visual cortex. NeuroImage 36, 1225–1235.

Smith, A.T., Singh, K.D., Williams, A.L., and Greenlee, M.W. (2001). Estimating Receptive Field Size from fMRI Data in Human Striate and Extrastriate Visual Cortex. Cereb. Cortex 11, 1182–1190.

Stephen, J.M., Aine, C.J., Christner, R.F., Ranken, D., Huang, M., and Best, E. (2002). Central versus peripheral visual field stimulation results in timing differences in dorsal stream sources as measured with MEG. Vision Res. 42, 3059–3074.

Sutherling, W.W., Akhtari, M., Mamelak, A.N., Mosher, J., Arthur, D., Sands, S., Weiss, P., Lopez, N., DiMauro, M., Flynn, E., et al. (2001). Dipole localization of human induced focal afterdischarge seizure in simultaneous magnetoencephalography and electrocorticography. Brain Topogr. 14, 101–116.

Tadel, F., Baillet, S., Mosher, J.C., Pantazis, D., and Leahy, R.M. (2011). Brainstorm: A User-Friendly Application for MEG/EEG Analysis, Brainstorm: A User-Friendly Application for MEG/EEG Analysis. Comput. Intell. Neurosci. Comput. Intell. Neurosci. 2011, 2011, e879716.

Tesche, C.D., Uusitalo, M.A., Ilmoniemi, R.J., Huotilainen, M., Kajola, M., and Salonen, O. (1995). Signal-space projections of MEG data characterize both distributed and well-localized neuronal sources. Electroencephalogr. Clin. Neurophysiol. 95, 189–200.

Troebinger, L., López, J.D., Lutti, A., Bestmann, S., and Barnes, G. (2014). Discrimination of cortical laminae using MEG. NeuroImage 102, Part 2, 885–893.

*Uusitalo, M.A., and Ilmoniemi, R.J. (1997). Signal-space projection method for separating MEG or EEG into components. Med. Biol. Eng. Comput. 35, 135–140.* 

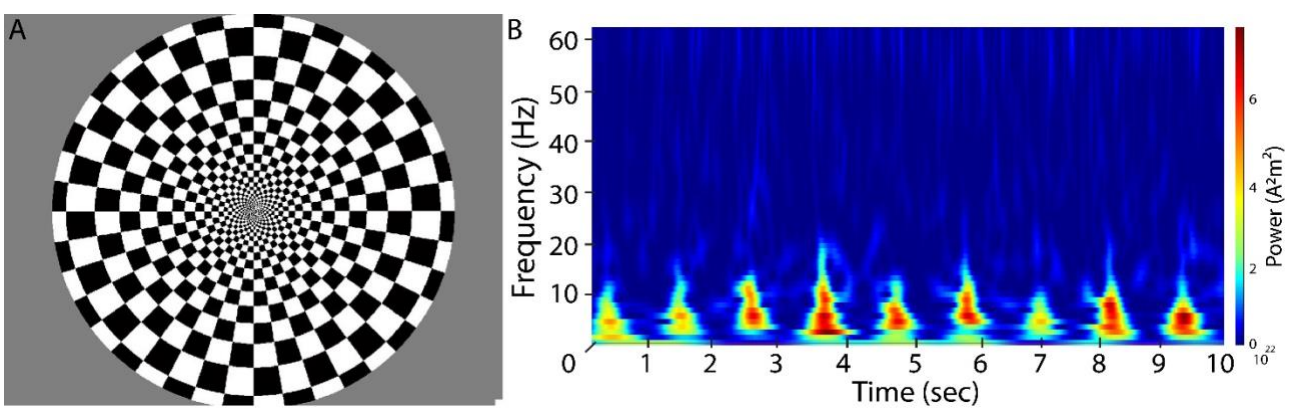
Van Essen, D.C., Newsome, W.T., and Maunsell, J.H.R. (1984). The visual field representation in striate cortex of the macaque monkey: Asymmetries, anisotropies, and individual variability. Vision Res. 24, 429–448.

Wandell, B.A., Dumoulin, S.O., and Brewer, A.A. (2007). Visual field maps in human cortex. Neuron 56, 366–383.

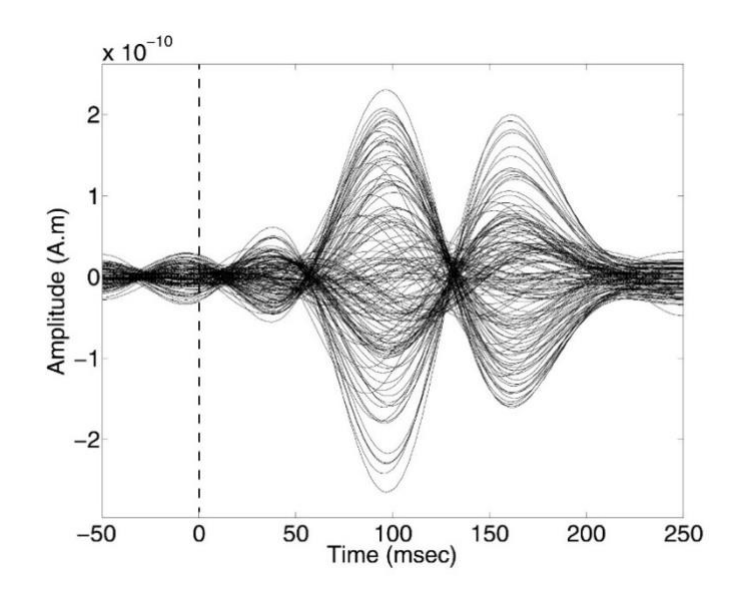
White, B.R., and Culver, J.P. (2010). Phase-encoded retinotopy as an evaluation of diffuse optical neuroimaging. NeuroImage 49, 568–577.

Zeki, S.M. (1978). Uniformity and diversity of structure and function in rhesus monkey prestriate visual cortex. J. Physiol. 277, 273–290.

# 2.8 Supplementary Figures - Appendix



Appendix 1. (A) Stimulus that was used in a pilot experiment to elicit visually responses. The subjects maintained fixation at a dot located at the center of the screen, and the stimulus appeared for 100 ms every second. (B) Time-frequency decomposition of the signal from a VI source during the pilot experiment. There is increased power in the 1-12Hz band.

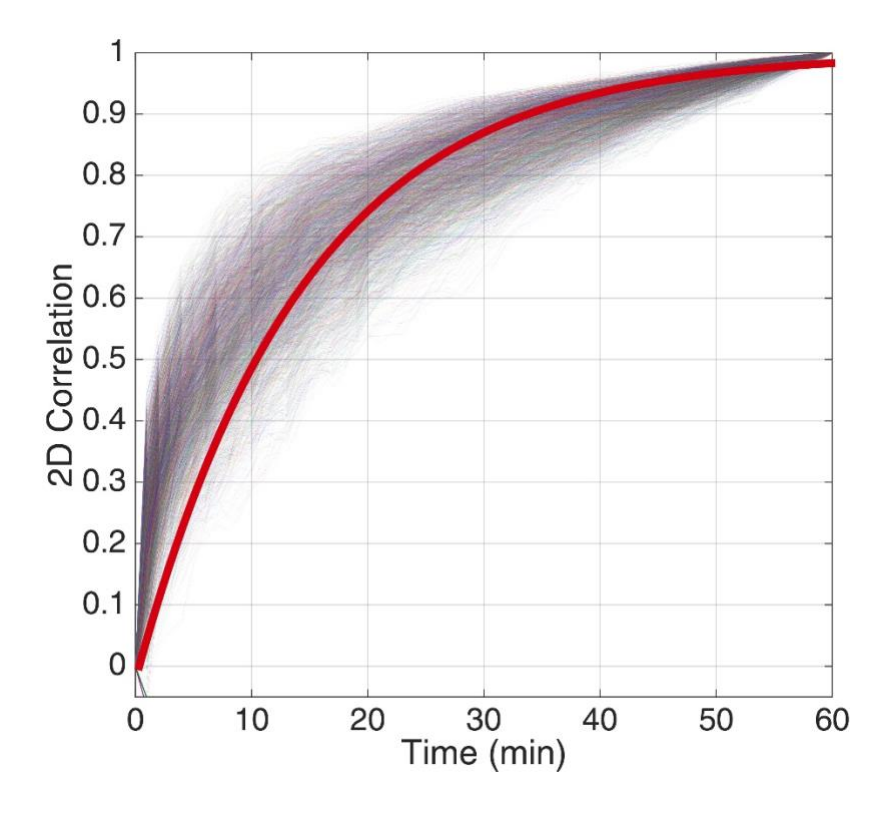


Appendix 2. Overlap of all VI responses from 259 averaged trials. The figure demonstrates the averaged responses of the filtered signals of all VI sources located in the left hemisphere of one subject. The responses elicited by the stimulus are bimodal.

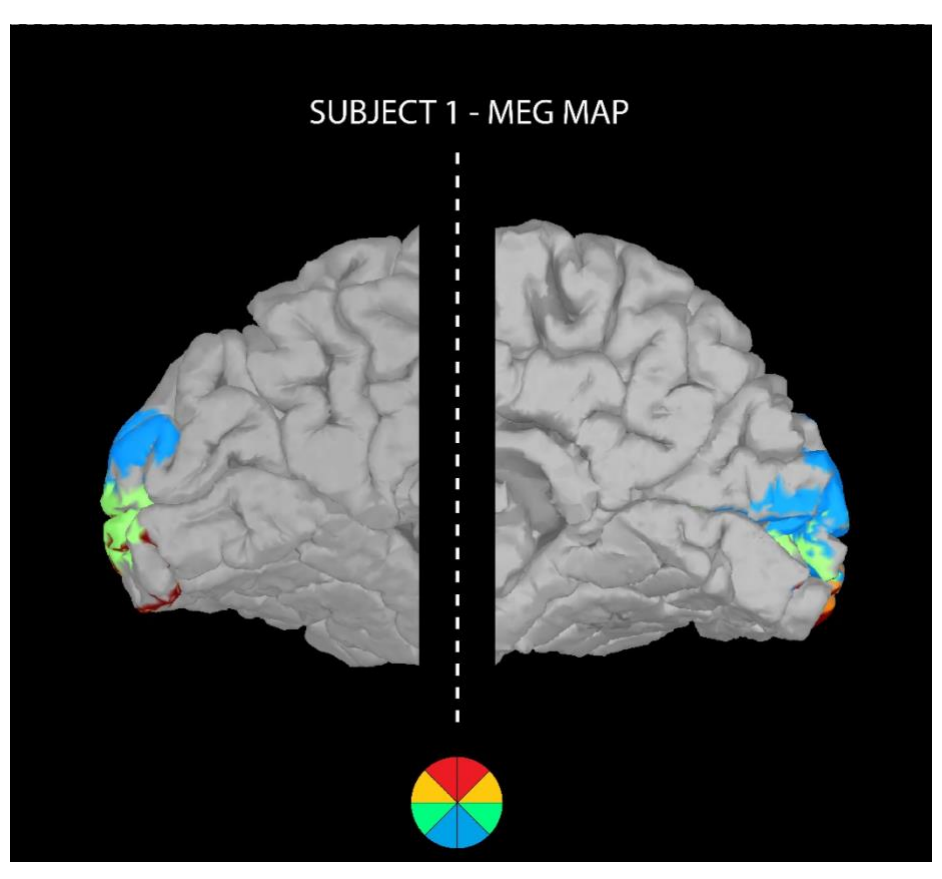
## 2.8.1 Efficiency of receptive field estimation with MEG

The receptive field shown in Figure 3 is the result of averaging responses over the full data record, which lasted for 60 minutes. To determine retrospectively if similar results could have been obtained with a shorter experimental duration, we estimated receptive fields from shorter segments of data, using 2,859 statistically significant receptive fields (see Methods) recovered from the primary visual cortex from both hemispheres of the two subjects.

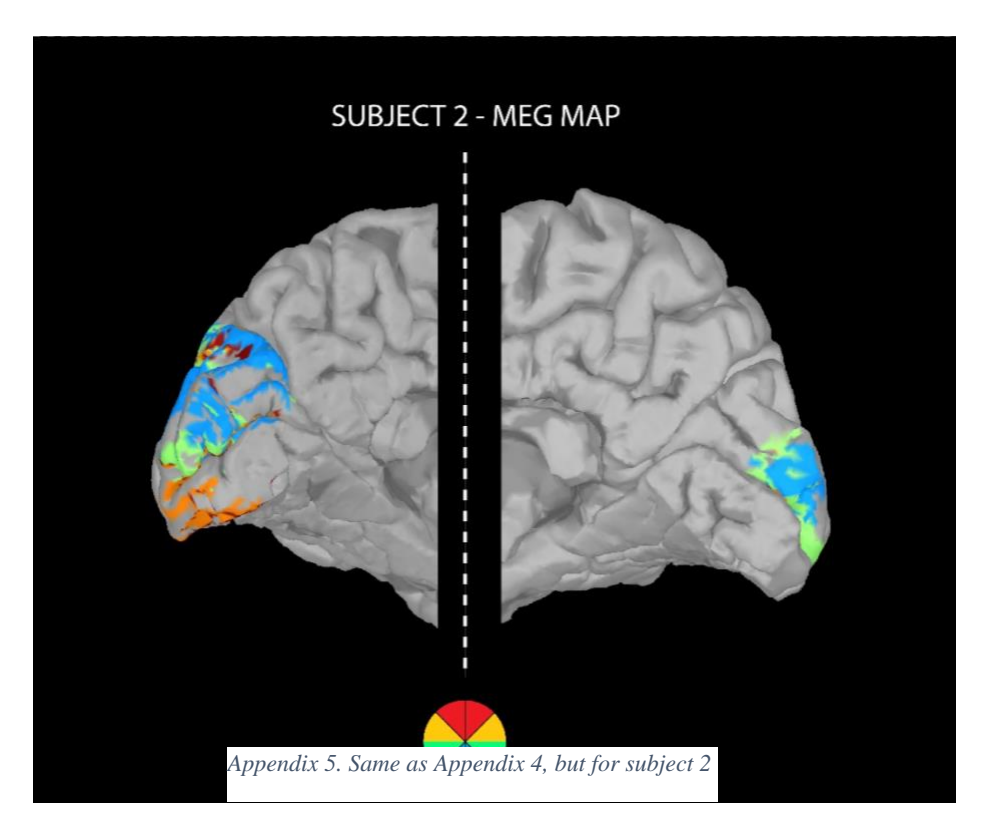
Appendix 3 shows the average 2-D correlation between the receptive fields calculated from the full experimental data and those obtained from data over increasing durations. After fitting an exponential function to this statistics, we obtained a mean time constant of  $14.6 \pm 2.9$  minutes (adjusted  $r^2$ =0.9276) to retrieve receptive fields that were similar to those obtained with the full 60-minute data set.

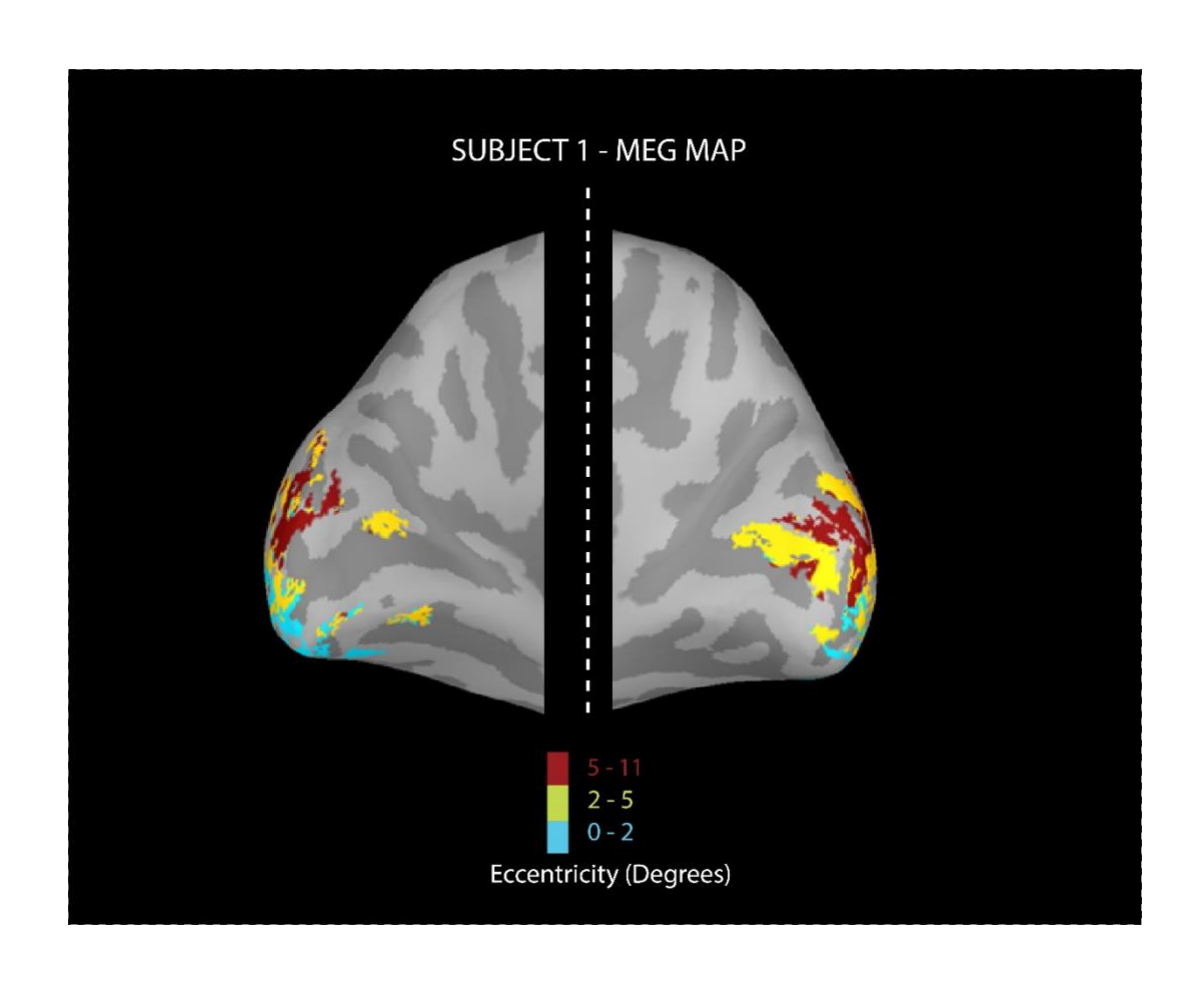


Appendix 3 Time-course of receptive field estimation relative to the final receptive field for every minute of the experiment. Each data-point represents the 2D correlation of the receptive field of each source, calculated based on data recorded up to that time point, with the source's final receptive field calculated from the full data record. The red line represents the fit on the data points. Each faded line corresponds to the 2d correlation of the receptive field of a single source.



Appendix 4. Angle retinotopic map of Subject 1. The receptive fields were binned based on their angle. The color assigned is relative to the position of the center of the receptive field on the visual field.





Appendix 6. The same retinotopic map as the one computed in Figure 5 but now projected on an inflated cortex. Dark grey areas represent the sulci. The blue, yellow and red colored sources represent eccentricities of 0-2, 2-5, 5-11 respectively. The calculation for the receptive fields was performed only for the sources located posteriorly to the parieto-occipital sulcus. Only sources with significant receptive fields are projected. Most of the sources that are located inside the sulci do not demonstrate significant receptive fields.

# Chapter 3 - Transient shifting of attentional encoding measured with magnetoencephalography

Konstantinos Nasiotis<sup>a</sup>,\*, Sujaya Neupane<sup>b</sup>, Shahab Bakhtiari<sup>c</sup>, Sylvain Baillet<sup>a</sup>, and Christopher C. Pack<sup>a</sup>,\*

<sup>a</sup> Montreal Neurological Institute, 3801 University Street, Montreal, H3A 2B4, QC, Canada

<sup>b</sup> McGovern Institute for Brain Science, 43 Vassar St., Cambridge, MA 02139, USA

<sup>c</sup> Mila, 6666 St. Urbain St., Montreal, H2S3H1, QC, Canada

\*Correspondence: konstantinos.nasiotis@mail.mcgill.ca, christopher.pack@mcgill.ca.

# 3.1 Abstract

Visual neurons encode information about our environment through hardwired connections to the retina that get established during early development. These connections create a neural mapping of the visual field to the cortical surface. However, it has been shown that the functional encoding of the visual space changes around the timing of eye-movements (saccades). This phenomenon has been termed visual remapping and has been approached by researchers with two separate schools of thought: some studies considered remapping as a compensating mechanism that contributes to visual stability (forward remapping), and others as a manifestation of spatial attention (saccade target remapping). A previous study (Neupane et al., 2016a) confirmed the existence of both types of remapping within visual area V4 of non-human primates, and showed an early visual response that confirms the first type of remapping, followed by a later response that corresponds to saccade target remapping. Here, we used magnetoencephalography (MEG)

to investigate cortical areas that are involved in the transient shift of receptive fields during an attention task. We utilized MEG's excellent temporal resolution to map multiple cortical areas and show significant activity in the parietal and visual areas, with space- and time-signatures that indicate distinct involvement of those areas in remapping. Time frequency decompositions showed that remapping information is gated by  $\beta$ -band activity in the parietal cortex, followed by sluggish  $\beta$ -band increased responses in the lateral-occipital cortex. Our results don't confirm the presence of both types of remapping within a single area, but rather a memory encoding trace on the parietal cortex, followed by a late inhibitory-gated response in the lateral-occipital cortex.

Additionally, we show sequential activation of the superior parietal areas of each hemisphere around the timing of the saccade when the remapping information needs to transfer across hemispheres, which could potentially be indicative of visual information propagation from the retinotopic to the remapped areas.

# 3.2 Introduction

Eye movements move the high-resolution part of the eye, the fovea, to the target. Whenever we explore the visual scene, retinal displacements occur several times per second. Although these abrupt displacements should create a chaotic image, we instead perceive a stable one. Remapping is one of the mechanisms that is considered to help the brain compensate for these shifts in the visual scene and contribute to the maintenance of a stable image. During remapping, neurons transiently shift their receptive fields and respond to stimuli that were presented to the location where their receptive field is going to land after the completion of the eye-movement.

How remapping contributes to this information transfer is not understood yet. (Neupane et al., 2017) hypothesized that neuronal populations that encode the current and future fields establish a channel of coherent oscillations in the alpha band. Importantly, this was shown for neurons in area V4 that encoded receptive fields connected across multiple saccade vectors, confirming the assumption that a mechanism responsible for visual stability should be present for any saccade direction (Heiser and Colby, 2006; Mirpour and Bisley, 2012; Neupane et al., 2017).

However, when saccades were directed close to the receptive fields there have been indications of expansion of the receptive fields towards the saccade target, in FEF (Chen et al., 2018; Zirnsak et al., 2014), MT (Niknam et al., 2019) and V4 (Hartmann et al., 2017; Neupane et al., 2016b, 2016a; Tolias et al., 2001). This type of remapping is assumed to be influenced by attentional shifts to the saccade target. Indeed, a series of psychophysical (Cavanagh et al., 2010; Rolfs and Szinte, 2016; Rolfs et al., 2011; Szinte et al., 2016, 2018) and electrophysiological (Bisley and Goldberg, 2003, 2010; Gottlieb et al., 1998; Joiner et al., 2011; Mirpour and Bisley, 2016; Yao et al., 2016; Zelinsky and Bisley, 2015) studies have confirmed the modulatory effect of attention to the remapping mechanism. Attention has been hypothesized to prioritize only specific objects of interest perisaccadically, which effectively would not activate all connections between current and future fields.

The plethora of studies that support either type of remapping, constitutes evidence of the potential expression of remapping in both forms. Here, we investigate perisaccadic activity by using magnetoencephalography (MEG); a modality that provides sub-millisecond temporal precision and the ability to monitor multiple cortical areas simultaneously. We report perisaccadic responses in cortical space, frequency and time during an attentional paradigm. Our results indicate distinct engagement of the parietal cortex to forward remapping, and traces of the lateral-occipital cortex that could facilitate saccade-target remapping through an inhibitory-gating mechanism.

## 3.3 Methods

## 3.3.1 Participants

Data were recorded from 8 healthy, right-handed subjects, all of whom had normal or corrected to normal vision. All subjects gave written consent prior to participation in multiple sessions, involving structural MRI, and MEG recordings. All experimental protocols were approved by the Research Ethics Board of the Montreal Neurological Institute.

#### 3.3.2 Structural MRI

For the MRI scans, each subject was positioned on his back with a 32-channel surface coil centered over the occipital pole. Three-dimensional T1-weighted anatomical MR image volumes covering the entire brain were acquired on a Siemens TIM Trio scanner (3D-MPRAGE, TR/TE= 2300/2.98 ms, TI = 900 ms, 176 sagittally oriented slices, slice thickness = 1 mm, 256 x 240 acquisition matrix).

#### 3.3.3 MEG Data Collection

Data were recorded using a 275-channel (axial gradiometers) whole-head MEG system (CTF MEG International Services Ltd.). Each subject's head was digitized (typically 200 points) with a 6 degree-of-freedom digitizer (Patriot - Polhemus) prior to MEG data collection. This was used to mark the scalp, eyebrows and nose, and to optimize co-registration with the anatomical MRI. Three head positioning coils were attached to fiducial anatomical locations (nasion, left/right pre-auricular points) to track head movement inside the MEG. Eye movements and blinks were recorded using 2 bipolar electro-oculographic (EOG) channels. EOG leads were placed above and below one eye (vertical channel) and the second channel was placed laterally to the two eyes (horizontal channel). Heart activity was recorded with one channel (ECG), with electrical reference at the opposite clavicle, for subsequent MEG artifact detection and removal. All data were sampled at 2400 Hz.

Visual stimuli were presented onto a screen placed in front of the subjects at a viewing distance of 45 cm, which permitted visual stimulation up to 25x20 degrees of eccentricity. The display system consisted of a projector (VPixx Technologies, PROPPixxx) located outside the magnetically shielded room and three reflecting mirrors that directed images to the screen. The refresh rate of the projector was 120 Hz with a resolution of 1920x1080 pixels.

#### 3.3.4 Stimulus

Subjects were seated in a dimly illuminated room (0.13 cd/m2) and asked to fixate on one of two possible red dots of 0.3 degrees radius and perform saccades between these two targets (10-degrees distance) when they appeared. A probe was presented on the lower visual field between the two targets. After the subjects performed a saccade, they had to report the orientation (left or right tilt) of the last probe presented, through a button press. If no response was given by the

subject within five seconds, a new trial was initiated. Feedback was given to the subjects for their selection by turning the fixation dot green or gray, for correct and failed trials respectively.

Each trial was separated into two segments: P1 and P2 probe presentations. Depending on each of the two cases, a 4-degree side square probe (34.59 cd/m2) appeared on the lower visual field between the two targets on a black background (0.94 cd/m2) – Figure 1:

P1: the probe was presented for 50 ms, while the subject maintains fixation on one of the two targets. This probe was a white square displayed at maximum contrast against the background and appeared 500-1500 ms after the target was presented. This delay assumes that the subject has already fixated on the next target, and the P1 probe was expected to elicit retinotopic responses to the cortical sources that their receptive field was within the probe's location.

P2: the P2 probe was also presented for 50 ms and was turned on for 50-150 ms (adjusted on the response latency of each subject) after the new target location was presented. The P2 probe was comprised of a series of parallel dark lines against a white background, with their orientation tilted +5 or -5 degrees relative to the vertical orientation. This probe was expected to elicit the remapped responses to the sources that their receptive field would overlap with the probe's position, after the eye movement was performed. It should be noted that it is imperative this probe was completely off before the eye-movement was initiated to accurately measure remapped responses, so extra attention was paid to these two parameters.

Once the P2 probe has been presented, the subject was asked to report the orientation of the lines within it (right tilt/left tilt). The subjects use their index or middle finger (left vs right conditions) of their right hand to report the orientation. In case no response was performed by the subject after 5 seconds, a timeout initiated the next trial.

Monitoring of the probes' on and off states was performed by a photodiode that was located at the corner of the screen, hidden from the subject's visual field. A P2 trial was considered successful only when the saccade was initiated after the probe was completely off. The photodiode was sampled from the acquisition system at the same rate as the MEG signals.

At the end of the experiment, every subject also participated in a 10-minute run where the subjects performed saccades between the two targets, and no probes were displayed (saccades in the dark). These trials were used during the analysis for baseline correction.

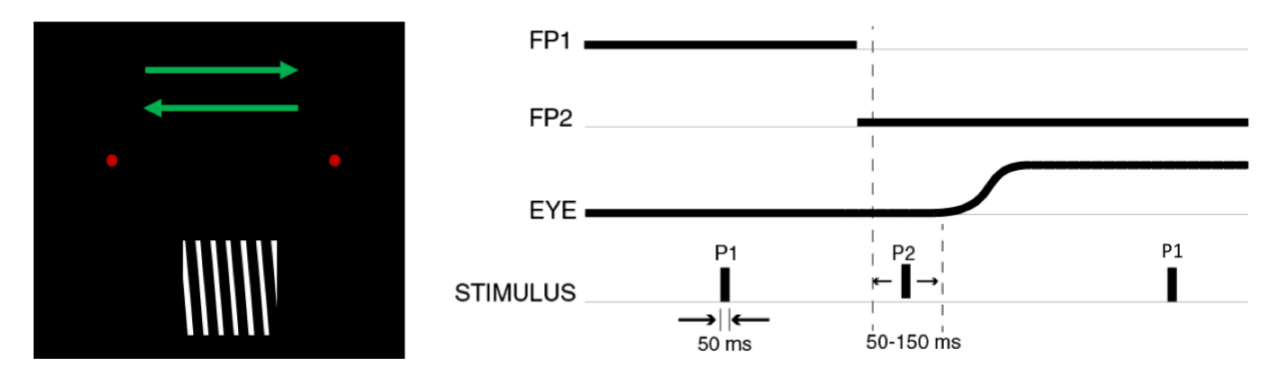


Figure 1. Experimental design. Subjects were asked to perform saccades between two targets while a probe appeared at the lower visual field between the targets. Probe P1 was a solid white square presented at maximum contrast during fixation to elicit retinotopic responses (not shown on the figure). Probe P2 contained orientation lines (tilted 5 degrees left/right) and the subjects were asked to report their orientation through a button press (depicted on the left of the figure). P2 probes were presented close to the saccade onset to elicit remapped responses.

#### 3.3.5 Artifact Removal

The eye acts as a dipole. MEG is very sensitive to eye-movements and the eyes' transition between the two targets influences the MEG signals extensively. We used independent component analysis (ICA) with InfoMax (Bell and Sejnowski, 1995) to isolate those components that originate from the eye-dipole and reject them. The top part of Figure 2 shows a 40-seconds example segment of the EOG signals (vertical-VEOG and horizontal-HEOG, 3 blinks are distinctly shown on this segment), and the bottom part shows the first 12 ICA components of the MEG signals. The 3<sup>rd</sup> component (in red) is clearly highly correlated to the eye-movements and is removed. The topography of the component (not displayed on Figure 2) is localized anteriorly and is associated to the eyes' dipoles. ICA decomposition revealed components that captured the eye movement artifact presence on the MEG signals in all subjects.

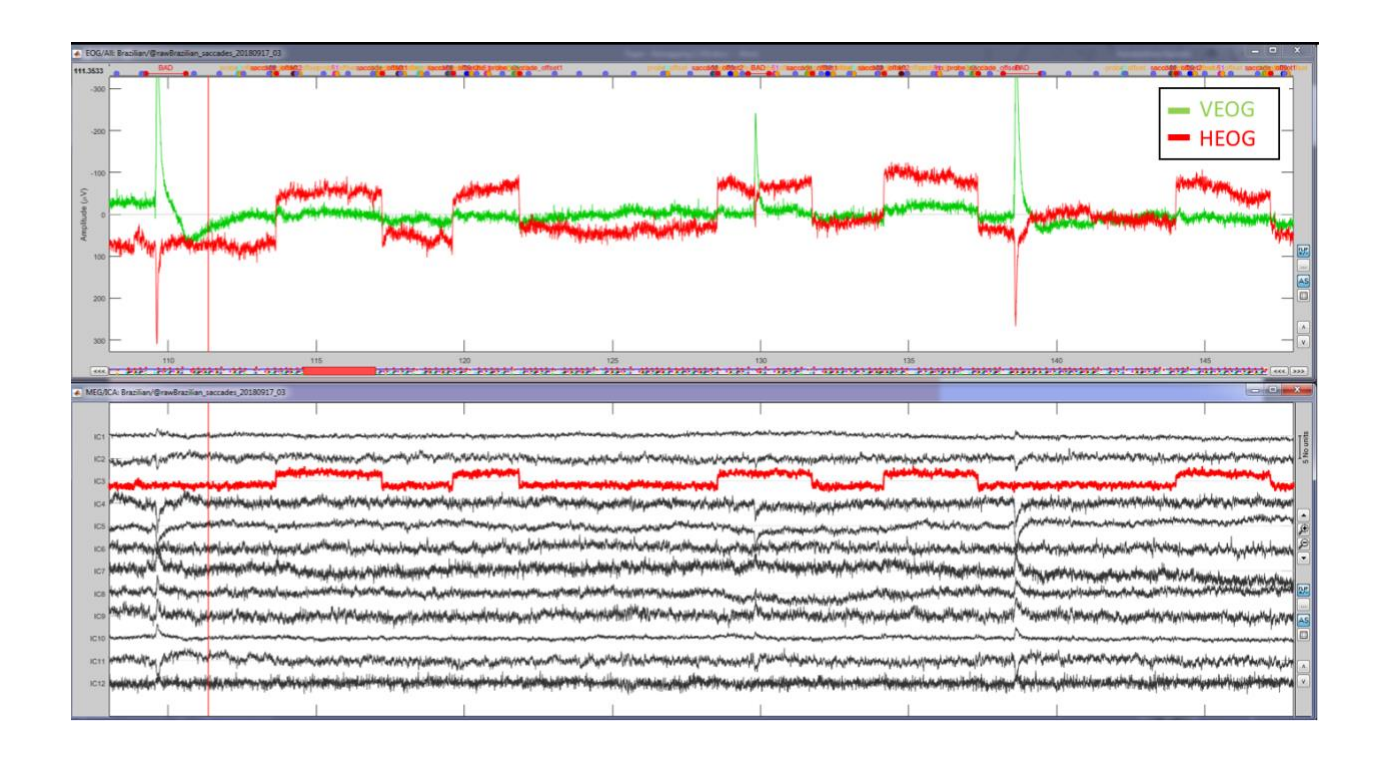


Figure 2. ICA Analysis components. Top row: Electrooculography signals (EOG). The large deflections on the vertical EOG (VEOG) channel reflect eye blinks. Since the saccades were performed on the horizontal axis, the horizontal EOG channel (HEOG) follows the trajectory of the eyes. Bottom row: 20 first MEG ICA components. For all subjects, ICA decomposition revealed a single component that was highly correlated with the HEOG. On this example, component 3 is highlighted to indicate the resemblance to the eye movement.

## 3.3.6 Time-segments of interest

Conditions were separated based on:

- 1. P1 probes' onset, while fixating on the first or the second target.
- 2. Saccade offset, for saccade to the left and saccade to the right, after a P2 probe was presented.
- 3. Saccade offset, for saccade to the left and saccade to the right, when no probe was presented (saccades in the dark).

Successful retinotopic trials (aligned on P1 probe onset: [-500,500] ms) were considered those that the subject maintained fixation around the probe onset on one of the targets.

Successful remapped trials (aligned on saccade offset: [-1000, 1000] ms) were considered those that the P2 probe was completely off (based on the photodiode's trace) before the saccade onset. As an additional quality-control for the trials selection, the maximum latency between the P2 probe offset and the successive saccade onset, was selected to be 150 ms, since remapping has been observed to be stronger when the saccade initiation is closer to the probe presentation (Umeno and Goldberg, 2001).

All trials that contained a blink were discarded.

## 3.3.7 MEG data analysis

MEG forward modeling was completed with the overlapping spheres approach (Huang et al., 1999). This method fits a sphere to the scalp surface under each sensor. A sphere can be used as a simplified model, since the magnetic fields are virtually undistorted by the skull (Barth et al., 1986; Okada et al., 1999).

Noise covariance across MEG sensors was estimated from a 2-minute resting state session. Weighted Minimum Norm Estimates (wMNE) (Lin et al., 2006) of cortically constrained, distributed sources were obtained using Brainstorm's default parameters (Depth weighting: 0.5, Regularized noise covariance: 0.1, Whitening: PCA / SNR: 3). Source orientations were constrained to be perpendicular to the cortical surface. 15,000 cortical sources where used for modeling each subject's structural morphology.

The signals were first projected on the cortical surface of each subject's anatomy with the wMNE inverse model, and all of the signal processing functions that are described below were applied on the signals from the individual cortical sources.

For population analysis (multiple subjects' analysis), the average signals from each subject were projected to the template brain, and statistical computations were performed on that common space.

#### 3.3.8 Statistical analysis

For the statistical analysis, all trials for each condition were averaged for each subject, and all individual source maps were mapped to, rectified, and smoothed on the MNI/ICBM152 brain template (Fonov et al. 2009), which is part of the default anatomy in Brainstorm's protocol (methodology described in (Tadel et al., 2019)).

A 1,000 randomizations paired permutation test was applied on the averages of all subjects between the saccade conditions where a saccade was performed with the presence of a P2 probe, and the conditions where a saccade was performed in the absence of the P2 probe (saccades in the dark). Separate tests were performed for the saccades to the left and right directions. The statistical significance threshold was set to  $\alpha = 0.05$  (uncorrected). These tests were performed for every timesample.

#### 3.3.9 Time-Frequency analysis

Time frequency wavelet decompositions were performed on each trial, for each subject, at the 6-90 Hz range. Each conditions' wavelets were then averaged for each subject.

Sequentially, an event related synchronization/desynchronization (ERSD) analysis was performed on each wavelet average, with respect to a baseline set at [-800, -200] ms before the saccade offset.

Each subjects' ERSDs were then averaged, ending up with 8 ERSD files for each condition.

This measure provides information of the modulation of the power of each frequency relative to the presaccadic baseline.

#### 3.3.10 Regions of interest for information flow

The regions of interest described here, were selected based on the combination of the statistical and the ERSD results. In order to have the same point of reference for all subjects, we used the Mindboggle Atlas (Klein et al., 2017), and specifically the superior parietal and lateral-occipital areas (in green and blue respectively in Figure 3).

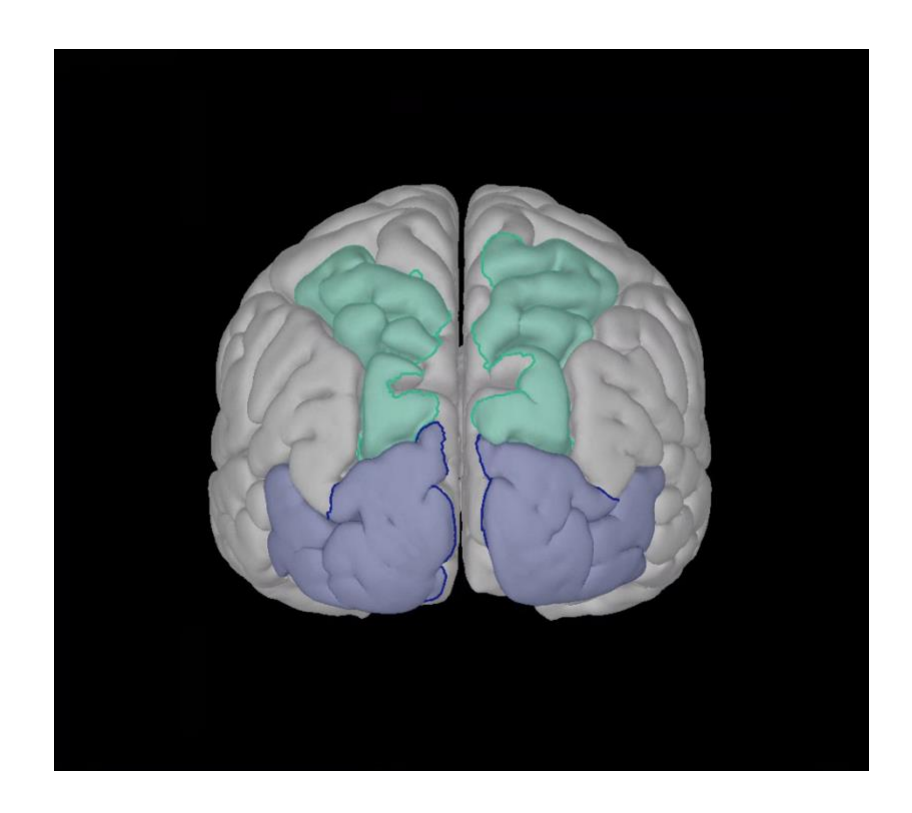


Figure 3. Superior parietal and lateral-occipital cortices were selected as regions of interest based on the results

#### 3.3.11 Computation of information flow

MEG sources can suffer from cross-talk from strong neighboring sources (Nasiotis et al., 2017). The placement of the probe between the two targets was expected to elicit retinotopic and remapped responses into two different hemispheres. In order to make sure that the retinotopic response was not leaking to the opposite hemisphere and provided a false positive remapped indication, we performed a principal component analysis to the ROIs that were located on the "retinotopic"/contralateral hemisphere, and regressed out the strongest components that were above a threshold of 0.3, from every source in the "remapped"/ipsilateral parietal cortex.

For example, for a saccade to the left condition, the subject was initially fixating on the right target, and the P2 probe was presented on the lower left visual field right before the saccade initiation. Therefore, the right hemisphere would encode the retinotopic information, and the left hemisphere the remapped. In order to reduce the crosstalk between the retinotopic to the remapped response, we computed the significant principle components on the right superior-parietal regions of interest, and sequentially we regressed out the components that crossed the threshold, from the left superior-parietal ROI. The selection of the regression technique was based on the fact that source crosstalk was expected to be time-locked. Additionally, the regression was also an effective tool for crosstalk removal even in source flip-sign occurrences that are present near the sulci.

This process was performed separately for each subject, and then the signals were projected to the average cortex.

#### 3.3.12 Software

Stimulation was programmed in Matlab (Mathworks), using Phychophysics toolbox (Brainard, 1997; Kleiner et al., 2007). MEG data analysis was performed with Brainstorm (Tadel et al., 2011). Cortical reconstruction and volumetric segmentation were performed with the Freesurfer image analysis suite (http://surfer.nmr.mgh.harvard.edu/) (Dale et al., 1999; Fischl et al., 1999, 2001).

## 3.4 Results

We investigated the cortical responses around the timing of eye-movements in 8 human subjects. Subjects were engaged by reporting the orientation of a small patch of lines within a probe that was presented between two targets. The selection of the location of the probe between the two targets dissociated retinotopic and remapped responses into two different hemispheres.

In this section, we demonstrate the biomarkers that indicate the manifestation of visual remapping in MEG.

## 3.4.1 Time Frequency – ERSD

All trials were segmented around the timing of the saccade offset, for both saccades to the left and to the right (-1000:1000 ms). Frequencies between [6, 90] Hz were monitored for ERSD metrics, and all subjects' cortical responses were projected and smoothed (3mm smoothing) on the average brain. ERSD provides the percentage of modulation of the power of each frequency compared to a pre-saccadic baseline. Figure 4 shows the power modulation on the  $\beta$ -band, for a timestamp 100 ms after the saccade offset, for 4 conditions of interest (saccade left/right, with probe/without probe). By contrasting the different conditions, we observed a differentiation on the power modulation on the ipsilateral parietal cortex when a probe was presented and when the subjects performed saccades in the dark.

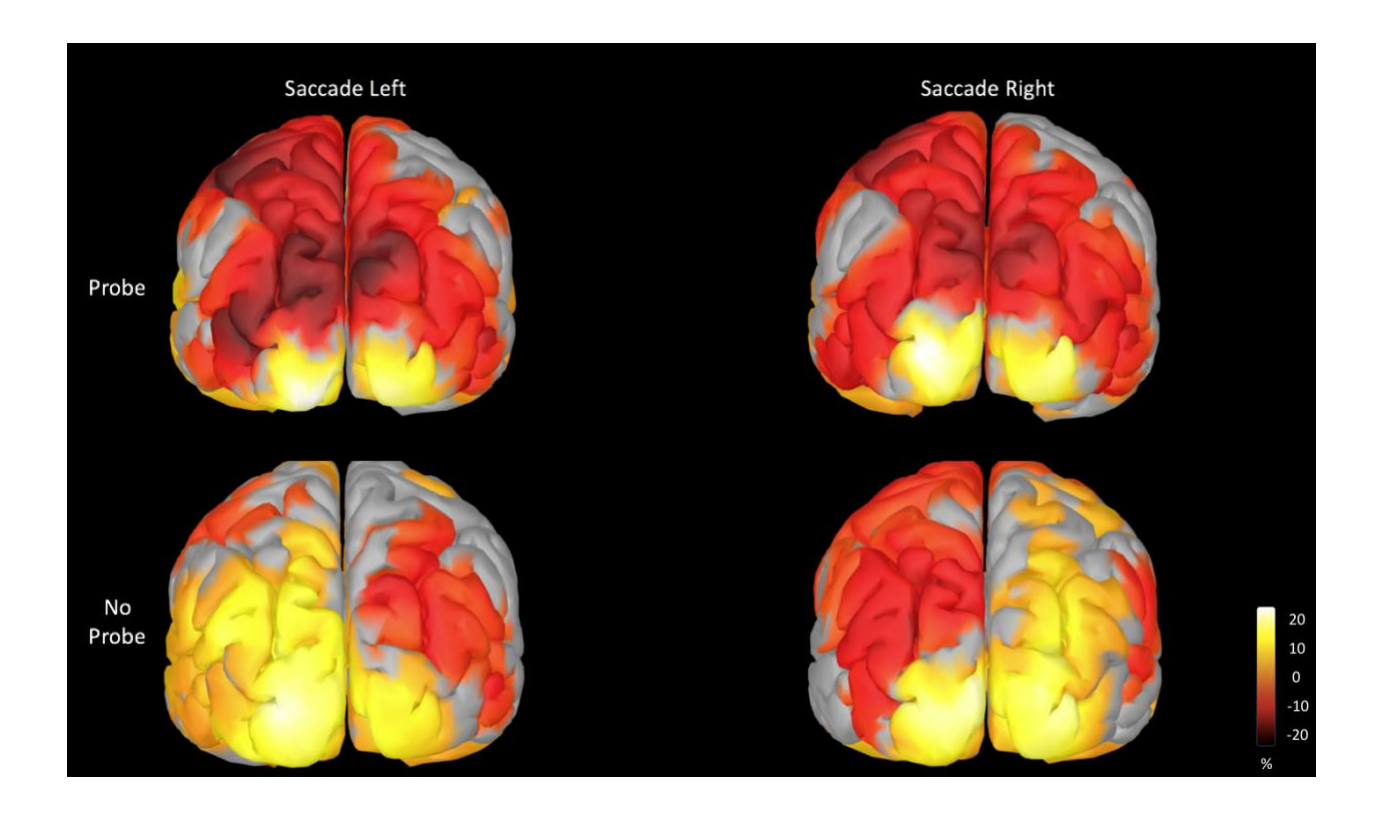


Figure 4. ERSD maps of the probe/no probe conditions for both saccade directions. All figures are synced at 100ms after the saccade offset for the  $\beta$ -band. Power modulation was normalized to a baseline [-800,-200]ms relative to the saccade offset. The presence or the absence of a P2 probe right before the saccade, distinctly affects the  $\beta$ -band activity on the ipsilateral parietal cortex for both saccadic directions.

Event related synchronization has been linked to decreased neural activity and desynchronization to activity increase (Pfurtscheller and Lopes da Silva, 1999).

The superior parietal cortex on the ipsilateral hemisphere shows synchronization on the conditions were there was no probe presented, and desynchronization when the P2 probe was presented.

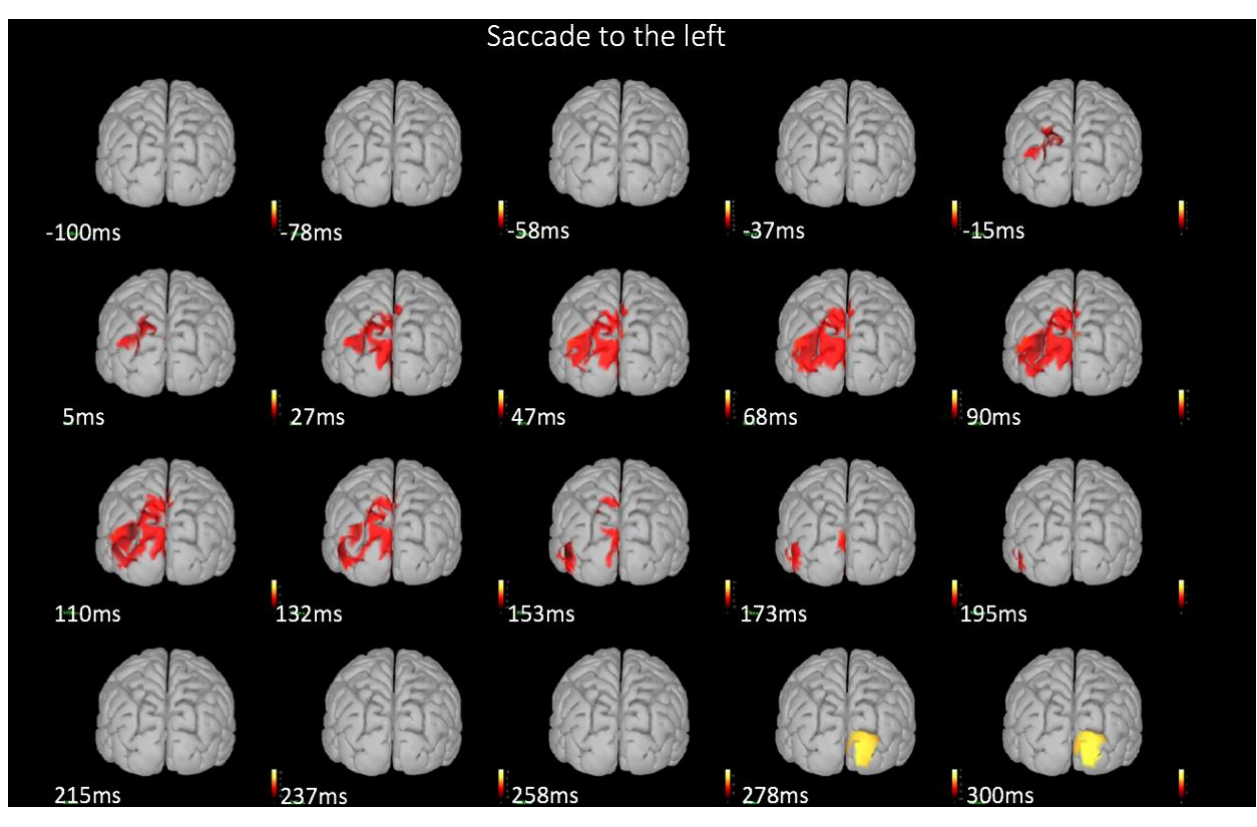
This result indicates that the superior parietal cortex on the ipsilateral cortex engages during the execution of the saccade only when a P2 probe was presented right before the saccade.

#### 3.4.2 Statistical significance of remapped responses

The ERSD analysis indicated on which frequency band there was modulation of the probe/no probe conditions' power relative to their baselines and indicate the contrast between probe/no probe conditions. To verify that the difference between the probe/no probe conditions was statistically significant, we filtered all probe/no probe trials on  $\beta$ -band and performed the permutation test described in the methods section for both saccade directions.

The permutation test was performed on each time-sample, allowing us to create a real-time statistical map of the entire cortical surface. The results indicate which areas are engaged in the task, on which frequencies, and their temporal characteristics. Figure 5 shows the statistical map created, for both saccade directions, in different timestamps ranging [-100,300] relative to the saccade offset.

Our results reveal a statistically significant early  $\beta$ -band suppression between the probe/no probe conditions in the ipsilateral superior parietal cortex, followed by a late  $\beta$ -band increased response (starting ~280ms after the saccade offset) on the contralateral visual cortex.



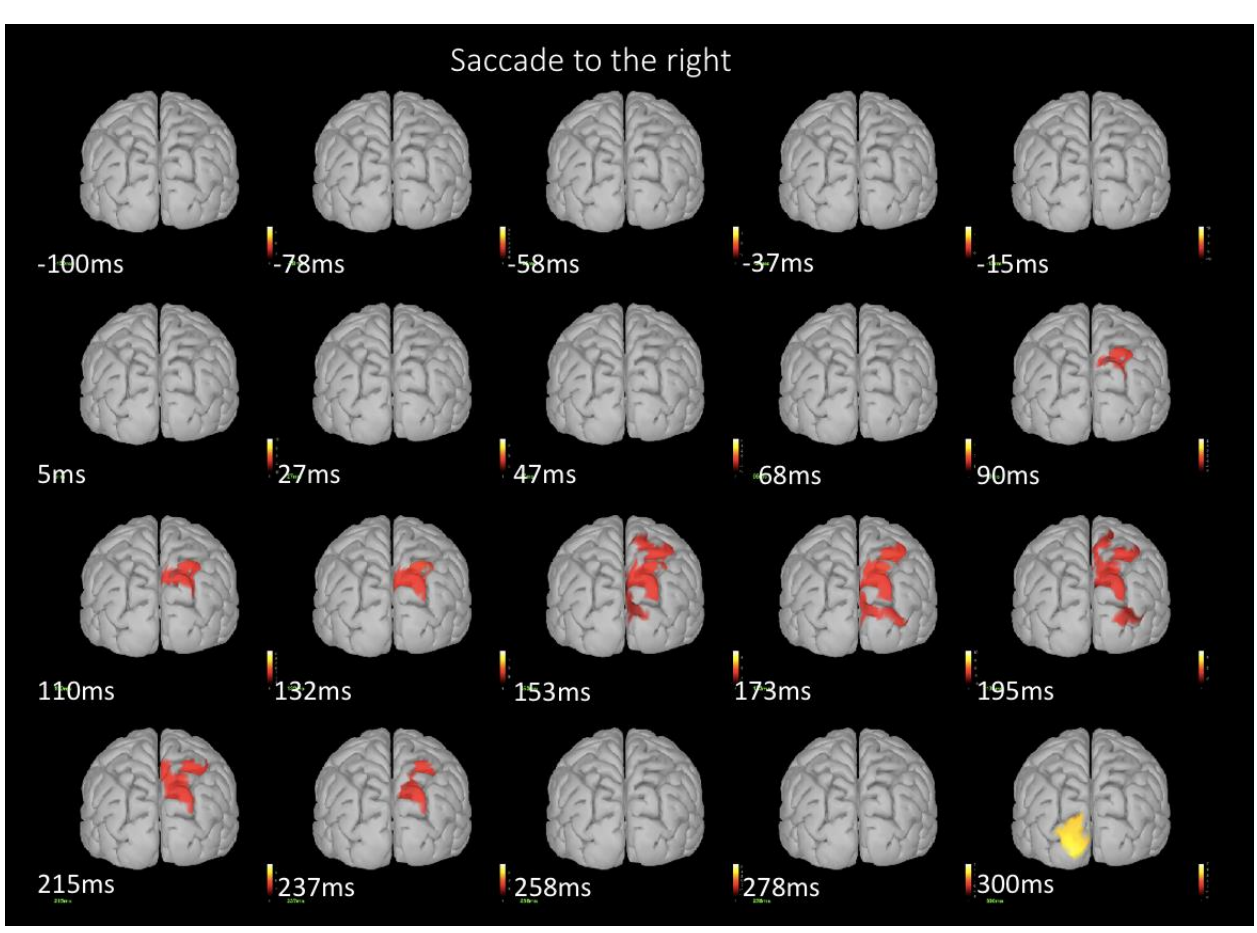


Figure 5. Two-tailed permutation test (1000 repetitions) between probe/no probe conditions, for saccades to the left (Top) and to the right (Bottom). The test was performed separately for every time-sample. The figure displays multiple snapshots on different timestamps ranging [-100,300]ms relative to the saccade offset. Due to the selection of the position of the probe, saccades to the left would showcase forward remapping on the left hemisphere (equally saccades to the right, on the right hemisphere). The maps indicate an early remapped response in the ipsilateral parietal cortex, followed by a sluggish  $\beta$ -band increase in the contralateral lateral-occipital cortex.

#### 3.4.3 Information flow

Crosstalk from the contralateral to the ipsilateral hemisphere has been regressed out (see Methods) in order to monitor the timing that each ROI was getting engaged in the task.

Forward remapping requires information exchange with the other hemisphere (since the probe is presented between the two targets) and it is expected that the information about the probe would reach the "retinotopic" hemisphere before it gets transferred to the "remapped" (Merriam et al., 2003).

The figure below shows the mean time trace within each ROI (superior parietal ROIs on both hemispheres), for both saccade directions. The traces correspond to unfiltered signals and indicate the engagement of the contralateral superior parietal cortex approximately 40ms before the ipsilateral counterpart. Moreover, the mean activity of the contralateral parietal cortex is consistently higher that the ipsilateral (Figure 6).

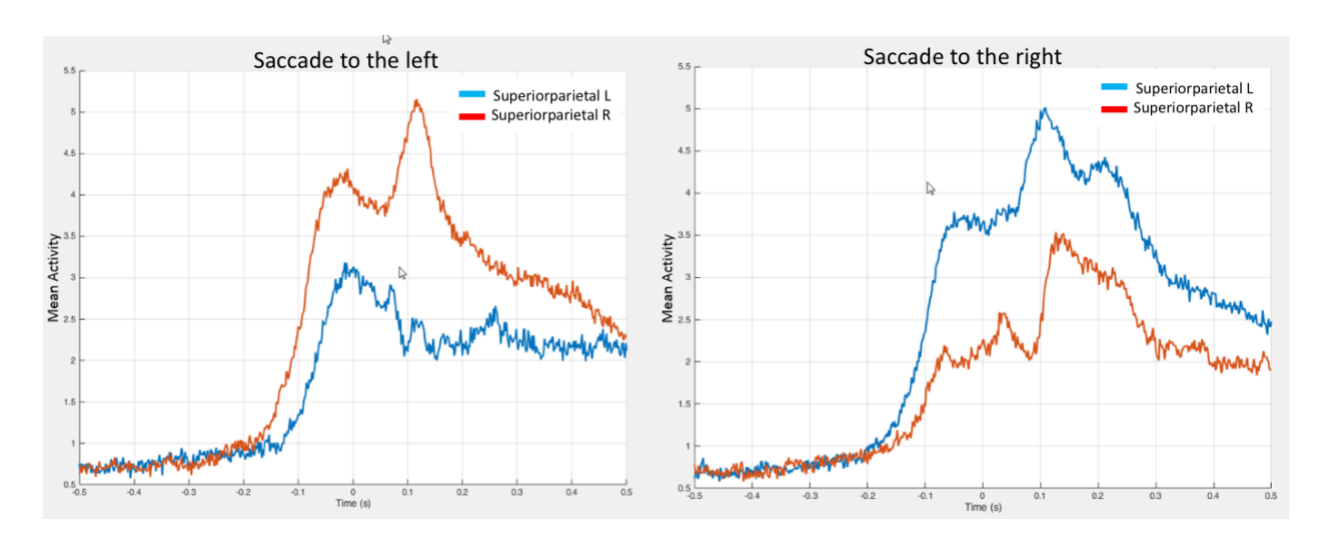


Figure 6. Mean z-scored activity around the saccade offset (-500, 500 ms) of the superior parietal cortices on the population average. Signals were rectified before being projected on the average topography and sequentially z-scored relative to a baseline [-1000, -200]ms before the saccade offset. Time-locked influence of the contralateral hemisphere to the ipsilateral was regressed out (see methods). For saccades to the left, the left hemisphere would encode forward remapped information (and the right hemisphere for saccades to the right respectively). The results suggest a sequential activation of the contralateral and then ipsilateral superior parietal cortices, which could be indicative of the information flow from the retinotopic to the remapped areas. The latency of the information flow presaccadically appears to be  $\sim$ 40ms.

## 3.5 Discussion

#### 3.5.1 Brief summary of results

In this study we have demonstrated remapping activity in the parietal and lateral-occipital cortex. Time frequency decomposition analysis around the timing of the saccade showed modulation in the  $\beta$ -band (Figure 4) in both areas. Statistical analysis revealed an early beta decrease on the ipsilateral parietal cortex, followed by a late  $\beta$ -band increase on the contralateral lateral-occipital area for an attentional task designed to dissociate forward and saccade target remapping into two separate hemispheres.

Temporal analysis of the parietal cortex in both hemispheres showed sequential activation from the retinotopic to the remapped areas, which can be indicative of the visual updating information flow.

#### 3.5.2 Previous work

Remapping has been observed in several brain regions through invasive electrophysiological methods in non-human primates: Superior Colliculus: (Churan et al., 2011; Walker et al., 1995), Frontal Eye Fields (FEF): (Umeno and Goldberg, 1997), Lateral Intraparietal Area (LIP): (Duhamel et al., 1992; Wang et al., 2016; Kusunoki and Goldberg, 2003), V4: (Neupane et al., 2016b, 2016a, 2017; Tolias et al., 2001), MT: (Yao et al., 2016), MST (Inaba and Kawano, 2014), or non-invasively with functional magnetic resonance imaging (fMRI) in parietal, striate and extra-striate cortex: (Merriam et al., 2003, 2007) (however, a replication attempt of the fMRI study wasn't able to show evidence of visual remapping in humans with fMRI (Lescroart et al., 2016)).

Remapping was shown to be mediated by a corollary discharge from the superior colliculus, through the mediodorsal thalamus, to the FEF (Sommer and Wurtz, 2006) and is less prominent descending along the visual hierarchy (Merriam et al., 2007; Nakamura and Colby, 2002). This has been hypothesized that is caused by the fewer connections from FEF (Nakamura and Colby, 2002; Schall et al., 1995; Stanton et al., 1995) or LIP to early visual areas. Further justification of the effect of visual hierarchy on remapping is that neurons in the superficial layers of the superior colliculus don't respond predictively to the future field and

these are the layers that project mostly to the retina, the striate and the early extrastriate visual cortex (in contrast to the intermediate layers of the SC that show remapping) (Walker et al., 1995). Additionally, the neuronal latency relative to the saccade onset increases in visual areas lower in the visual hierarchy (Nakamura and Colby, 2002). This observation, along with the observation of fewer projections from areas that exhibit remapping to the earlier visual areas support the notion of a top-down mechanism.

Remapping is considered to be a mechanism that contributes to visual stability. Although this would dictate that the saccadic shift would imply remapping of every point of the visual field, several studies have approached the remapping phenomenon as a shift of attentional pointers to regions of interest (Cavanagh et al., 2010; Rolfs and Szinte, 2016; Rolfs et al., 2011; Szinte et al., 2016, 2018). These studies support the claim that only points of interest get remapped are effectively remapped.

Yet, one study showed that within a single area, both mechanisms (remapping contributes to spatial constancy but also to attentional modulation) can be observed (Neupane et al., 2016a).

Previous eye-movement/remapping MEG studies (Moon et al., 2007) investigated the sensorimotor transformation in FEF and LIP during anti-saccades, but didn't demonstrate the selective spatial neuronal shift. (Medendorp et al., 2007) investigated single and double step saccades but the temporal delay used in their paradigm allowed them to investigate the memory aspect of LIP involvement in the saccades, rather than spatial remapping intrinsically.

Two studies tried to monitor remapping along the visual track between the receptive field (RF) of neurons, and the future field (FF) they will have after the saccade. Visual probes projected at the midpoint between the RF and FF (along the saccade vector that connects the two receptive fields) have been reported both to elicit (Wang et al., 2016 - in LIP) and not elicit (Sommer and Wurtz, 2006 - in FEF) remapped responses; resulting to conflicting reports as to whether this mechanism involves a "jump" of the remapped responses, or a propagating "wave" of activity (receptive field expansion) that connects the two cortical locations that encode the CF and FF through the associated intermediate neuronal populations.

## 3.5.3 Where we expected to see remapping with MEG

Electrophysiological techniques applied on non-human primates found that the strength of remapping was roughly monotonic with position in the visual hierarchy. Almost no remapping was observed in the primary visual cortex (1/64 neurons (Nakamura and Colby, 2002)). Equivalent fMRI experiments in humans, showed the same result (Merriam et al., 2007) but with higher distribution of remapped sources along the visual cortex: remapped responses were small in V1 and V2 (around 20% of the voxels exhibited remapping) and larger in V3A and human V4 (hV4) (~50% of hV4 voxels showed remapping). The increased capacity of fMRI to show remapping even in the primary visual cortex was attributed to the effective response fields of the fMRI voxels (Merriam et al., 2007).

Our study (Nasiotis et al., 2017) revealed that MEG was capable of estimating high-resolution V1 retinotopic maps. We measured the effective receptive fields of individual sources on a high-resolution cortical tessellation, and our results suggests that they were roughly 10 times bigger from individual neurons and about 2 times bigger than V1 population receptive fields estimated with fMRI. It is due to this larger cortical integration that in theory, MEG would be able to summate the remapped responses of populations of neurons.

Regarding the subcortical superior colliculus, the MEG signal attenuates within deeper structures due to the electromagnetic properties of the sources (although there are reports that show it can be achieved (Backus et al., 2016; Coffey et al., 2016)).

Although MEG studies have been able to localize FEF from increased presaccadic activity (loannides et al., 2004, 2010), our results weren't able to identify statistical significance in any of the areas that FEF have been localized with MEG or other imaging modalities (Vernet et al., 2014).

Therefore, we focused our investigation on the superficial areas that demonstrated significance: the parietal and the lateral-occipital cortex.

## 3.5.4 Experimental Design

#### 3.5.4.1 Selection of the probe's position

The P1 and P2 probes appeared at a location that was between the two targets. The P1 probes were expected to elicit responses in the contralateral hemisphere as is expected from the retinotopic map. However, the P2 probes were expected to activate the contralateral hemisphere (retinotopic responses), but also the ipsilateral hemisphere (remapped responses). The selection of the P2 probe's horizontal location between the two targets, ultimately dissociates the retinotopic and remapped responses into different hemispheres.

The location of the probe was selected to be on the lower visual field. The lower visual field has been associated with stronger visual responses and was expected to increase the signal to noise ratio (Fylan et al., 1997; Nasiotis et al., 2017; Perry et al., 2011; Poghosyan and Ioannides, 2007; Portin and Hari, 1999).

## *3.5.4.2 Number of probes*

Pilot experiments on this study used multiple locations for probe presentation (6 possible locations on the visual field, and one control on the upper field). The initial design of this experiment intended to also investigate inter-areal, and intra-areal interactions, since our previous study (Nasiotis et al., 2017) showed that the spatial resolution of MEG would be able to achieve that. However, there is a striking difference between this remapping and our previous retinotopic study: the design of the reverse correlation – retinotopic study, allowed visual stimulation every 100ms, leading to 36,000 frames presented to each subject every hour. The remapping pilot study with the 7 potential probes on the other hand, allowed on average approximately 50 successful trials on every session. This led us to reduce the number of potential probes, initially to three, and finally to just one, to increase the number of trials per condition and ultimately the signal to noise ratio.

#### 3.5.4.3 Attention on the remapping task

The first subject underwent a series of pilot studies until we refined the remapping paradigm.

These studies experimented with the size of the probe, its spatial frequency, temporal frequency

(frequency tagging), and the engagement, or not, of the subject with the paradigm (introducing attention).

Attention has been shown to play a modulatory effect in remapping (Rolfs and Szinte, 2016; Rolfs et al., 2011; Yao et al., 2016). In order to investigate this modulation in MEG, the first subject underwent 3 total modifications of the experiment:

- 1. The first session was the one described in the manuscript: one probe was presented between the two targets, and the subject had to pay attention on the P2 probe and report the orientation of the lines within the probe.
- 2. The first control disengaged the subject from the task. The P2 probe was presented at the same location but had no orientation within it (probe consisted of a white square at maximum contrast) and the subject wasn't asked to give any feedback. This first control took out the attention component.
- 3. The second control session tried to rule out the engagement of the ipsilateral hemisphere solely due to the attentional engagement and the saccadic movement; or in other words, that the location of the probe is important for the ipsilateral activation. In order to control for that, the location of the probe was moved further from the saccade target on the direction of the saccade; for example, for a saccade to the left the probe was presented further left from the target. By positioning the probe to that location, remapping was expected to be isolated within the right hemisphere and the left hemisphere shouldn't show any significant activity.

These controls revealed that the ipsilateral parietal cortex was engaged only when attention was involved in the paradigm and only when a probe was presented at a location that the activity needed to be remapped to the ipsilateral hemisphere.

## 3.5.5 Two types of remapping

Neural oscillations play an important role in the establishment of communication between brain regions. The nature of a communication structure is to show selectivity in the information that is passed through. Remapping involves memory since neurons respond to stimuli that have been omitted from the screen. Short-

term memory requires communication between multiple brain regions that collectively mediate the encoding and maintenance of sensory information (Liebe et al., 2012). Throughout the maintenance period, the signature of the encoded memory should be sustained (D'Esposito, 2007) even if the stimulus has been eliminated.

Our results suggest the manifestation of two types of remapping with distinct spatial and temporal characteristics, as shown in Figure 5. The early component is revealed in the ipsilateral superior parietal cortex after the time of the saccade, which is consistent with the idea of forward/memory trace remapping.

A more sluggish component appears in the contralateral lateral-occipital cortex ~280ms after the saccade offset. The visual cortex shows increased  $\beta$ -band activity only on the hemisphere that encodes receptive fields in the direction of the saccade. A similar result has been observed in V4 with the same temporal (~250ms) and spatial signature (only for saccades towards the RF of the neurons, Neupane et al., 2016a), linking this late component to saccade target remapping. Since our study utilized only a single probe, it is still an open question if the response is elicited by neurons that encode the probe, the saccade target, or a convoluted spatial mix of the two (Zirnsak et al., 2014). Future experiments with more thorough probing of the visual space would be able to shed light to this question.

The parietal cortex showed decreased  $\beta$ -band activity post-saccadically. Decreased power in the lower frequency ranges (less than 20 Hz) has been observed during memory encoding, on items that were remembered compared to those not remembered (Burke et al., 2014; Fellner et al., 2013; Hanslmayr et al., 2016; Long et al., 2014; Noh et al., 2014). Lower power in  $\beta$ -band oscillations have been linked to increased attentional modulation (Friese et al., 2016) and to encoding and maintenance of memory load in the parietal region (Proskovec et al. 2018).

In contrast, the lateral-occipital cortex showed a late increase in the  $\beta$ -band activity. Higher  $\beta$ -band oscillatory power is assumed to result from the rhythmic activity of inhibitory interneurons (Klimesch et al., 2007; Jensen and Mazaheri, 2010). Inhibition has been described as a modulatory factor that can increase signal to noise ratio by enabling neurons to fire during specific cycles of ongoing oscillations (Klimesch, 2012; Shen et al., 2011; Yizhar et al., 2011). This temporally precise,

tuned interplay between inhibition/excitation can be the gating mechanism of the saccade target remapping component.

#### 3.5.6 Remapping information flow

Our experimental design forced the retinotopic and the forward-remapped information to be encoded in two separate hemispheres since the probe was located between the two targets. The contralateral hemisphere encodes the probe's characteristics before the eye movement and transfers the information through a complicated network all the way to the ipsilateral hemisphere.

Split-brain experiments in the macaque monkey, have shown that across-hemifield remapping of stimulus traces occur even in the absence of the forebrain commissures, but the remapped responses are smaller and appear later (Heiser et al., 2005). In other words, there are redundant cortico-cortical and sub-cortical connections that mediate remapping.

(Crapse and Sommer, 2009) have shown that FEF is getting information regarding the ipsilateral visual field from the opposite superior colliculus in the midbrain. LIP is connected to FEF (Anderson et al., 2011), therefore it could potentially receive the ipsilateral information from that pathway. Although MEG cannot monitor the information flow through the subcortical areas, the relative timing of the information flow between the two hemispheres appears to be ~40ms for transfer across parietal cortices.

## 3.5.7 Why we didn't see remapping in all expected areas

FEF was also monitored for remapping since it is a cortical area. However, FEF is located within sulci where the MEG signal shows weaker responses (Goldenholz et al., 2009; Nasiotis et al., 2017). The striate and extrastriate cortex on the other hand, although more accessible with MEG, are expected to show weaker remapping responses. hV4 has been a subject of controversy among researchers (Winawer and Witthoft, 2015) and the homology with the monkey V4 and human V4 has been under debate. However, (Merriam et al., 2007) found remapping in area hV4 (ventral area adjacent to ventral V3 - (Wandell et al., 2005, 2007)). This area is located on the ventral stream, in greater distance to the MEG sensors which is expected to reduce the signal to noise ratio. Moreover, (Merriam et al., 2007) showed that remapped responses were smaller in

magnitude that the visual response. This is consistent with physiological studies in monkeys in which cells have remapped responses that are on average half as large as the responses to stimuli in the receptive field (Duhamel et al., 1992) or 75.3% in amplitude of the visual response (Nakamura and Colby, 2002) and with our own results from this study.

Besides the obvious problem that a noisy signal would create, we hypothesize another plausible reason for not being able to localize cortical sources that elicit remapping responses. The spatial resolution of invasive electrophysiological methods that can detect activity from individual neurons is far more precise than the MEG signal. Namely, the weakest MEG signal that can be detected is considered to be generated by simultaneous activity of 10,000-50,000 neurons (Murakami and Okada, 2006). Therefore, comparing MEG to invasive methods that have shown remapping effects with event related approaches in several areas is not appropriate due to the uneven, in orders of magnitude, spatial resolution.

However, remapping has been shown with fMRI as well, where each voxel also representing the summated activity of large populations of neurons. There is a fundamental difference between the two brain imaging methods that could cause fMRI methods to be able to show remapping and MEG to be insensitive to it. The BOLD signal in fMRI studies is created by changes in brain metabolism (Bandettini et al., 1992; Kwong et al., 1992; Ogawa et al., 1990). Any localized activity will cause oxygen consumption and therefore a change in the BOLD signal. The neurons that contribute to the BOLD signal are not required to be perfectly time locked, since the BOLD signal is very sluggish and is only affected by the total neuronal activity; either neurons fire and consume oxygen, or they don't. Time-locked responses from the voxel integrated neurons are not detrimental. MEG on the other hand, has excellent temporal resolution. Considering that neurons in very close proximity (neurons picked up from different electrodes on the same 10x10 Utaharray – 4x4mm) can show very smeared remapped latencies (unpublished data from our lab showed latency-difference as extreme as 300ms between remapping neurons within the same Utah array) and that the MEG sources integrate a considerable number of nearby neurons, it is probable that the MEG sources effectively integrate the activity of many non-time locked neurons, leading to a significantly attenuated remapping signal. Therefore, a MEG source would be able to

show the remapping activity only if the neurons it integrated where time-locked. Figure 7 shows a schematic that demonstrates this potential explanation.

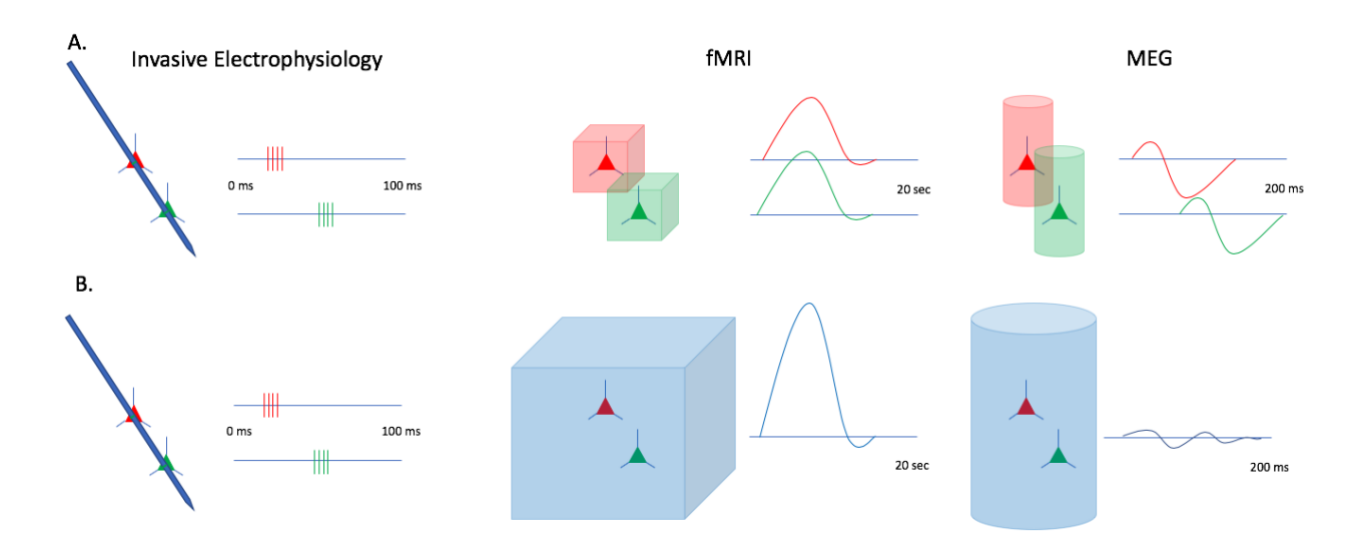


Figure 7. Schematic showing a possible explanation why MEG might not be able to show remapping in all areas. The cartoon shows two neurons that are not time-locked and how different recording methods/modalities would pick up their activity. (A) shows a hypothetical situation of what the BOLD and the MEG signals would be if the fMRI voxels and MEG sources had the spatial resolution to monitor activity from individual neurons. The BOLD signal would be insensitive to the temporal difference in firing of the two neurons, whereas the MEG sources would be able to reveal it. (B) In a more realistic scenario, the fMRI voxels and MEG sources, incorporate the activity of multiple neurons. However, the BOLD signal is affected from the summated energy consumption of the neurons within the voxel and the signal would be strengthened. MEG sources on the other hand, would average out the total activity, resulting in an attenuated signal.

#### 3.5.8 Future research

Short term memories are suggested to be physiologically stored through patterns of physical activity (Buschman et al., 2011; Fell and Axmacher, 2011; Lisman and Idiart, 1995; Lisman and Jensen, 2013). These studies suggest that the physiological capacity of this storage is influenced by nested oscillations that co-exist within slower oscillations. In the example of theta-gamma nested oscillations, the storage limit would be the number of  $\gamma$  sub-cycles that can fit within a  $\theta$ -cycle. Remapping could be an example of this memory storage mechanism and the number of objects/probes that can be remapped could be limited by the number of faster oscillations that are nested (perhaps in the  $\beta$ -oscillations that we observed). Although this idea is fundamentally

contradictory to the relation of remapping to spatial constancy (spatial constancy wouldn't be achieved if only 5-7 spatial locations remap), it could potentially provide the upper limit of objects on the approach of remapping as a mechanism of attentional pointers. Future studies can investigate the storage capacity of spatial features during remapping.

## 3.6 Conclusion

We have shown that remapping can be observed with MEG through an experimental paradigm that utilizes subject's attention. We have shown the presence of two potential types of remapping in real-time on human subjects; the real-time engagement of the parietal cortex in the mechanism, and evidence of a late, possibly saccade target remapping. Finally, our results show the sequential activation of the retinotopic and the remapped superior parietal cortex in the two opposite hemispheres.

# 3.7 Acknowledgements

We would like to thank Elizabeth Bock for help in data acquisition, Pooya Laamerad, Dr. Dan Guitton and Dr. Matthew Krause for analysis input. This work was funded by a Molson Neuro-Engineering Scholarship (the Molson Foundation) to K.N., by grants from National Science and Engineering Research Council of Canada (NSERC 436355-13) and National Institutes of Health (NIH-2R01EB009048-05) to S.B. and a grant from NSERC (NSERC RGPIN/341534-2012) to C.P.

## 3.8 References

Anderson, J.C., Kennedy, H., and Martin, K.A.C. (2011). Pathways of Attention: Synaptic Relationships of Frontal Eye Field to V4, Lateral Intraparietal Cortex, and Area 46 in Macaque Monkey. J. Neurosci. *31*, 10872–10881.

Backus, A.R., Schoffelen, J.-M., Szebényi, S., Hanslmayr, S., and Doeller, C.F. (2016). Hippocampal-Prefrontal Theta Oscillations Support Memory Integration. Curr. Biol. *26*, 450–457.

Bandettini, P.A., Wong, E.C., Hinks, R.S., Tikofsky, R.S., and Hyde, J.S. (1992). Time course EPI of human brain function during task activation. Magn. Reson. Med. *25*, 390–397.

Barth, D.S., Sutherling, W., Broffman, J., and Beatty, J. (1986). Magnetic localization of a dipolar current source implanted in a sphere and a human cranium. Electroencephalogr. Clin. Neurophysiol. *63*, 260–273.

Bell, A.J., and Sejnowski, T.J. (1995). An information-maximization approach to blind separation and blind deconvolution. Neural Comput. *7*, 1129–1159.

Bisley, J.W., and Goldberg, M.E. (2003). Neuronal activity in the lateral intraparietal area and spatial attention. Science 299, 81–86.

Bisley, J.W., and Goldberg, M.E. (2010). Attention, intention, and priority in the parietal lobe. Annu. Rev. Neurosci. *33*, 1–21.

Brainard, D.H. (1997). The Psychophysics Toolbox. Spat. Vis. 10, 433–436.

Burke, J.F., Long, N.M., Zaghloul, K.A., Sharan, A.D., Sperling, M.R., and Kahana, M.J. (2014). Human intracranial high-frequency activity maps episodic memory formation in space and time. NeuroImage *85*, 834–843.

Buschman, T.J., Siegel, M., Roy, J.E., and Miller, E.K. (2011). Neural substrates of cognitive capacity limitations. Proc. Natl. Acad. Sci. *108*, 11252–11255.

Cavanagh, P., Hunt, A.R., Afraz, A., and Rolfs, M. (2010). Visual stability based on remapping of attention pointers. Trends Cogn. Sci. *14*, 147–153.

Chen, X., Zirnsak, M., and Moore, T. (2018). Dissonant Representations of Visual Space in Prefrontal Cortex during Eye Movements. Cell Rep. 22, 2039–2052.

Churan, J., Guitton, D., and Pack, C.C. (2011). Context dependence of receptive field remapping in superior colliculus. J. Neurophysiol. *106*, 1862–1874.

Coffey, E.B.J., Herholz, S.C., Chepesiuk, A.M.P., Baillet, S., and Zatorre, R.J. (2016). Cortical contributions to the auditory frequency-following response revealed by MEG. Nat. Commun. 7, 11070.

Crapse, T.B., and Sommer, M.A. (2009). Frontal Eye Field Neurons with Spatial Representations Predicted by Their Subcortical Input. J. Neurosci. 29, 5308–5318.

Dale, A.M., Fischl, B., and Sereno, M.I. (1999). Cortical Surface-Based Analysis: I. Segmentation and Surface Reconstruction. NeuroImage *9*, 179–194.

D'Esposito, M. (2007). From cognitive to neural models of working memory. Philos. Trans. R. Soc. B Biol. Sci. *362*, 761–772.

Duhamel, J.R., Colby, C.L., and Goldberg, M.E. (1992). The updating of the representation of visual space in parietal cortex by intended eye movements. Science 255, 90–92.

Fell, J., and Axmacher, N. (2011). The role of phase synchronization in memory processes. Nat. Rev. Neurosci. *12*, 105–118.

Fellner, M.-C., Bäuml, K.-H.T., and Hanslmayr, S. (2013). Brain oscillatory subsequent memory effects differ in power and long-range synchronization between semantic and survival processing. NeuroImage *79*, 361–370.

Fischl, B., Sereno, M.I., and Dale, A.M. (1999). Cortical Surface-Based Analysis: II: Inflation, Flattening, and a Surface-Based Coordinate System. NeuroImage *9*, 195–207.

Fischl, B., Liu, A., and Dale, A.M. (2001). Automated manifold surgery: constructing geometrically accurate and topologically correct models of the human cerebral cortex. IEEE Trans. Med. Imaging *20*, 70–80.

Friese, U., Daume, J., Göschl, F., König, P., Wang, P., and Engel, A.K. (2016). Oscillatory brain activity during multisensory attention reflects activation, disinhibition, and cognitive control. Sci. Rep. *6*, 1–11.

Fylan, F., Holliday, I.E., Singh, K.D., Anderson, S.J., and Harding, G.F.A. (1997). Magnetoencephalographic Investigation of Human Cortical Area V1 Using Color Stimuli. NeuroImage *6*, 47–57.

Goldenholz, D.M., Ahlfors, S.P., Hämäläinen, M.S., Sharon, D., Ishitobi, M., Vaina, L.M., and Stufflebeam, S.M. (2009). Mapping the signal-to-noise-ratios of cortical sources in magnetoencephalography and electroencephalography. Hum. Brain Mapp. *30*, 1077–1086.

Gottlieb, J.P., Kusunoki, M., and Goldberg, M.E. (1998). The representation of visual salience in monkey parietal cortex. Nature *391*, 481–484.

Hanslmayr, S., Staresina, B.P., and Bowman, H. (2016). Oscillations and Episodic Memory: Addressing the Synchronization/Desynchronization Conundrum. Trends Neurosci. *39*, 16–25.

Hartmann, T.S., Zirnsak, M., Marquis, M., Hamker, F.H., and Moore, T. (2017). Two Types of Receptive Field Dynamics in Area V4 at the Time of Eye Movements? Front. Syst. Neurosci. 11.

Heiser, L.M., and Colby, C.L. (2006). Spatial updating in area LIP is independent of saccade direction. J. Neurophysiol. *95*, 2751–2767.

Heiser, L.M., Berman, R.A., Saunders, R.C., and Colby, C.L. (2005). Dynamic Circuitry for Updating Spatial Representations. II. Physiological Evidence for Interhemispheric Transfer in Area LIP of the Split-Brain Macaque. J. Neurophysiol. *94*, 3249–3258.

Huang, M.X., Mosher, J.C., and Leahy, R.M. (1999). A sensor-weighted overlapping-sphere head model and exhaustive head model comparison for MEG. Phys. Med. Biol. *44*, 423.

Inaba, N., and Kawano, K. (2014). Neurons in cortical area MST remap the memory trace of visual motion across saccadic eye movements. Proc. Natl. Acad. Sci. 111, 7825–7830.

Ioannides, A.A., Corsi-Cabrera, M., Fenwick, P.B.C., Portilla, Y. del R., Laskaris, N.A., Khurshudyan, A., Theofilou, D., Shibata, T., Uchida, S., Nakabayashi, T., et al. (2004). MEG Tomography of Human Cortex and Brainstem Activity in Waking and REM Sleep Saccades. Cereb. Cortex *14*, 56–72.

Ioannides, A.A., Fenwick, P.B., Pitri, E., and Liu, L. (2010). A step towards non-invasive characterization of the human frontal eye fields of individual subjects. Nonlinear Biomed. Phys. *4*, S11.

Joiner, W.M., Cavanaugh, J., and Wurtz, R.H. (2011). Modulation of shifting receptive field activity in frontal eye field by visual salience. J. Neurophysiol. *106*, 1179–1190.

Klein, A., Ghosh, S.S., Bao, F.S., Giard, J., Häme, Y., Stavsky, E., Lee, N., Rossa, B., Reuter, M., Chaibub Neto, E., et al. (2017). Mindboggling morphometry of human brains. PLoS Comput. Biol. *13*.

Kleiner, M., Brainard, D., Pelli, D., Ingling, A., Murray, R., and Broussard, C. (2007). What's new in psychtoolbox-3. Perception *36*, 1–16.

Klimesch, W. (2012). Alpha-band oscillations, attention, and controlled access to stored information. Trends Cogn. Sci. *16*, 606–617.

Kusunoki, M., and Goldberg, M.E. (2003). The Time Course of Perisaccadic Receptive Field Shifts in the Lateral Intraparietal Area of the Monkey. J. Neurophysiol. *89*, 1519–1527.

Kwong, K.K., Belliveau, J.W., Chesler, D.A., Goldberg, I.E., Weisskoff, R.M., Poncelet, B.P., Kennedy, D.N., Hoppel, B.E., Cohen, M.S., and Turner, R. (1992). Dynamic magnetic resonance imaging of human brain activity during primary sensory stimulation. Proc. Natl. Acad. Sci. U. S. A. 89, 5675–5679.

Lescroart, M.D., Kanwisher, N., and Golomb, J.D. (2016). No Evidence for Automatic Remapping of Stimulus Features or Location Found with fMRI. Front. Syst. Neurosci. 10.

Liebe, S., Hoerzer, G.M., Logothetis, N.K., and Rainer, G. (2012). Theta coupling between V4 and prefrontal cortex predicts visual short-term memory performance. Nat. Neurosci. *15*, 456–462.

Lin, F.-H., Witzel, T., Ahlfors, S.P., Stufflebeam, S.M., Belliveau, J.W., and Hämäläinen, M.S. (2006). Assessing and improving the spatial accuracy in MEG source localization by depthweighted minimum-norm estimates. NeuroImage *31*, 160–171.

Lisman, J.E., and Idiart, M.A. (1995). Storage of 7 +/- 2 short-term memories in oscillatory subcycles. Science 267, 1512–1515.

Lisman, J.E., and Jensen, O. (2013). The Theta-Gamma Neural Code. Neuron 77, 1002–1016.

Long, N.M., Burke, J.F., and Kahana, M.J. (2014). Subsequent memory effect in intracranial and scalp EEG. NeuroImage *84*, 488–494.

Medendorp, W.P., Kramer, G.F.I., Jensen, O., Oostenveld, R., Schoffelen, J.-M., and Fries, P. (2007). Oscillatory Activity in Human Parietal and Occipital Cortex Shows Hemispheric Lateralization and Memory Effects in a Delayed Double-Step Saccade Task. Cereb. Cortex *17*, 2364–2374.

Merriam, E.P., Genovese, C.R., and Colby, C.L. (2003). Spatial Updating in Human Parietal Cortex. Neuron *39*, 361–373.

Merriam, E.P., Genovese, C.R., and Colby, C.L. (2007). Remapping in Human Visual Cortex. J. Neurophysiol. *97*, 1738–1755.

Mirpour, K., and Bisley, J.W. (2012). Anticipatory Remapping of Attentional Priority across the Entire Visual Field. J. Neurosci. *32*, 16449–16457.

Mirpour, K., and Bisley, J.W. (2016). Remapping, Spatial Stability, and Temporal Continuity: From the Pre-Saccadic to Postsaccadic Representation of Visual Space in LIP. Cereb. Cortex N. Y. NY 26, 3183–3195.

Moon, S.Y., Barton, J.J.S., Mikulski, S., Polli, F.E., Cain, M.S., Vangel, M., Hämäläinen, M.S., and Manoach, D.S. (2007). Where left becomes right: a magnetoencephalographic study of sensorimotor transformation for antisaccades. NeuroImage *36*, 1313–1323.

Murakami, S., and Okada, Y. (2006). Contributions of principal neocortical neurons to magnetoencephalography and electroencephalography signals. J. Physiol. *575*, 925–936.

Nakamura, K., and Colby, C.L. (2002). Updating of the visual representation in monkey striate and extrastriate cortex during saccades. Proc. Natl. Acad. Sci. U. S. A. 99, 4026–4031.

Nasiotis, K., Clavagnier, S., Baillet, S., and Pack, C.C. (2017). High-resolution retinotopic maps estimated with magnetoencephalography. NeuroImage *145*, *Part A*, 107–117.

Neupane, S., Guitton, D., and Pack, C.C. (2016a). Two distinct types of remapping in primate cortical area V4. Nat. Commun. 7, 10402.

Neupane, S., Guitton, D., and Pack, C.C. (2016b). Dissociation of forward and convergent remapping in primate visual cortex. Curr. Biol. CB 26, R491-492.

Neupane, S., Guitton, D., and Pack, C.C. (2017). Coherent alpha oscillations link current and future receptive fields during saccades. Proc. Natl. Acad. Sci. *114*, E5979–E5985.

Niknam, K., Akbarian, A., Clark, K., Zamani, Y., Noudoost, B., and Nategh, N. (2019). Characterizing and dissociating multiple time-varying modulatory computations influencing neuronal activity. PLoS Comput. Biol. *15*.

Noh, E., Herzmann, G., Curran, T., and de Sa, V.R. (2014). Using single-trial EEG to predict and analyze subsequent memory. NeuroImage *84*, 712–723.

Ogawa, S., Lee, T.M., Kay, A.R., and Tank, D.W. (1990). Brain magnetic resonance imaging with contrast dependent on blood oxygenation. Proc. Natl. Acad. Sci. U. S. A. 87, 9868–9872.

Okada, Y.C., Lahteenmäki, A., and Xu, C. (1999). Experimental analysis of distortion of magnetoencephalography signals by the skull. Clin. Neurophysiol. *110*, 230–238.

Perry, G., Adjamian, P., Thai, N.J., Holliday, I.E., Hillebrand, A., and Barnes, G.R. (2011). Retinotopic mapping of the primary visual cortex – a challenge for MEG imaging of the human cortex. Eur. J. Neurosci. *34*, 652–661.

Pfurtscheller, G., and Lopes da Silva, F.H. (1999). Event-related EEG/MEG synchronization and desynchronization: basic principles. Clin. Neurophysiol. *110*, 1842–1857.

Poghosyan, V., and Ioannides, A.A. (2007). Precise mapping of early visual responses in space and time. NeuroImage *35*, 759–770.

Portin, K., and Hari, R. (1999). Human parieto-occipital visual cortex: lack of retinotopy and foveal magnification. Proc. R. Soc. B Biol. Sci. 266, 981–985.

Rolfs, M., and Szinte, M. (2016). Remapping Attention Pointers: Linking Physiology and Behavior. Trends Cogn. Sci. 20, 399–401.

Rolfs, M., Jonikaitis, D., Deubel, H., and Cavanagh, P. (2011). Predictive remapping of attention across eye movements. Nat. Neurosci. *14*, 252–256.

Schall, J.D., Morel, A., King, D.J., and Bullier, J. (1995). Topography of visual cortex connections with frontal eye field in macaque: convergence and segregation of processing streams. J. Neurosci. *15*, 4464–4487.

Shen, W., McKeown, C.R., Demas, J.A., and Cline, H.T. (2011). Inhibition to excitation ratio regulates visual system responses and behavior in vivo. J. Neurophysiol. *106*, 2285–2302.

Sommer, M.A., and Wurtz, R.H. (2006). Influence of the thalamus on spatial visual processing in frontal cortex. Nature *444*, 374–377.

Stanton, G.B., Bruce, C.J., and Goldberg, M.E. (1995). Topography of projections to posterior cortical areas from the macaque frontal eye fields. J. Comp. Neurol. *353*, 291–305.

Szinte, M., Jonikaitis, D., Rolfs, M., Cavanagh, P., and Deubel, H. (2016). Presaccadic motion integration between current and future retinotopic locations of attended objects. J. Neurophysiol. *116*, 1592–1602.

Szinte, M., Jonikaitis, D., Rangelov, D., and Deubel, H. (2018). Pre-saccadic remapping relies on dynamics of spatial attention. ELife 7, e37598.

Tadel, F., Baillet, S., Mosher, J.C., Pantazis, D., and Leahy, R.M. (2011). Brainstorm: A User-Friendly Application for MEG/EEG Analysis, Brainstorm: A User-Friendly Application for MEG/EEG Analysis. Comput. Intell. Neurosci. 2011, 2011, e879716.

Tadel, F., Bock, E., Niso, G., Mosher, J.C., Cousineau, M., Pantazis, D., Leahy, R.M., and Baillet, S. (2019). MEG/EEG Group Analysis With Brainstorm. Front. Neurosci. *13*.

Tolias, A.S., Moore, T., Smirnakis, S.M., Tehovnik, E.J., Siapas, A.G., and Schiller, P.H. (2001). Eye Movements Modulate Visual Receptive Fields of V4 Neurons. Neuron *29*, 757–767.

Umeno, M.M., and Goldberg, M.E. (1997). Spatial Processing in the Monkey Frontal Eye Field. I. Predictive Visual Responses. J. Neurophysiol. *78*, 1373–1383.

Umeno, M.M., and Goldberg, M.E. (2001). Spatial Processing in the Monkey Frontal Eye Field. II. Memory Responses. J. Neurophysiol. *86*, 2344–2352.

Vernet, M., Quentin, R., Chanes, L., Mitsumasu, A., and Valero-Cabré, A. (2014). Frontal eye field, where art thou? Anatomy, function, and non-invasive manipulation of frontal regions involved in eye movements and associated cognitive operations. Front. Integr. Neurosci. 8, 66.

Walker, M.F., Fitzgibbon, E.J., and Goldberg, M.E. (1995). Neurons in the monkey superior colliculus predict the visual result of impending saccadic eye movements. J. Neurophysiol. *73*, 1988–2003.

Wandell, B.A., Brewer, A.A., and Dougherty, R.F. (2005). Visual field map clusters in human cortex. Philos. Trans. R. Soc. Lond. B Biol. Sci. *360*, 693–707.

Wandell, B.A., Dumoulin, S.O., and Brewer, A.A. (2007). Visual field maps in human cortex. Neuron *56*, 366–383.

Wang, X., Fung, C.C.A., Guan, S., Wu, S., Goldberg, M.E., and Zhang, M. (2016). Perisaccadic Receptive Field Expansion in the Lateral Intraparietal Area. Neuron 0.

Winawer, J., and Witthoft, N. (2015). Human V4 and ventral occipital retinotopic maps. Vis. Neurosci. 32, E020.

Yao, T., Treue, S., and Krishna, B.S. (2016). An Attention-Sensitive Memory Trace in Macaque MT Following Saccadic Eye Movements. PLOS Biol. *14*, e1002390.

Yizhar, O., Fenno, L.E., Prigge, M., Schneider, F., Davidson, T.J., O'Shea, D.J., Sohal, V.S., Goshen, I., Finkelstein, J., Paz, J.T., et al. (2011). Neocortical excitation/inhibition balance in information processing and social dysfunction. Nature *477*, 171–178.

Zelinsky, G.J., and Bisley, J.W. (2015). The what, where, and why of priority maps and their interactions with visual working memory. Ann. N. Y. Acad. Sci. *1339*, 154–164.

Zirnsak, M., Steinmetz, N.A., Noudoost, B., Xu, K.Z., and Moore, T. (2014). Visual space is compressed in prefrontal cortex before eye movements. Nature *507*, 504–507.

Chapter 4 contains			
neurophysiology. It pro through intuitive pipeli			

# Chapter 4 - Integrated open-source software for multiscale electrophysiology

Konstantinos Nasiotis<sup>a,\*</sup>, Martin Cousineau<sup>a</sup>, François Tadel<sup>b</sup>, Adrien Peyrache<sup>a</sup>, Richard M. Leahy<sup>c</sup>, Christopher C. Pack<sup>a</sup>, Sylvain Baillet<sup>a</sup>

<sup>a</sup> Montreal Neurological Institute, McGill University, Montreal, QC, Canada

<sup>b</sup> Grenoble Institute of Neuroscience, Grenoble, France

<sup>c</sup> Signal & Image Processing Institute, University of Southern California, Los Angeles, USA

\* Correspondence: <u>konstantinos.nasiotis@mail.mcgill.ca</u>

#### 4.1 Abstract

The methods for electrophysiology in neuroscience have evolved tremendously over the recent years with a growing emphasis on dense-array signal recordings. Such increased complexity and augmented wealth in the volume of data recorded, have not been accompanied by efforts to streamline and facilitate access to processing methods, which too are susceptible to grow in sophistication. Moreover, unsuccessful attempts to reproduce peer-reviewed publications indicate a problem of transparency in science. This growing problem could be tackled by unrestricted access to methods that promote research transparency and data sharing, ensuring the reproducibility of published results.

Here, we provide a free, extensive, open-source software that provides data-analysis, data-management and multi-modality integration solutions for invasive neurophysiology. Users can perform their entire analysis through a user-friendly environment without the need of programming skills, in a tractable (logged) way. This work contributes to open-science, analysis standardization, transparency and reproducibility in invasive neurophysiology.

#### 4.2 Introduction

Invasive electrode recordings are a unique source of in-vitro and in-vivo neurophysiological data at high resolution in both space and time, recorded in relation to complex animal and human behavior. The complexity of this kind of data has increased in recent years, with the advent of increasingly dense multi-channel and multi-site electrode arrays. This evolution provides exciting opportunities to explore the relationship between local events, such as action potentials, and more global dynamics at the systems level, such as fluctuations in oscillatory network activity. At the same time, these multiscale explorations require different analytical methods from those traditionally used in the field.

Challenges in exploring high-dimensional spatio-temporal data sets are not specific to electrophysiology: they occur frequently in neuroimaging data, as scanners produce increasingly large volumes of data, which are often shared across multiple groups or research centres. In response, the brain imaging community has made significant strides in developing shared software platforms to harmonize analytical methods and to facilitate data sharing(Abraham et al., 2014; Gorgolewski et al., 2011; Gramfort et al., 2013b, 2014; Hanke et al., 2009; Tadel et al., 2011). Indeed, free, open-source software toolkits have been critical for facilitating training and augmenting research productivity. This approach has transferred to the field of scalp electrophysiology(Baillet et al., 2011), but as of yet it has not found widespread use in invasive neurophysiology (IN). Software tools do exist for specific segments of the IN data workflow, such as for spike detection and sorting and time-series analysis(Fee et al., 1996; Hazan et al., 2006; Hill et al., 2011; Mitra and Bokil, 2007; Oostenveld et al., 2011; Pachitariu et al., 2016b; Quiroga et al., 2004; Siegle et al., 2017), but they remain relatively specialized, some with limited support and documentation and most with restricted interoperability with other tools.

While we acknowledge significant efforts in harmonizing data formats for electrophysiology ((Rübel et al., 2019; Stead and Halford, 2016; Teeters et al., 2015), Neuroshare - http://neuroshare.sourceforge.net/index.shtml), it does seem that this field lags behind others in meeting the demands of recommended practices for data management and transparency(Gorgolewski and Poldrack, 2016; Larson and Moser, 2017). In this regard, well-supported software tools are required to produce analytical workflows that are validated, well-

documented and reproducible. Important components include data organization, review and quality control, verified implementations of signal extraction and decomposition methods, solutions for advanced visualization registered to anatomy, and sound approaches to machine learning and statistical inference. As in the brain imaging field, such tools would facilitate the reproducibility of published results and the dissemination of methods within and between research groups. They would also save considerable time and resources currently required to recode published methods. In addition, re-coding presents challenges in code verification relative to a published method, raising possible concerns about the validity of the end results and limiting the long-term value of the effort.

Here we deploy and share open-source software (called *Invasive Neurophysiology*-Brainstorm, or *IN-Brainstorm*) that integrates multiple aspects of data analysis for most modalities and signal types for basic electrophysiology: from single cells to distributed channel arrays, from spiking events to local field potentials, from ongoing recordings to event-related responses, and from in vitro preparations to free-behaving models. We also emphasize the importance of an extensive graphical interface for user-friendly access to advanced analytical methods, of flexible scripting features for high-performance computing, and of traceable code execution. The proposed tool is accompanied by extensive online documentation and support from a user community web forum.

This free application builds on the foundations of the *Brainstorm* platform(Tadel et al., 2011), which is well-established (21,000 user accounts), free open-source software for magnetoencephalography (MEG) and electroencephalography (EEG). Brainstorm can integrate multimodal data volumes in addition to scalp electrophysiology e.g., magnetic resonance imaging (MRI), CT-scans and functional near-infrared spectroscopy (fNIRS). It also features advanced source modeling for electrophysiological signals.

The IN-Brainstorm application provides a comprehensive suite that interoperates with other, more specific and constantly evolving IN tools available from the open-source community e.g., for performing spike sorting. The end result is a unique and expansive software toolkit that bridges across recording scales and data modalities, registers invasive neurophysiology with structural

anatomy data, and thereby delivers a unifying analytical environment to the neurophysiology research community.

# 4.3 Results

The IN-Brainstorm functionalities described here offer comprehensive solutions for data importation and analysis, including spike-sorting, extraction of local field potentials, and correlations among these measures across multiple channels. Importantly, thanks to an intuitive graphical user interface, no programming skills are required for accessing and using the advanced methods available, including for assembling and sharing advanced data analysis pipelines. A summary of these software features is provided in Table 1, and a schematic of the workflow enabled by the toolbox is shown in FIGURE 1.

The bedrock of the present developments is the Brainstorm platform. Brainstorm(Tadel et al., 2011) is written in Matlab (Matlab2008a and higher) and Java. It is therefore independent of the operating system (Windows, MacOS and Linux). Community code management is via <u>GitHub</u>. Users without access to a Matlab license can use a fully executable version of the application compiled for the above operating systems. Extensive documentation is freely available online, with specialized tutorials, datasets and videos (<a href="https://neuroimage.usc.edu/brainstorm/e-phys/Introduction">https://neuroimage.usc.edu/brainstorm/e-phys/Introduction</a>). A thorough comparison of Brainstorm and other open source toolboxes was published recently(Unakafova and Gail, 2019).

In the following sections, we describe a broad spectrum of analysis options for multiscale electrophysiology that are enabled by IN-Brainstorm and illustrate these features with the processing of an example raw data file.

#### 4.3.1 Importing, reviewing and pre-processing raw data

#### 4.3.1.1 Raw data importation

Data to be analyzed must first be imported into the software. Brainstorm can read raw electrophysiology data from 80 different file formats. We have added new data formats specific to single- and multi-unit electrophysiology, including Plexon (.plx, .pl2), Blackrock (.nsX), Ripple (.nsX), Intan (.rhd, .rhs), Tucker Davis Technologies, and Neurodata Without Borders (.nwb). New formats can be added on demand. Raw data can also be read directly from ASCII and basic binary data formats, with header file parameters easily specified from a GUI.

#### 4.3.1.2 Data review

Raw files of continuous data from chronic preparations can be voluminous due to hours-long durations, tens of kilo-Hertz sampling rate and simultaneous recording from multi-channel electrode arrays. Hence loading such large raw files at once into computer memory can be impractical. For this reason, we have implemented efficient data review solutions of the raw signals, that load portions of the raw data on the fly depending on the visualization parameters set by the user (e.g., virtual page length, selection of a subset of channels or montages for review, keyboard and mouse shortcuts for navigating and marking events).

Task events (e.g., stimulus types and presentation times, behavioral responses) and ancillary recordings (electrooculograms, electrocardiogram, eye and body movements, video recordings of behaviour, etc.) are readily registered to the electrophysiological data in IN-Brainstorm, for multimodal data review, quality control and event-related processing. We emphasize that when a raw file is reviewed, the physical data is not duplicated as a Brainstorm file. Instead, the header of the original data file is automatically parsed to extract metadata, such as channel parameters, sampling rate, time stamps, event codes, etc.

Figure 2 (left) shows an example of IN-Brainstorm display for data review, including sub-menus for displaying and navigating through files and events. The right panel shows an example of raw data collected with a Plexon MAP system and a 32-channel linear electrode implanted in cortical areas MT and MST of a non-human primate. The animal maintained fixation during the presentation of a motion stimulus comprising of dots that translated in 8 different directions.

The red line in the figure shows the time of a "Stim On O" event, extracted from the data. Spikes detected online (labelled as Spikes Channel) were extracted directly from the raw file contents by IN-Brainstorm, with automatic registration to the data time series.

The bottom right panel of Figure 2 shows a selection of 4 channels temporally aligned with the top figure. The spikes from a neuron that was isolated on the first electrode are marked with green circles at the top of the full time-series displayed in the top panel. Users can browse the raw traces using point-and-click GUI and a series of keyboard shortcuts. On-the-fly bandpass and notch filtering can be applied to the signals.

#### 4.3.1.3 Quality control & data pre-processing

Starting from the kind of raw data shown in Figure 2, users can easily navigate through the recordings and experimental trials and events for quality control. Data segments, channels and entire trials can be marked as "bad" and excluded from further analyses using automatic processes or based on user evaluations.

The IN-Brainstorm pre-processing toolkit features solutions for adjustments of recording baseline, data resampling and frequency filtering (with linear phase filters). Additionally, detection and attenuation of artifacts (e.g., heartbeats, eye and body movements, stimulation and juice artifacts) can be achieved with principal(Uusitalo and Ilmoniemi, 1997) or independent component analysis(Bell and Sejnowski, 1995; Cardoso, 1999). Finally, combining sensor data with the actual geometry of the recording array(s) enables many 2-D and 3-D visualization possibilities for timeseries and realistic topographical plots, as illustrated further below.

#### 4.3.2 Spike detection and spike sorting

Following the importation and preprocessing of data, IN data is often processed to extract spiking events from single or multiple neurons. This entails detecting spike occurrences and classifying these events according to their respective neural sources (Quiroga, 2007). Most data acquisition systems feature online spike detection and sorting. These online events can be imported directly into IN-Brainstorm with the corresponding raw recordings. Yet, usual IN practice is to refine spike

classification with a two-step procedure consisting of 1) unsupervised clustering, which automatically assigns each spike to a neural source based on waveform features, then 2) supervised clustering, which requires manual reviewing and editing of the labels from unsupervised clustering and the elimination of spurious spike events.

For IN-Brainstorm, we have enabled the direct interoperability with a selection of existing and openly-available spike-sorting toolkits: *Waveclus*(Quiroga et al., 2004), *UltraMegaSort2000*(Fee et al., 1996; Hill et al., 2011) and *Kilosort*(Pachitariu et al., 2016b). Those packages can be downloaded and installed automatically, in a completely transparent procedure. Sequentially, these tools are called by and interact with IN-Brainstorm without programming interventions from users.

#### 4.3.2.1 Unsupervised spike sorting

Figure 3 (left) shows IN-Brainstorms' GUI for unsupervised spike-sorting. Raw files are dragged and dropped into the GUI process box before a spike-sorting tool is selected from the IN-Brainstorm toolkit. Next, spike events are detected on each electrode and classified according to their putative neuronal generators.

The unsupervised spike events produced overwrite the online counterparts that were detected during data acquisition. The output of the spike-sorting process (Figure 3 Box 1) is automatically registered to and accessible from the IN-Brainstorm database and linked to the corresponding raw file. The spike events are labelled in a principled manner (per channel and source cell number – Figure 3 Box 2).

#### 4.3.2.2 Supervised spike sorting

As *WaveClus* and *UltraMegaSort2000* have built-in supervised spike sorting graphical user interfaces, we synchronized their GUIs with IN-Brainstorm's. For *Kilosort*, we developed specific GUI bridges via *Klusters*(Hazan et al., 2006). The user-selected supervised clustering tool is called from Brainstorm's main window after an unsupervised spike-sorted file is selected (Figure 4a). The user then switches to the GUI of the selected supervised spike clustering tool (Figure 4b-d). Once

supervised spike clustering is complete, the spike events are updated accordingly and registered into the software's file system. Double-clicking on the link to the raw data file lets the user review the updated spike events along with the raw electrophysiological traces as shown in Figure 2 (Right).

Spike events and categories from other spike-sorting tools can be readily imported as Brainstorm events, following the procedure described in the online documentation (https://neuroimage.usc.edu/brainstorm/e-phys/ConvertToBrainstormEvents).

#### 4.3.3 Extraction of local field potentials

In addition to spiking activity, IN recordings yield local field potentials (LFPs), which provide direct measures of the summed post-synaptic electrical activity in the vicinity of recording electrodes(Legatt et al., 1980). These can be useful as a complement to spiking activity or a surrogate for some aspects of neural activity (e.g., (Mineault et al., 2013)), provided that LFP traces can reliably be filtered and separated from spike waveforms (Zanos et al., 2011).

Figure 5a shows the IN-Brainstorm's GUI for extracting LFP traces from raw recordings. The application features efficient tools to remove spike traces (Zanos et al., 2011), to perform antialiasing bandpass filtering and to down-sample the raw data. The de-spiking method proposed by Zanos et al. (Zanos et al., 2011) increases the accuracy of subsequent spike-field coherence measures and of spike-triggered average signals.

The resulting LFP traces and experimental events are automatically registered in IN-Brainstorm's data repository for further review and analysis with a vast library of tools and pipelines – as described below – or for easy exportation to other software or plain files.

LFP extraction produces a new IN-Brainstorm down-sampled time-series binary file (Figure 5b) with all the corresponding metadata, such as channel description (e.g., electrode labels and locations), and spike and experimental events. This file is easily sharable among researchers since its size is typically ~20-30 times smaller than the original raw file. Figure 5C shows a segment of the LFP file created.

#### 4.3.4 Epoching

Once the relevant neural signals (LFPs and spikes) have been extracted from the raw data, they can be divided according to experimental epochs. Epochs are typically comprised of experimental trials, with the time window selection defined around a stimulation or behavioral event of interest. These can be imported directly into the IN-Brainstorm file system.

To illustrate these functions, we make use of the example visual cortex recording described previously (Figure 2). The experiment involved presentations of moving stimuli while the animal maintained fixation; we defined the relevant epochs as segments of [-500, 1000] ms around the onset of each visual stimulus (Figure 6 Left). In total we considered 8 different directions of the visual stimulus moving pattern; each stimulus condition was repeated 4 times (one condition was repeated for 96 trials for usage in the raster plot, and noise correlation functions). Imported trials to the database are shown in (Figure 6 – Right).

The following analysis steps can then be applied on the epoched trials.

#### 4.3.5 Analysis of individual LFP signals

LFP traces can be analyzed using Brainstorm's extensive library originally developed for EEG and MEG research(Tadel et al., 2011). We show in Table 1 a list of the main data processing categories that are available for LFP analysis. There is extensive online documentation, accompanied by data files, that describes in detail the methods and practices of LFP signal analysis (http://neuroimage.usc.edu/brainstorm).

We briefly provide below a few examples of these functions and their implementation in IN-Brainstorm.

#### 4.3.5.1 Time-frequency decompositions

Having extracted the LFP signal and defined an appropriate analysis epoch, one can compute the LFP power at different frequencies and at different times relative to a stimulus event. Such information is often used to infer stimulus selectivity, anatomical sources of input, and other

factors that are not necessarily apparent in spiking activity(Buzsáki, 2006; Fries et al., 2008; Pesaran et al., 2002; Wilke et al., 2006; Womelsdorf et al., 2006).

IN-Brainstorm provides functionality for spectral and time-frequency decompositions, which can be derived using power spectrum density estimates, Hilbert or wavelet transforms. An example time-frequency decomposition (wavelet) is shown in Figure 7a for the example LFP data corresponding to a single stimulus condition and epoch that shows strong alpha and beta responses after stimulation. The wavelet decomposition was z-scored with respect to a prestimulus baseline [-500:-100] ms.

#### 4.3.5.2 LFP-LFP signal analysis

LFP signals from multichannel recordings can be analyzed to detect occurrences of various forms of signal similarities in the time or frequency domain. These measures are often interpreted as representing functional connectivity between different sites(Fries, 2005; Fries et al., 2002, 2008; Womelsdorf et al., 2006). IN-Brainstorm provides support for widely-used measures based on amplitude or phase statistics as indicators of possible interregional brain interactions (coherence, phase-locking values, bandlimited amplitude envelope correlations, phase-transfer entropy) and parametric models (estimates of time- or frequency-domain Granger causality). Advanced measures of interdependence between oscillatory components of polyrhythmic brain activity can be derived with phase-amplitude coupling (PAC) estimation tools(Canolty et al., 2006; Samiee and Baillet, 2017). An example estimation of coherence among all combinations of electrodes is shown in Figure 7b for a single stimulus condition and epoch. The bimodal pattern that emerges (high coherence among some channels and low coherence among others) is an indication of the transition of the linear probe across neighboring cortical areas, from MT (electrodes 1:13) to MST (21:32).

#### 4.3.6 Analysis of individual neuron spiking activity

Spikes are registered in IN-Brainstorm as events; the corresponding features are 1) the time of occurrence and 2) a label for distinguishing between neuronal sources. We provide several features for visualization of epoched spiking data.

#### 4.3.6.1 Raster plot – Peristimulus Time Histograms

Raster plots and peristimulus time histograms (PSTH), are routinely used to visualize the relations between neuronal firing and a stimulus event or a behavioral response.

We provide three methods for visualizing spiking activity with IN-Brainstorm:

The first method (raster plot) shows the spiking data as trial vs. time for each neuron. Similarly, the second method (PSTH) shows the average binned firing rate for each neuron, along its 95% confidence intervals. Raster plots and PSTHs of spiking rates are displayed after interactive selection of the cell to be reviewed. Figure 8a shows the raster plot of the first neuron detected from contact AD01 (top), and its equivalent PSTH with 10-ms binning (bottom). The PSTH of the neuron's firing rate from 96 trials of a single condition revealed a stimulus-onset-to-maximum-firing latency of about 150 ms.

The third method is embedded within the topographical plots section as shown below.

#### 4.3.6.2 Tuning curves

Tuning curves capture the relationship between an experimental variable (e.g., the orientation of a visual stimulus) and a scalar measure of neural activity (e.g., a single neuron's trial-averaged firing rate).

Tuning curves are readily produced from continuous data files that contain the event markers of interest to the study. Tuning curves are displayed with IN-Brainstorm after manual assignment of the order of the experimental conditions (x-axis), the selection of the neurons to be displayed, and the selection of the time window of interest for reporting spiking activity. A separate tuning curve figure is produced for each neuron selected.

We selected the events and individual neurons previously identified from spike sorting via IN-Brainstorm's GUI. Figure 8b shows the tuning curves of one example neuron (labeled as "Spikes Channel ADO7 |1|") for the 8 different conditions (Stim On -3/4 pi, Stim On -2/4 pi etc.) of the motion stimuli, and its 95% confidence intervals. The tuning curve shows the preference of this neuron for stimuli moving in the right direction (Stim On -1/4 pi condition).

#### 4.3.6.3 Topographical plots

When multichannel recording devices are used, neurophysiology data can be shown as topographically registered to structural anatomy. IN-Brainstorm can show neuronal firing at the 3-D locations of the recording probes/arrays. To illustrate this feature, we used a separate dataset that was collected from two 96-channel Utah arrays and one 32-linear probe(Krause et al., 2017). A structural T1-weighted MRI volume was acquired preoperatively. The head and brain surface envelopes were segmented with Freesurfer(Fischl et al., 2001) and directly imported in IN-Brainstorm. The electrode contact locations were co-registered to the 3-D anatomical volume by specifying the distance of the electrodes along the probe and locating the tip of the probe and the entry point through the skull, using Brainstorm's MRI volume viewer.

Neuronal firing was binned in 10-ms segments and displayed on the animal's anatomy as shown in Figure 9a (a single bin is displayed in the figure). This figure shows IN-Brainstorm's ability to overlay the segmented cortical surface, MRI orthogonal slices, the implanted devices with actual geometry, and color-coded displays of raw or processed electrophysiology data (here instantaneous firing rates). Figure 9b shows a zoomed-in version of Figure 9a over the Utah array implanted in the prefrontal cortex.

#### 4.3.7 Spike-spike analysis: Noise correlations

While tuning curves capture neuronal sensitivity to stimulus properties, the fidelity of a population code is thought to be limited by noise that is common across neurons (Zohary et al., 1994); for example, neurons would be noise correlated if for each stimulus their activities are correlated (Eyherabide and Samengo, 2013). Such noise correlations are typically quantified as the

Pearson correlation coefficient between the firing rates of two neurons across trials. Such correlations strongly influence the accuracy of population coding(Abbott and Dayan, 1999;

Averbeck et al., 2006; Liu et al.; Panzeri et al., 1999; Sompolinsky et al., 2001).

Noise correlation statistics are displayed with IN-Brainstorm from the correlation of the spike

trains that each neuron elicited within a given epoch, for all neuronal combinations. The end result

is a nxn matrix (with n the number of unique neurons that produced spikes during the selected

trials) that shows noise correlation estimates between the selected neurons.

Figure 8c shows the noise correlation profile across the 32-channel array of the example dataset,

for 53 unique neurons that elicited spikes across all trials at the 8 conditions of presentation of the

moving stimulus in the original data set from Figure 2. Spikes included in the correlation

computations were selected in the [0,300]-ms time range of each trial.

The computed noise correlation showed 2 pairs of neurons with abnormally high noise correlation

(above 0.8). After further inspection, it was revealed that this was due to the fact that the spike-

sorter that was used was not taking into account the relative position of the electrodes, and the

same neurons were picked up from neighbouring channels:

Neurons: AD01 | 1 | - AD02 | 2 | and AD08 | 1 | - AD09 | 1 | were the same neuron.

4.3.8 Spike-LFP analysis

Spikes are local events, reflecting outputs from individual neurons. LFPs in contrast can capture

activity over regions, including subthreshold post-synaptic activity, and therefore reflect the state

of a broader network (Cui et al., 2016). There is considerable interest in relating the two types of

signals for estimating the dependence of spiking activity on the broader context in which the

neuron is embedded.

4.3.8.1 Spike-field coherence

Spike-field coherence (SFC) estimates the consistency between the time occurrence of spike trains

and the phase of co-localized LFP cycles as a function of frequency (Arce-McShane et al., 2018).

108

SFC can also be used to evaluate synchronized activity between distant brain regions, as a marker of neuronal communication(Fries, 2005; Gregoriou et al., 2009; Liebe et al., 2012; Singer, 1999; Womelsdorf et al., 2007). IN-Brainstorm features the spike-field coherence estimator proposed by Fries(Fries et al., 2001). The user can derive SFC estimates for each GUI-selected neuron, for all electrodes and frequencies of interest.

Figure 8d shows SFC up to 50 Hz between a single neuron detected at channel AD07 of the example data set and the LFP traces at all the 32 channels of the probe. The time window selected around the spiking events was [-150, 150] ms. The horizontal white line indicates the electrode where the neuron was detected.

#### 4.3.8.2 Spike-triggered average of the LFP

Spike-triggered averaging (STA) of the LFP reveals how neuronal spiking is related to the dynamics of proximal or distant LFPs(Jin et al., 2008; Nauhaus et al., 2009; Ray and Maunsell, 2011). STA proceeds with trial averaging of LFP traces time-locked to a designated neuron's spike events, followed by normalization with the total spike count.

Analogous to spike-field coherence, STA is computed over a user-selected time window around each spiking event. STA scores are per neuron, showcasing the average LFP amplitude around the occurrence of the spikes of each neuron. STA can be visualized on topological 2-D representations of the recording array, to reveal time-locked associations between neuronal spiking activity and local or remote LFP recordings.

Figure 8e shows the STA time-locked to the firing of the first neuron detected by electrode AD01 across trials and conditions. The topographical 2-D plot is produced with IN-Brainstorm using multidimensional scaling of the actual 3-D location and geometry of the implanted probe. The LFP epoch around spike event was [-150,150] ms.

#### 4.3.9 Statistical inference and machine learning

Once measures have been extracted from spiking or LFP data, tools to conduct inferential statistical analysis in the multiple dimensions of electrophysiological data (space, time, frequency, connectivity) are available from Brainstorm's library.

Parametric (one- and two-sample tests) and nonparametric permutation tests, descriptive and distribution statistics from histograms (Q-Q plot and Shapiro-Wilk test for data normality) are available. Here too, the software architecture emphasises interoperability with other toolkits, for expanded resources. For instance, multidimensional and nonparametric cluster statistics can be run on LFP and time-frequency data, from Brainstorm, via calls to FieldTrip(Oostenveld et al., 2011).

In addition, statistical learning tools for decoding and multivariate pattern analysis (MVPA) are also available (see e.g. Cichy et al., Cichy et al., 2014)). The Brainstorm library also includes support vector machine (SVM) and linear discriminant analysis (LDA) classification of LFP time series based on experimental events and conditions.

#### 4.3.10 Additional features

#### 4.3.10.1 Processing Power

Hardware acceleration in the processing of long recordings is enabled by Matlab's standard parallel computing (e.g., multi-core) features, which are controlled directly from Brainstorm's GUI. Flexible management of memory resources is also accessible to users, with the specification of the amount of RAM allocated to data manipulations while executing the LFP extraction process. Moreover, GPU acceleration computations are enabled through Kilosort for the spike-sorting step.

#### 4.3.10.2 Data management

Generally speaking, formal data management plans are seldom adopted by electrophysiology labs. Instead, the handling of data is typically project-based, with trainees managing their individual data collection and analyses until publication. When they move on to another project or to the next step of their career, they frequently leave data, analysis pipelines and results behind, with minimal documented organization for sustainability and knowledge transfer. This limits the long-

term value of data and negatively impacts the reproducibility and verification of research results (Baker, 2016). Brainstorm has tools to improve and facilitate data management: data is hierarchically organized by Studies, followed by Subjects/Samples and (experimental) Conditions, which point to data elements such as links to raw data files, single-trial epochs, sample statistics, and other derivatives: power spectra, wavelet decompositions, measures of cross-frequency coupling and inter-regional connectivity, etc. As with all features in the application, user interactions with Brainstorm's data organization are facilitated both by the application's GUI and direct access via scriptable functions using Matlab code.

Another important aspect of Brainstorm is its capacity for importing entire data repositories at once, with associated metadata, when those datasets are organized according to the emergent Brain Imaging Data Structure (BIDS). Originally driven by the neuroimaging community, BIDS is a grassroots effort to harmonize data organization and documentation (Gorgolewski et al., 2016). BIDS has recently been extended to MEG electrophysiology(Niso et al., 2018) and is presently integrating EEG(Pernet et al.), and invasive neurophysiology(Holdgraf et al.).

#### 4.3.10.3 Batch processing

The software has a specific GUI for assembling data processing pipelines in an intuitive manner, choosing elementary processes from the (IN-)Brainstorm library and assembling them together into a logical progression along the workflow. These pipelines enable the reproduction of any data workflow with a click of a button. They can also be shared in Matlab format with collaborators or the entire user community. The Matlab code for pipelines can also be generated automatically by Brainstorm e.g., for execution in headless (no GUI) mode on high-performance computing servers and cloud resources.

#### 4.4 Discussion

We provide a free, extensive open-source software application for invasive electrophysiology. IN-Brainstorm is built on the foundations of Brainstorm, which was originally designed for human multimodal electrophysiology and imaging. IN-Brainstorm supports multiple data formats of raw signals from a variety of acquisition systems. The recorded traces and their LFP versions can be reviewed, quality-controlled and processed within a unique analytical environment, with easy GUI interactions, rich visualization, intuitive pipeline editing for scripting and sharing. We have built bridges for IN-Brainstorm to interoperate seamlessly with established, free spike-sorting tools.

A specific emphasis was put on providing versatile solutions for multidimensional data visualization, including 2-D and 3-D topographical plots registered to structural anatomy from coregistered MRI data. Source modeling of array data is also available using boundary element modeling of head and brain tissues(Gramfort et al., 2010; Kybic et al., 2005) and a variety of source modeling techniques available in Brainstorm(Baillet et al., 2001). Videos synchronised to electrophysiological traces can also be imported and visualized simultaneously in synchrony, for marking behavioral events.

The software is supported by an expansive online documentation (with tutorial data) and online user forum. The active Brainstorm user community contributes to an efficient peer-reviewing/debugging process, and daily updates deliver bug fixes and software improvements that are readily available to the users.

With IN-Brainstorm, electrophysiologists are provided a free, integrated software environment that promotes and facilitates harmonized principles of data management, methods, documentation, code verification and reproducibility of data analyses. Such practical and user-friendly tools also accelerate the education of electrophysiologist trainees and promotes the adoption and expansion of data harmonization efforts, such as BIDS and *Neurodata Without Borders*.

Every instance of data processing is logged, with the filenames of the data used and time stamps of execution. These simple, yet powerful features document the provenance of data derivatives

and analysis results. Custom IN analysis pipelines assembled for elementary processing blocks of the software's library can be shared with collaborators, publishers and the scientific community. Pipelines are constructed via the GUI and saved as Matlab files. The open-source code of IN-Brainstorm is thoroughly documented, verifiable and can benefit from contributions from any user via GitHub. Sharing is further encouraged and facilitated by Brainstorm's data organization in Studies, which can be zipped for archiving, exportation (e.g., as a BIDS repository) or importation into the Brainstorm environment of a collaborator. Batch processing of multiple data volumes is automated, thanks to the systematic organization of Brainstorm's file system and can be executed on high-performance computing servers without requiring GUI interactions.

For all these reasons, we believe that IN-Brainstorm responds to an unmet need of the electrophysiology community. By providing a unique environment with a common set of analytical tools, the application also provides a unique bridge between recording scales, data types and researchers, and additionally, between the methods used in human, animal and slice preparations. It also represents a scalable framework to developments and integration of existing or future tools and data formats for the entire field of electrophysiology.

# 4.5 Methods

#### 4.5.1 Code availability

The toolbox can be acquired as part of Brainstorm's GitHub repository: <a href="https://github.com/brainstorm-tools/brainstorm3">https://github.com/brainstorm-tools/brainstorm3</a>

# 4.6 Data Availability

The dataset that was used for showcasing this toolbox, is available as part of the tutorial for the toolbox's features: https://neuroimage.usc.edu/brainstorm/e-phys/Introduction

# 4.7 Acknowledgements

We are grateful to Dr. Matthew Krause, Dr. Pedro Vieira, Dr. Christos Gkogkas, Bennet Csorba, Nardin Nakhla and Yavar Korkian for providing datasets. Dr. Shahab Bakhtiari for his input in data analysis. We also thank Elizabeth Bock for early testing of the tools featured. We also extend acknowledgments to Dr. Michael Petrides, Sebastien Tremblay and Veronika Zlatkina for their input.

This work was supported by a Molson Neuro-Engineering Scholarship (the Molson Foundation) to K.N., by grants from the National Science and Engineering Research Council of Canada (NSERC 436355-13 to S.B. and 341534-2012 to C.C.P.), the National Institutes of Health (NIH-1R01EB026299) and the Brain Canada Foundation (PSG15-3755) to S.B.

# 4.8 Author Contributions

K.N. designed, coded and made the toolbox compatible to Brainstorm. M.C. and F.T. refined the code for Brainstorm compatibility. C.P., S.B., A.P. and R.L. provided input to manuscript and toolbox utilities. K.N., C.P. and S.B. wrote the paper.

# 4.9 Competing Interests

No competing interests declared by the authors.

#### 4.10 References

Abbott, L.F., and Dayan, P. (1999). The effect of correlated variability on the accuracy of a population code. Neural Comput. 11, 91–101.

Abraham, A., Pedregosa, F., Eickenberg, M., Gervais, P., Mueller, A., Kossaifi, J., Gramfort, A., Thirion, B., and Varoquaux, G. (2014). Machine learning for neuroimaging with scikit-learn. Front. Neuroinformatics 8.

Arce-McShane, F., Sessle, B.J., Ross, C.F., and Hatsopoulos, N.G. (2018). Primary sensorimotor cortex exhibits complex dependencies of spike-field coherence on neuronal firing rates, field power, and behavior. J. Neurophysiol.

Averbeck, B.B., Latham, P.E., and Pouget, A. (2006). Neural correlations, population coding and computation. Nat. Rev. Neurosci. 7, 358–366.

Baillet, S., Mosher, J.C., and Leahy, R.M. (2001). Electromagnetic brain mapping. IEEE Signal Process. Mag. 18, 14–30.

Baillet, S., Friston, K., and Oostenveld, R. (2011). Academic Software Applications for Electromagnetic Brain Mapping Using MEG and EEG.

Baker, M. (2016). 1,500 scientists lift the lid on reproducibility. Nat. News 533, 452.

Bell, A.J., and Sejnowski, T.J. (1995). An information-maximization approach to blind separation and blind deconvolution. Neural Comput. 7, 1129–1159.

Buzsáki, G. (2006). Rhythms of the Brain (Oxford University Press).

Canolty, R.T., Edwards, E., Dalal, S.S., Soltani, M., Nagarajan, S.S., Kirsch, H.E., Berger, M.S., Barbaro, N.M., and Knight, R.T. (2006). High Gamma Power Is Phase-Locked to Theta Oscillations in Human Neocortex. Science 313, 1626–1628.

Cardoso, J.F. (1999). High-order contrasts for independent component analysis. Neural Comput. 11, 157–192.

Cichy, R.M., Pantazis, D., and Oliva, A. (2014). Resolving human object recognition in space and time. Nat. Neurosci. 17, 455.

Cui, Y., Liu, L.D., McFarland, J.M., Pack, C.C., and Butts, D.A. (2016). Inferring Cortical Variability from Local Field Potentials. J. Neurosci. Off. J. Soc. Neurosci. 36, 4121–4135.

Eyherabide, H.G., and Samengo, I. (2013). When and Why Noise Correlations Are Important in Neural Decoding. J. Neurosci. 33, 17921–17936.

Fee, M.S., Mitra, P.P., and Kleinfeld, D. (1996). Automatic sorting of multiple unit neuronal signals in the presence of anisotropic and non-Gaussian variability. J. Neurosci. Methods 69, 175–188.

Fischl, B., Liu, A., and Dale, A.M. (2001). Automated manifold surgery: constructing geometrically accurate and topologically correct models of the human cerebral cortex. IEEE Trans. Med. Imaging 20, 70–80.

Fries, P. (2005). A mechanism for cognitive dynamics: neuronal communication through neuronal coherence. Trends Cogn. Sci. 9, 474–480.

Fries, P., Reynolds, J.H., Rorie, A.E., and Desimone, R. (2001). Modulation of Oscillatory Neuronal Synchronization by Selective Visual Attention. Science 291, 1560–1563.

Fries, P., Schröder, J.-H., Roelfsema, P.R., Singer, W., and Engel, A.K. (2002). Oscillatory neuronal synchronization in primary visual cortex as a correlate of stimulus selection. J. Neurosci. Off. J. Soc. Neurosci. 22, 3739–3754.

Fries, P., Womelsdorf, T., Oostenveld, R., and Desimone, R. (2008). The Effects of Visual Stimulation and Selective Visual Attention on Rhythmic Neuronal Synchronization in Macaque Area V4. J. Neurosci. 28, 4823–4835.

Gorgolewski, K.J., and Poldrack, R.A. (2016). A Practical Guide for Improving Transparency and Reproducibility in Neuroimaging Research. PLOS Biol. 14, e1002506.

Gorgolewski, K., Burns, C.D., Madison, C., Clark, D., Halchenko, Y.O., Waskom, M.L., and Ghosh, S.S. (2011). Nipype: A Flexible, Lightweight and Extensible Neuroimaging Data Processing Framework in Python. Front. Neuroinformatics 5.

Gorgolewski, K.J., Auer, T., Calhoun, V.D., Craddock, R.C., Das, S., Duff, E.P., Flandin, G., Ghosh, S.S., Glatard, T., Halchenko, Y.O., et al. (2016). The brain imaging data structure, a format for organizing and describing outputs of neuroimaging experiments. Sci. Data 3, 160044.

Gramfort, A., Papadopoulo, T., Olivi, E., and Clerc, M. (2010). OpenMEEG: opensource software for quasistatic bioelectromagnetics. Biomed. Eng. OnLine 9, 45.

Gramfort, A., Luessi, M., Larson, E., Engemann, D.A., Strohmeier, D., Brodbeck, C., Goj, R., Jas, M., Brooks, T., Parkkonen, L., et al. (2013). MEG and EEG data analysis with MNE-Python. Front. Neurosci. 7.

Gramfort, A., Luessi, M., Larson, E., Engemann, D.A., Strohmeier, D., Brodbeck, C., Parkkonen, L., and Hämäläinen, M.S. (2014). MNE software for processing MEG and EEG data. NeuroImage 86, 446–460.

Gregoriou, G.G., Gotts, S.J., Zhou, H., and Desimone, R. (2009). High-Frequency, Long-Range Coupling Between Prefrontal and Visual Cortex During Attention. Science 324, 1207–1210.

Hanke, M., Halchenko, Y.O., Sederberg, P.B., Olivetti, E., Fründ, I., Rieger, J.W., Herrmann, C.S., Haxby, J.V., Hanson, S.J., and Pollmann, S. (2009). PyMVPA: a unifying approach to the analysis of neuroscientific data. Front. Neuroinformatics 3.

Hazan, L., Zugaro, M., and Buzsáki, G. (2006). Klusters, NeuroScope, NDManager: a free software suite for neurophysiological data processing and visualization. J. Neurosci. Methods 155, 207–216.

Hill, D.N., Mehta, S.B., and Kleinfeld, D. (2011). Quality metrics to accompany spike sorting of extracellular signals. J. Neurosci. Off. J. Soc. Neurosci. 31, 8699–8705.

Holdgraf, C., Appelhoff, S., Bickel, S., Bouchard, K., D'Ambrosio, S., David, O., Devinsky, O., Dichter, B., flinker, adeen, Foster, B., et al. BIDS-iEEG: an extension to the brain imaging data structure (BIDS) specification for human intracranial electrophysiology.

Jin, J.Z., Weng, C., Yeh, C.-I., Gordon, J.A., Ruthazer, E.S., Stryker, M.P., Swadlow, H.A., and Alonso, J.-M. (2008). On and off domains of geniculate afferents in cat primary visual cortex. Nat. Neurosci. 11, 88–94.

Krause, M.R., Zanos, T.P., Csorba, B.A., Pilly, P.K., Choe, J., Phillips, M.E., Datta, A., and Pack, C.C. (2017). Transcranial Direct Current Stimulation Facilitates Associative Learning and Alters Functional Connectivity in the Primate Brain. Curr. Biol. 27, 3086-3096.e3.

Kybic, J., Clerc, M., Abboud, T., Faugeras, O., Keriven, R., and Papadopoulo, T. (2005). A common formalism for the Integral formulations of the forward EEG problem. IEEE Trans. Med. Imaging 24, 12–28.

Larson, M.J., and Moser, J.S. (2017). Rigor and replication: Toward improved best practices in human electrophysiology research. Int. J. Psychophysiol. 111, 1–4.

Legatt, A.D., Arezzo, J., and Vaughan, H.G. (1980). Averaged multiple unit activity as an estimate of phasic changes in local neuronal activity: effects of volume-conducted potentials. J. Neurosci. Methods 2, 203–217.

Liebe, S., Hoerzer, G.M., Logothetis, N.K., and Rainer, G. (2012). Theta coupling between V4 and prefrontal cortex predicts visual short-term memory performance. Nat. Neurosci. 15, 456–462.

Liu, L.D., Haefner, R.M., and Pack, C.C. A neural basis for the spatial suppression of visual motion perception. ELife 5.

Mineault, P.J., Zanos, T.P., and Pack, C.C. (2013). Local field potentials reflect multiple spatial scales in V4. Front. Comput. Neurosci. 7, 21.

Mitra, P., and Bokil, H. (2007). Observed Brain Dynamics (Oxford; New York: Oxford University Press).

Nauhaus, I., Busse, L., Carandini, M., and Ringach, D.L. (2009). Stimulus contrast modulates functional connectivity in visual cortex. Nat. Neurosci. 12, 70–76.

Niso, G., Gorgolewski, K.J., Bock, E., Brooks, T.L., Flandin, G., Gramfort, A., Henson, R.N., Jas, M., Litvak, V., T. Moreau, J., et al. (2018). MEG-BIDS, the brain imaging data structure extended to magnetoencephalography. Sci. Data 5, 180110.

Oostenveld, R., Fries, P., Maris, E., and Schoffelen, J.-M. (2011). FieldTrip: Open Source Software for Advanced Analysis of MEG, EEG, and Invasive Electrophysiological Data.

Pachitariu, M., Steinmetz, N.A., Kadir, S.N., Carandini, M., and Harris, K.D. (2016). Fast and accurate spike sorting of high-channel count probes with KiloSort. In Advances in Neural Information Processing Systems 29, D.D. Lee, M. Sugiyama, U.V. Luxburg, I. Guyon, and R. Garnett, eds. (Curran Associates, Inc.), pp. 4448–4456.

Panzeri, S., Schultz, S.R., Treves, A., and Rolls, E.T. (1999). Correlations and the encoding of information in the nervous system. Proc. R. Soc. B Biol. Sci. 266, 1001–1012.

Pernet, C.R., Appelhoff, S., Flandin, G., Phillips, C., Delorme, A., and Oostenveld, R. BIDS-EEG: an extension to the Brain Imaging Data Structure (BIDS) Specification for electroencephalography.

Pesaran, B., Pezaris, J.S., Sahani, M., Mitra, P.P., and Andersen, R.A. (2002). Temporal structure in neuronal activity during working memory in macaque parietal cortex. Nat. Neurosci. 5, 805–811.

Quiroga, R.Q. (2007). Spike sorting. Scholarpedia 2, 3583.

Quiroga, R.Q., Nadasdy, Z., and Ben-Shaul, Y. (2004). Unsupervised Spike Detection and Sorting with Wavelets and Superparamagnetic Clustering. Neural Comput. 16, 1661–1687.

Ray, S., and Maunsell, J.H.R. (2011). Network Rhythms Influence the Relationship between Spike-Triggered Local Field Potential and Functional Connectivity. J. Neurosci. 31, 12674–12682.

Rübel, O., Tritt, A., Dichter, B., Braun, T., Cain, N., Clack, N., Davidson, T.J., Dougherty, M., Fillion-Robin, J.-C., Graddis, N., et al. (2019). NWB:N 2.0: An Accessible Data Standard for Neurophysiology. BioRxiv 523035.

Samiee, S., and Baillet, S. (2017). Time-resolved phase-amplitude coupling in neural oscillations. NeuroImage 159, 270–279.

Siegle, J.H., López, A.C., Patel, Y.A., Abramov, K., Ohayon, S., and Voigts, J. (2017). Open Ephys: an open-source, plugin-based platform for multichannel electrophysiology. J. Neural Eng. 14, 045003.

Singer, W. (1999). Neuronal Synchrony: A Versatile Code for the Definition of Relations? Neuron 24, 49–65.

Sompolinsky, H., Yoon, H., Kang, K., and Shamir, M. (2001). Population coding in neuronal systems with correlated noise. Phys. Rev. E Stat. Nonlin. Soft Matter Phys. 64, 051904.

Stead, M., and Halford, J.J. (2016). A Proposal for a Standard Format for Neurophysiology Data Recording and Exchange. J. Clin. Neurophysiol. Off. Publ. Am. Electroencephalogr. Soc. 33, 403–413.

Tadel, F., Baillet, S., Mosher, J.C., Pantazis, D., and Leahy, R.M. (2011). Brainstorm: A User-Friendly Application for MEG/EEG Analysis, Brainstorm: A User-Friendly Application for MEG/EEG Analysis. Comput. Intell. Neurosci. 2011, 2011, e879716.

Teeters, J.L., Godfrey, K., Young, R., Dang, C., Friedsam, C., Wark, B., Asari, H., Peron, S., Li, N., Peyrache, A., et al. (2015). Neurodata Without Borders: Creating a Common Data Format for Neurophysiology. Neuron 88, 629–634.

Unakafova, V.A., and Gail, A. (2019). Comparing open-source toolboxes for processing and analysis of spike and local field potentials data. BioRxiv 600486.

*Uusitalo, M.A., and Ilmoniemi, R.J. (1997). Signal-space projection method for separating MEG or EEG into components. Med. Biol. Eng. Comput. 35, 135–140.* 

Wilke, M., Logothetis, N.K., and Leopold, D.A. (2006). Local field potential reflects perceptual suppression in monkey visual cortex. Proc. Natl. Acad. Sci. 103, 17507–17512.

Womelsdorf, T., Fries, P., Mitra, P.P., and Desimone, R. (2006). Gamma-band synchronization in visual cortex predicts speed of change detection. Nature 439, 733–736.

Womelsdorf, T., Schoffelen, J.-M., Oostenveld, R., Singer, W., Desimone, R., Engel, A.K., and Fries, P. (2007). Modulation of Neuronal Interactions Through Neuronal Synchronization. Science 316, 1609–1612.

Zanos, T.P., Mineault, P.J., and Pack, C.C. (2011). Removal of Spurious Correlations Between Spikes and Local Field Potentials. J. Neurophysiol. 105, 474–486.

Zohary, E., Shadlen, M.N., and Newsome, W.T. (1994). Correlated neuronal discharge rate and its implications for psychophysical performance. Nature 370, 140–143.

# 4.11 Figures

Figure 1. Workflow of the toolbox

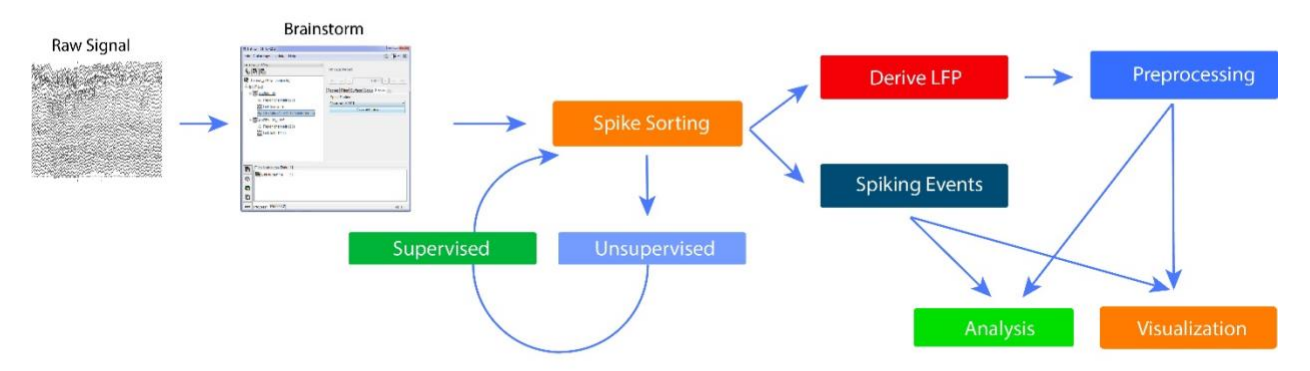


Figure 1. Workflow of the e-Phys toolbox. Users initially import the header to the raw binary signal. Once the data is identified, the users perform the spike-sorting step. The spike-sorting process is divided into two parts: Unsupervised (the algorithm creates neuronal clusters automatically) and Supervised (the user inspects the output of the unsupervised part). At this point of the workflow, the LFP can be extracted. All the spiking events that were previously computed and the down-sampled LFP signals are all encapsulated to a single binary file. The original binary file can be stored to an external source and is no-longer needed. Finally, users can now perform preprocessing and analyze their data, utilizing the spike-related function that have been introduced to Brainstorm by this toolbox.

e-PHYS TOOLBOX	
Acquisition Systems	Blackrock (.nsX), Ripple (.nsX), Plexon (.plx, .pl2), Intan (.rhd), Neurodata
	without borders (.nwb), Tucker Davis Technologies
Spike Sorters	WaveClus, UltraMegaSort2000, Kilosort (Klusters)
LFP spectral Artifact Removal	Bayesian spectral spiking-artifact removal
Spike-related Functions	Tuning Curves, Raster Plots, Spike Field Coherence, Spike triggered Average
Pre-processing	DC-offset removal, Band-pass / band-stop / notch filtering, resampling
Artifact Removal	SSP, ICA
Frequency	FFT, Welch Density, Morlet Wavelets, Hilbert transform, Multi-tapers, Phase Amplitude Coupling, Instantaneous frequency, Canolty Maps
Connectivity	Correlation, coherence, Bivariate Granger causality, Phase Locking Value, Amplitude Envelope Correlation, Phase Transfer Entropy
Statistics and machine learning	Parametric testing (zero / baseline), Partial Least Squares, Support Vector Machine classification, Linear Discriminant Analysis classification

Table 1. Synopsis of the e-Phys toolbox and the tools that can be used for LFP analysis. The e-Phys toolbox provides a working framework for every step of the e-Phys analysis and each module can easily be enriched with future additions.

Figure 2. Dataset navigation and pre-processing window

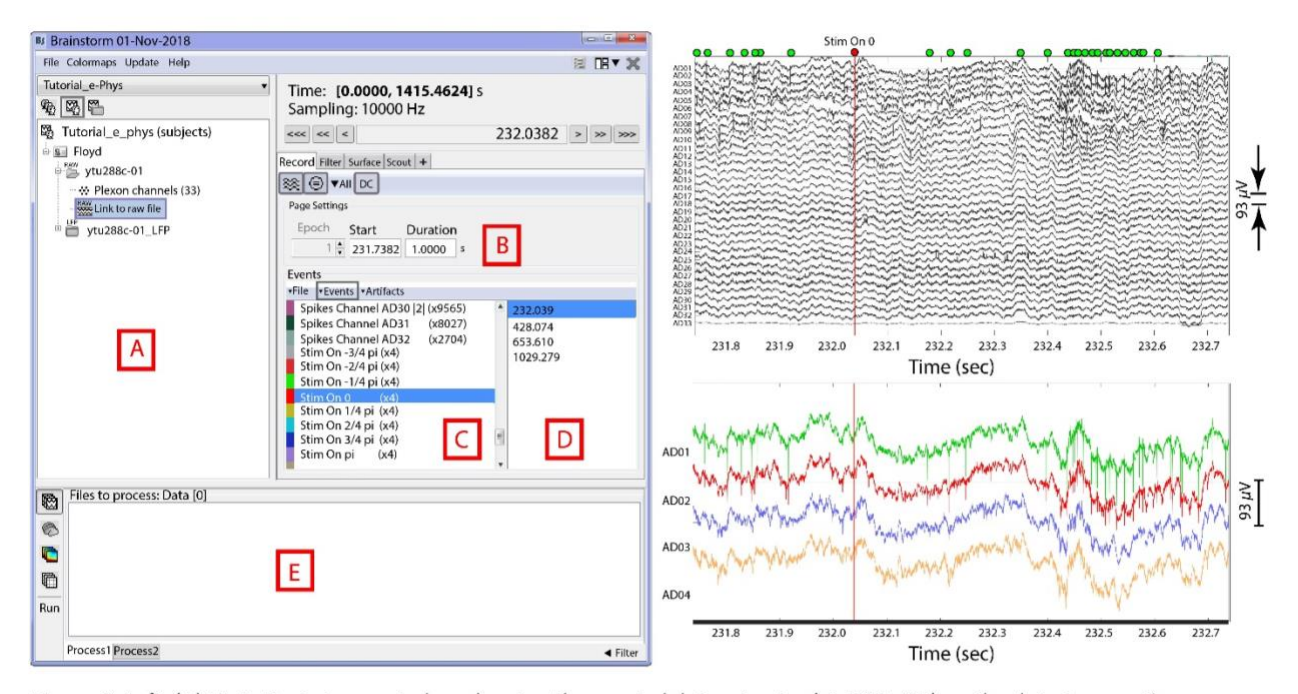


Figure 2. Left: (A) Main Brainstorm window showing the created dataset entry (ytu288c-01) on the data-tree section. (B) Selection of starting time point and duration of signal segment to be loaded for reviewing. (C) Experimental and spiking events are displayed. (D) An event is selected from the "Stim on 0" condition. This selection automatically synchronizes all reviewing windows to the timepoint of the event's occurrence. Right Top: 1 second segment displaying raw signals from all electrodes. The vertical red line indicates alignment around the selected event ("Stim On 0"). The green dots on the top of the figure represent the spiking events from the first neuron on electrode with label AD01. Right Bottom: A selection of the first 4 electrodes, aligned in time with the top figure.

Figure 3. Unsupervised Spike-sorting

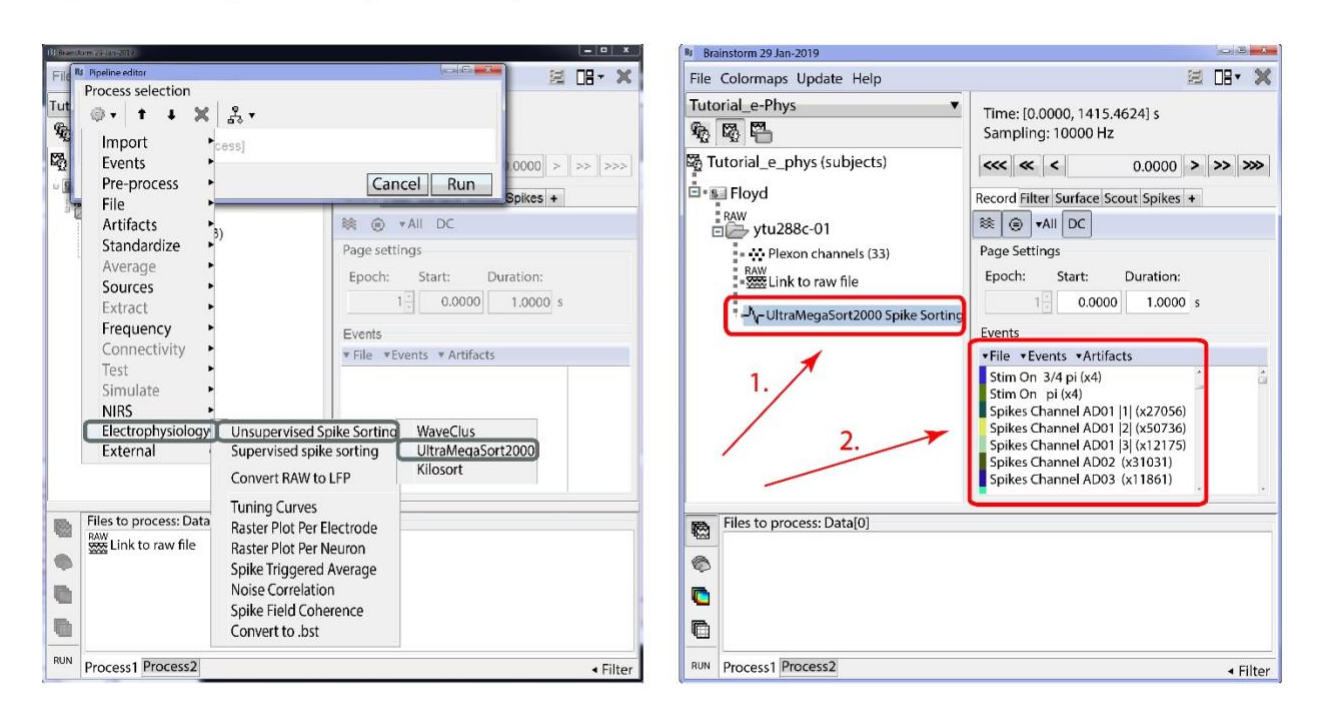


Figure 3. Left: Selection of the embedded spike-sorters for unsupervised spike-sorting within Brainstorm. Right: Example of a dataset spike-sorted with UltraMegaSort2000. (Box 1)A new entry in the database UltraMegaSort2000 Spike Sorting appears and indicates that this dataset has been spike-sorted. (Box 2). New events appear in the Events window, corresponding to the spikes that the spike-sorter clustered (Spikes Channel X).

Figure 4. Supervised spike-sorting

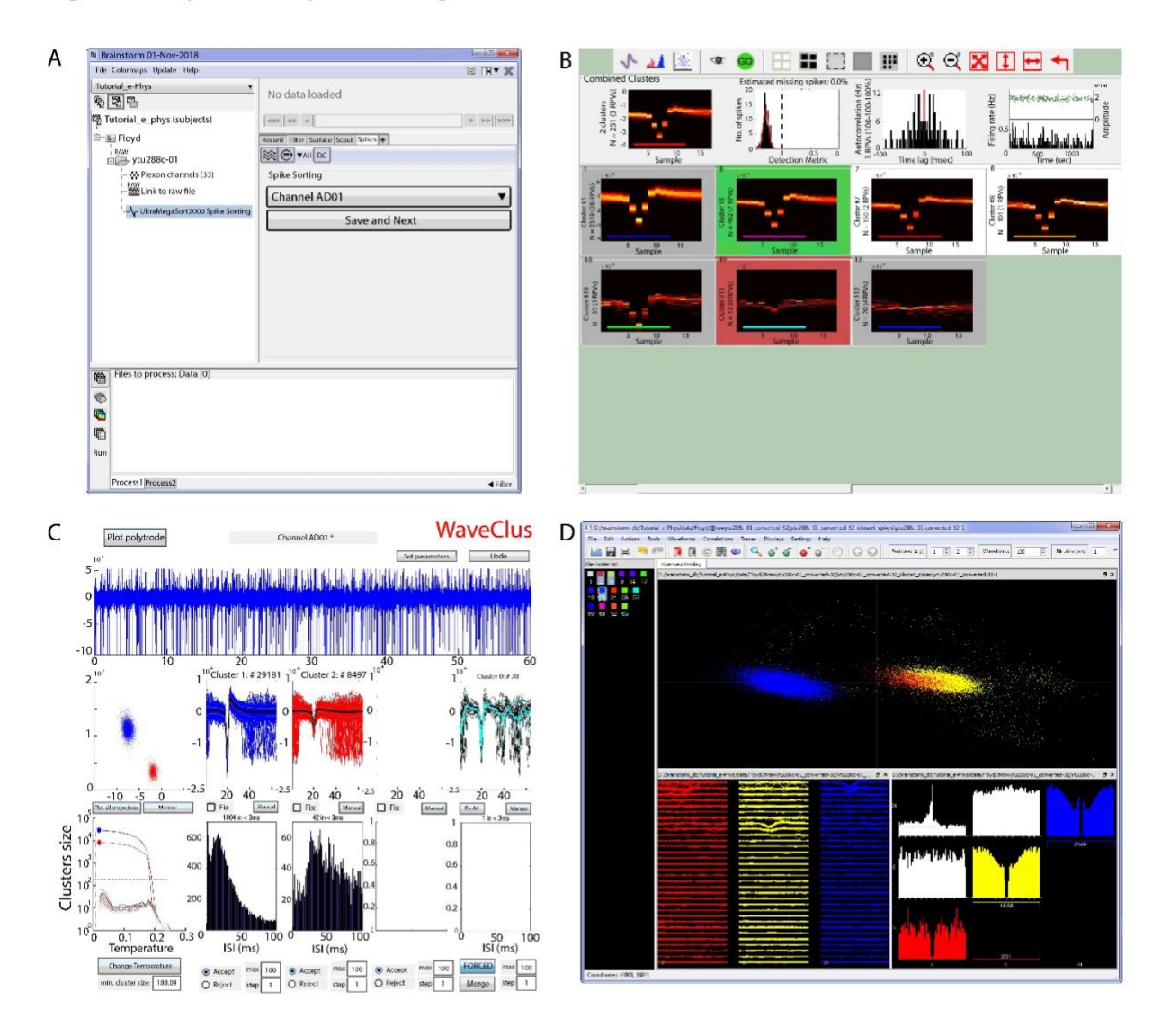


Figure 4. Supervised spike sorting. (A). Main window that the user selects the electrode (or group of electrodes for Klusters) and the spike sorted files automatically update the spike sorter in use. Once the neuronal clusters have been adjusted, the user presses the Save and Next button and the next electrode gets selected to continue the supervised spike-sorting. (B, C, D). Supervised GUI for UltraMegaSort, WaveClus and Klusters respectively.

Figure 5. Conversion from raw signals to LFPs

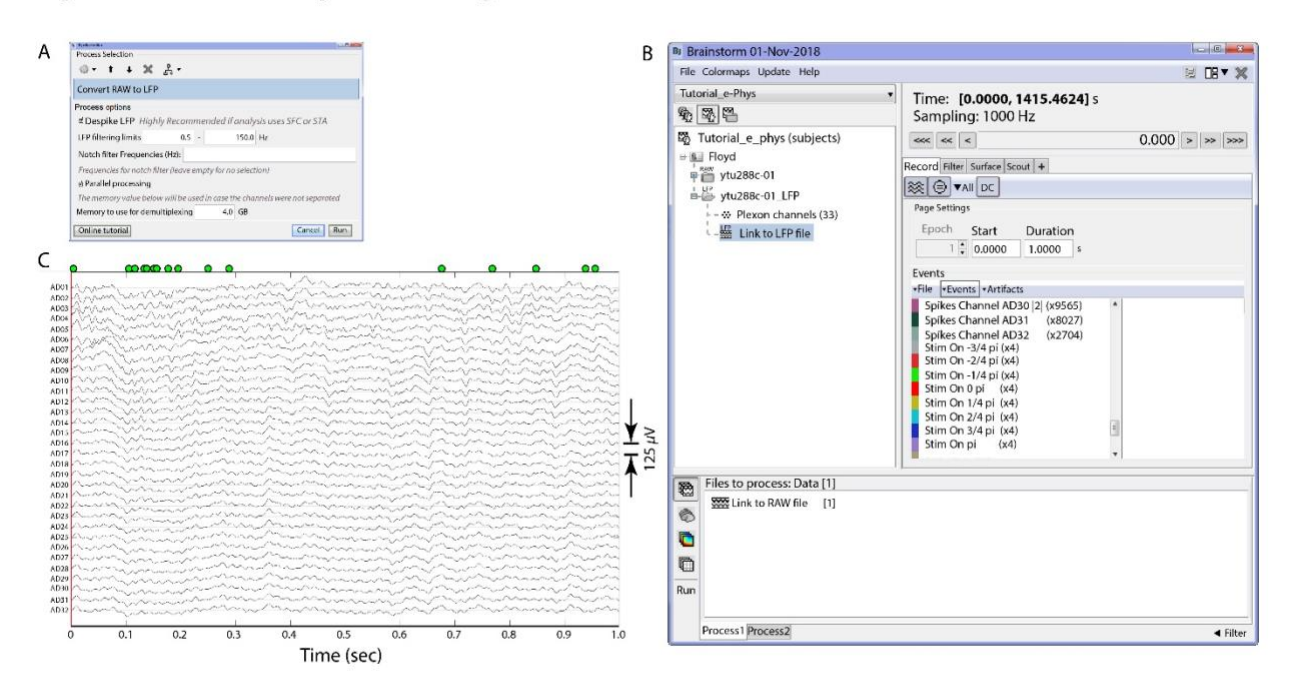


Figure 5. Converter from raw signals to LFPs. (A). Users can select the filtering limits of their LFP and apply a notch filter if necessary. The converter downsamples the raw signal to 1 KHz. (B). Once the conversion is complete, a single binary file (.bst) that contains all the necessary information (LFPs, experimental and spiking events) is stored on the hard drive, and automatically imported on the data-tree as a new dataset. (C). 1 second segment review of the created LFP signal traces. The spiking events from the first neuron of electrode AD01 are represented by the green dots on the top of the figure, as in Figure 2.

Figure 6. Importing of trials

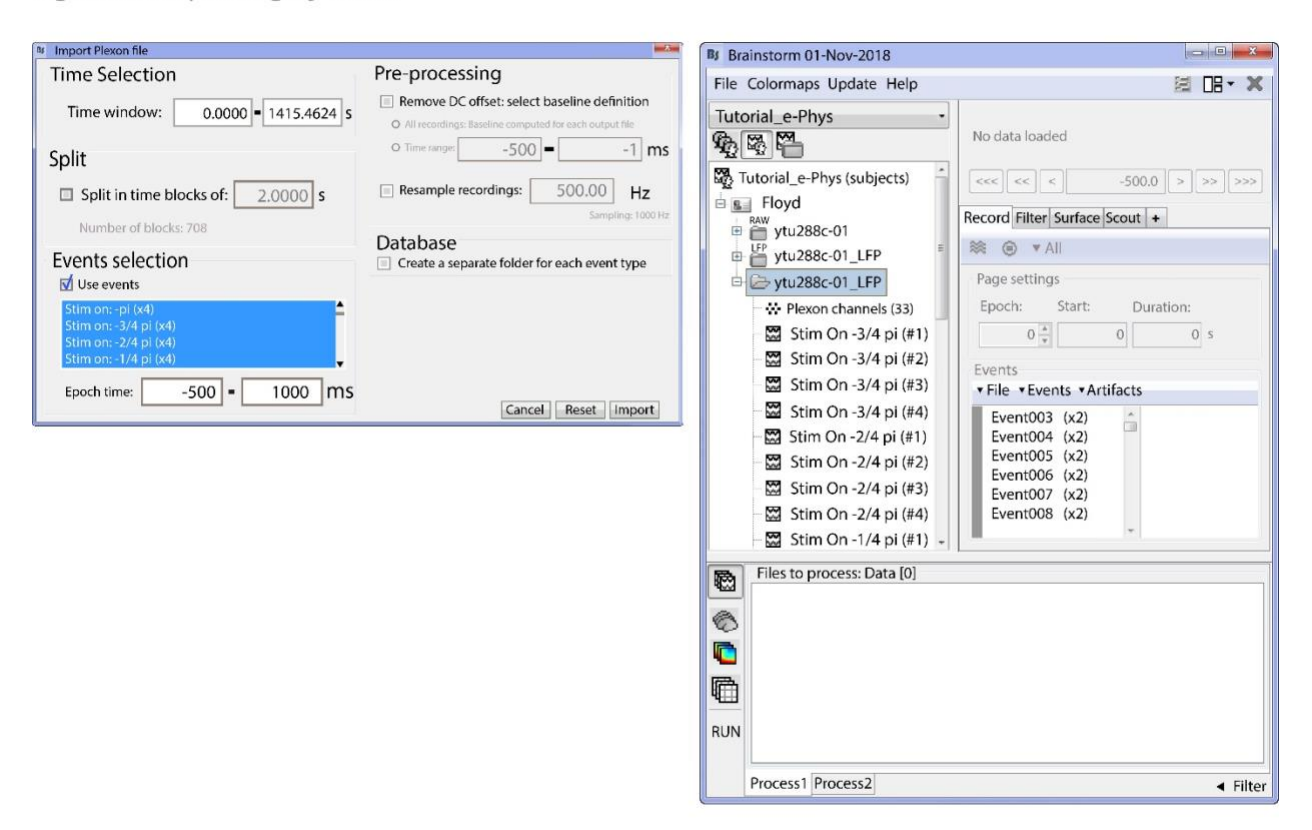


Figure 6. (Left) Selection of the events of interest and temporal boundaries around them, for importing the LFP segments. (Right) Imported LFP trials for the selected conditions in the Brainstorm database.

Figure 7. Analysis of LFP signals

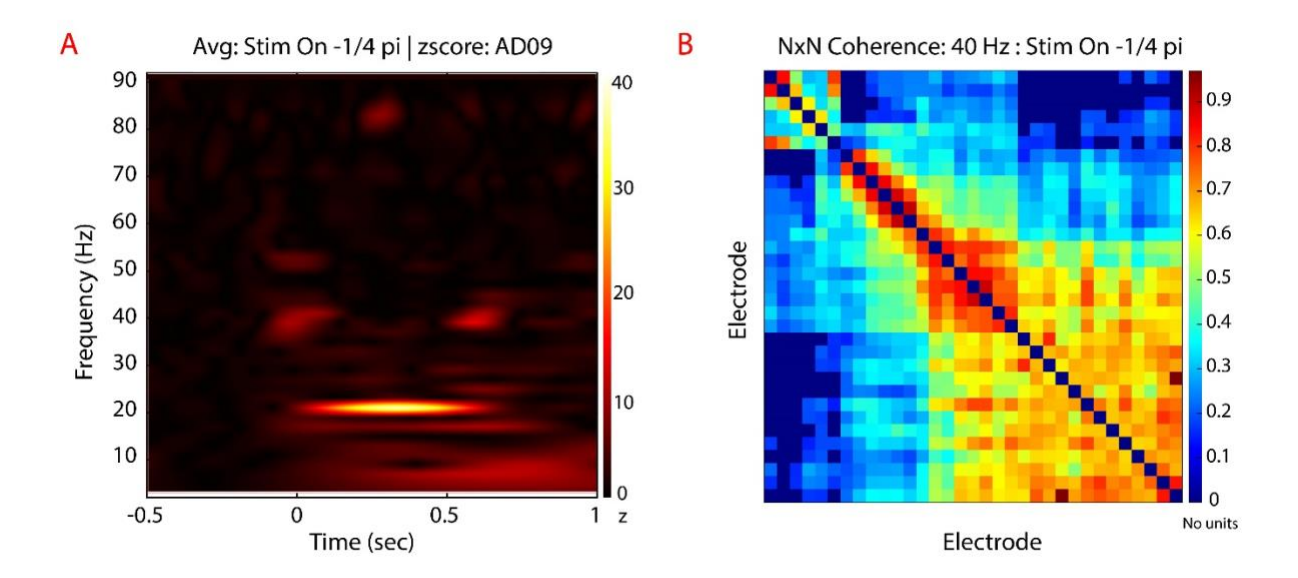


Figure 7. (A). Wavelet Decomposition ([2-90] Hz) of a single LFP trial from electrode labeled AD09 for moving stimulus condition towards -1/4 pi degrees direction. Users can select the channel they want to be displayed from a drop-down list on the main Brainstorm window.

(B). Estimation of NxN coherence for a single trial across all electrodes. The coherence values are color-coded for a specific frequency (on the example 40 Hz frequency is selected). Users can display coherence in the other frequencies by moving a sliding toggle.

Figure 8. Spike-LFP analysis functions

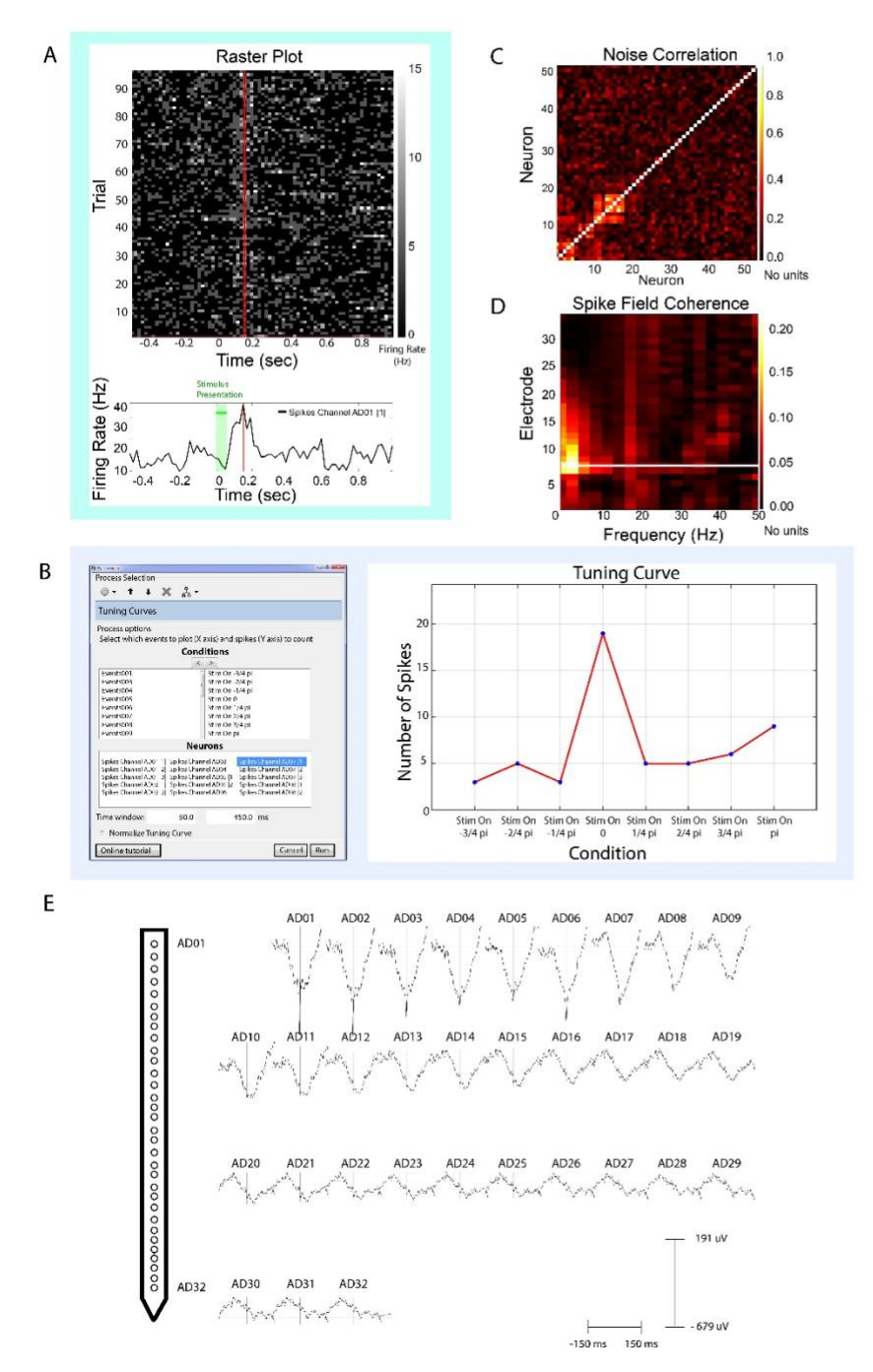


Figure 8. (A) Raster Plot. (Top) Example raster plot for 96 trials of a single condition for the first neuron picked up on electrode labeled 'AD01'. Firing has been binned into 10ms segments. The green shading indicates the period where the stimulus was presented on the screen. A single condition was repeated 96 times instead of 4 for the purpose of this raster plot. (Bottom) Average firing rate from all trials shows maximum firing "150ms after the stimulus onset for this neuron. The vertical red line indicates interactive temporal alignment between the two plots and the green shade the period of the stimulus presentation.

(B) Tuning curves function. (LEFT): Users select the neurons that they want to display the tuning curves, and sequentially the conditions (and their order) that would formulate the x-axis (right side of the conditions selection window). Additionally, we included a selection for the time-window where the spikes would be counted. (RIGHT): Tuning curve for an example neuron, selected from the window on the left of Figure B. The x-axis shows the different experimental conditions at the order selected on the previous window. This neuron expresses selectivity for the condition "Stim On O".

(C) Noise correlation. The function selects all the neurons that elicited spikes within the trials imported and displays a nxn figure where the noise correlation is computed for all combinations of neurons. Specifically for the dataset illustrated, there were 53 unique neurons picked up by the electrodes (according to the spike sorting step). This figure shows the computation of noise-correlation on all trials (a subset on a specific condition is also possible) for the presentation 96 trials of a motion stimulus, and spikes are selected on [0,300] ms around the stimuli presentations.

(D) Spike field coherence for an example neuron picked up from the first electrode (ADO7) for the motion stimulus condition "Stim On 0". The spike-field coherence window displays spectral influence of a single neuron to all 32 electrodes. Frequency is shown up to 60 Hz. Time selection around each spike was [-150, 150] ms

(E) Spike triggered average of a neuron picked up on electrode labeled ADO1. A graph of the linear probe with the relative electrode locations is displayed on the left of the figure. The time selection around the spikes was set to [-150,150] ms for all trials of all experimental conditions. The electrodes have been presented into four rows for easier visualization. In reality, the linear probe extends on a single dimension (1:32). The scale of the STA is shown on the bottom right. All traces have been aligned to the same time-selection (0 ms – time occurrence of the spikes of ADO1), indicated by the vertical line of each signal's display.

Figure 9. Topographical visualizations

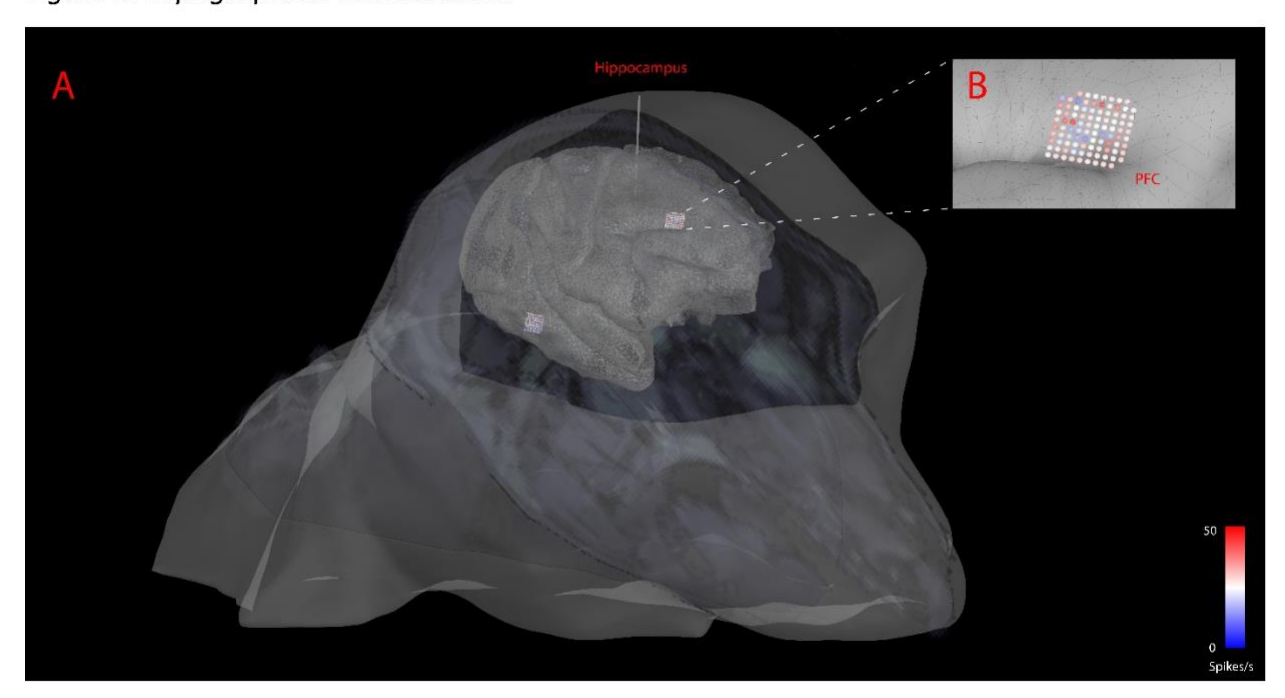


Figure 9. (A). Visualization of the implanted electrodes on the anatomical MRI of the non-human primate. The MR slices are superimposed on the figure. (B). Zoomed in version of an implanted Utah array on the cortical surface, with the spiking activity color-coded on the array's topography for a single time-bin.

Chapter 5 briefly summarizes the findings presented in this thesis and outlines the significance of this work and some possible future avenues of research that could potentially follow this PhD work.

# Chapter 5: Discussion

Chapters 2, 3 and 4 in this thesis constitute original scholarship and are published (chapters 2 and 4 in Neuroimage and Nature Scientific Data respectively) or in preparation for journal submission (chapter 3).

# 5.1 Summary of results and contribution to original knowledge 5.1.1 Retinotopy in MEG

The most elementary characteristic of a visual neuron would be its receptive field. Ever since neurophysiologists introduced the idea of visual spatial selectivity in the mid 20<sup>th</sup> century, countless invasive and imaging studies have utilized that spatial information to understand why neurons elicit responses and communicate among them.

MEG has been used for clinical applications and basic research studies that require real-time, non-invasive mapping of the human cortex. Although almost five decades have passed since the first MEG system (Cohen, 1968), the spatial selectivity of visual areas has been demonstrated very crudely with this modality, in accordance with the general acceptance that MEG provides "modest" spatial resolution.

Chapter 2 introduces a novel method for mapping the retinal input to the cortical manifold. In this study we used high-resolution cortical tessellations from each subject (~150,000 vertices) and we managed to isolate individual sources within the primary visual cortex that showed significant confined receptive fields. In order to measure the fidelity of our results, the same subjects additionally participated in fMRI retinotopic experiments, and the MEG retinotopic maps showed surprising alignment with those from the fMRI. Moreover, we estimated the cortical magnification achieved with MEG by selecting sources along the calcarine sulcus and formulating the relationship between their relative distance and receptive field eccentricity, comparing it with other imaging modalities (Duncan and Boynton, 2003; Endo et al., 1997; Engel et al., 1997; Horton JC and Hoyt WF, 1991; Qiu et al., 2006; Sereno et al., 1995). Having established the reliability of

the cortical responses within the primary visual cortex, we then investigated the seperability between adjacent sources in order to formulate an estimation for spatial resolution. Our calculations considered physical properties of MEG sources that were expected to affect resolution, and computed an estimator based on geodesic distance and relative orientation. Our resolution estimator indicated that with proper stimulation, MEG sources can be reliably differentiated if they're 7mm apart while their orientation is parallel. For regions of greater curvature (i.e. near a gyrus), resolution can be considerably greater (averaging 2-4 mm) — with the absolute limit of 0.49mm that is achieved at the noise level of 1x1 mm isotropic space voxels from MRI tessellations (Pienaar et al., 2008).

In order to put these numbers into perspective, the neuronal density in the human primary visual cortex is estimated to be ~40,000 cells / mm³ (Leuba and Garey, 1989). Taking into account that the weakest MEG signal was previously calculated to be elicited by the simultaneous activity of a population of ~50,000 neurons (Murakami and Okada, 2006), our results suggest that we disentangled signals from much smaller populations. Our study took full advantage of high-resolution cortical tessellations that provide anatomically precisely oriented sources. Usage of a lower resolution cortical surface could have led to improper source vector orientation, and would be likely to offer limited accuracy in source estimation (Bonaiuto et al., 2019). An extra step towards increased resolution would be to use head casts that can reduce movement inside MEG (Meyer et al., 2017; Troebinger et al., 2014). This study shows that proper stimulation of areas that are anatomically known to be located near gyri, can be properly detected by MEG sources.

#### 5.1.2 Remapping in MEG

Being able to estimate the receptive fields from individual sources, opens up the road to selectively include sources in MEG analysis for visual studies. Remapping is a prime candidate mechanism that relies on neuronal populations with specific spatial selectivity; receptive fields before and after the saccade. The initial studies on remapping demonstrated a shift of the receptive field of a neuron parallel to the saccade vector. Despite a plethora of studies that supported this remapping direction, (Tolias et al., 2001a; Zirnsak and Moore, 2014) showed remapping vectors that were

skewed towards the saccade target. The interpretation of these studies was that receptive field shifting reflects target selection rather than visual stability. (Neupane et al., 2016b, 2016a) created a bridge between these two lines of thinking, demonstrating that both types of remapping are present within V4 neurons.

The studies described in Chapter 3 show remapping manifestation in the superior parietal and visual cortices. The experimental paradigm was designed in such a way that the retinotopic and remapped responses were dissociated into two different hemispheres, by presenting the probe between the two targets (retinotopic responses were allocated on the contralateral hemisphere and remapped on the ipsilateral). Our results support the existence of the two aforementioned types of remapping; an early superior parietal component (40-150ms after saccade offset) showed significant responses consistent with the approach of "forward remapping", and a late (~280ms after saccade offset) early-visual-cortex component showed responses that were consistent with "convergent" remapping. Interestingly, we observed these late "convergent" remapping responses in the visual cortex (activation span across several visual areas), but not in the parietal cortex. Since our experimental design involved repeated saccades between two set targets, "convergent" remapping might be an epiphenomenon of covert attention from the anticipation of the fully predictable target appearance (Deubel, 2008; Neupane et al., 2016a).

In alignment with our results, two neurophysiological studies have demonstrated convergent remapping in the visual cortex and specifically in V4 (Neupane et al., 2016a; Tolias et al., 2001b).

Evidence of convergent remapping has been demonstrated in FEF (Zirnsak and Moore, 2014), but not in the parietal cortex. Based on our data, the parietal cortex might not be involved in the convergent remapping responses, although invasive neurophysiological studies would be able to provide better understanding due to their spatial resolution.

Importantly, several studies unsuccessfully attempted to observe remapping in area MT (Hartmann et al., 2011; Inaba and Kawano, 2014; Ong and Bisley, 2011), and this was achieved only when an attentional memory task was introduced to the paradigm (Yao et al., 2016). Attentional modulation of remapping has been observed in the parietal cortex as well (Gottlieb et al., 1998; Mirpour and Bisley, 2016), an area that inactivation studies have shown association to

visual spatial attention (Liu et al., 2010; Wardak et al., 2004). In our study, we attempted several pilot experimental paradigms that have been commonly used in remapping literature, but none of them elicited remapping responses. It was only until we introduced attention through an oriented probe in our paradigm that we were able to detect the remapping responses. Moreover, two of our subjects underwent a series of control experiments (attention / no attention) that further supported the modulatory role of attention in remapping and remapping's role in the creation of priority/saliency maps around eye movements.

## 5.1.3 Invasive neurophysiology analysis

Chapter 4 introduced a modern approach in invasive neurophysiology analysis, in accordance to values of open-science, transparency, standardization and reproducibility. The toolbox utilizes a set of features that enable the creation of a full pipeline for invasive neurophysiology analysis within Brainstorm — from importing signals from a wide variety of acquisition systems, to performing spike rate visualization on the anatomical modeling of the implants. It enables quick overview of the raw signals for quality control, artifact rejection, event-related analysis, and a set of pre-processing features. A series of spike-sorters are supported (WaveClus, UltraMegaSort2000 and Kilosort) for supervised and unsupervised spike-sorting, with interoperability with the main Brainstorm interface. A convenient LFP converter is included that downsamples and packages all experimental and spiking events along with the LFP signals into a single file for easy sharing among researchers.

A series of functions can be utilized for extracting LFP and spiking information. The toolbox is designed in a modular approach so its functionality can be easily enriched. Every instance of data-processing is logged, and the open-source code of every function is thoroughly documented. Additionally, an active user forum and daily GitHub updates provide an extra layer of support to the software.

This software responds to an unmet need of the electrophysiology community. By providing a unique environment with a common set of analytical tools, the application also provides a unique bridge between recording scales, data types and researchers, and additionally, between the

methods used in human, animal and slice preparations. It also represents a scalable framework to developments and integration of existing or future tools and data formats for the entire field of electrophysiology. Additionally, we emphasized on the efficiency of the software due to the trend of modern neurophysiology to move towards high-density electrodes. The software can run on headless mode on a cluster and benefit from GPU processing for spike-sorting (through Kilosort).

## 5.2 Future development

The retinotopic maps we computed in Chapter 2 have been created by projecting thousands of stimulation frames to the subjects. Our retinotopic maps showed significance only within the primary visual cortex and some within V2. This is probably due to the selection of the size of the probes between the nominal size of the receptive fields in V1 and V2 (Freeman and Simoncelli, 2011). Further studies can investigate the size effect of stimulation to different visual areas. Moreover, our selectivity detection method showed that only 3% of the frames that had a probe within the final receptive field of the source crossed the detection threshold. This is a potential indication of a phase-locking mechanism that can be exploited by a closed-loop system. Real-time MEG monitoring of ongoing oscillations in different frequencies coupled with a minimal latency projector can shed light to this question.

The functional role of remapping has not yet been demonstrated with neurophysiology. An extension to the analysis we performed on the current paradigm would be to separate the trials based on the orientation of the remapped probe, to explore if remapping also transfers feature information besides location. The small orientation differentiation used in this paradigm might be too prohibitive (we only used ±5°), but a bigger tilt should be able to be recovered by MEG as shown previously for cortical columns (Cichy et al., 2015 - they used ±45°). Moreover, (Neupane et al., 2017) showed coherent oscillations between the neurons that encode the current and the future receptive field. In our study we isolated the sources that encode these two points in the visual field within the visual and parietal cortex, but were not able to show significant communication by coherence (Fries, 2005) between these areas. Further investigation on the communication between remapping areas can include bicoherence methods (Shils et al., 1996).

The modular architecture of the invasive neurophysiology toolbox gives it enormous potential for further development. At the point that this thesis is written its functionality has already expanded to include more features compared to what was published in the work within Chapter 4; e.g. already included computation of place fields (for hippocampal recordings), support of the Allen Institute mouse atlas (for inter- and intra-areal analysis) and support for high density electrodes - Neuropixels.

## References

Baillet, S. (2017). Magnetoencephalography for brain electrophysiology and imaging. Nat. Neurosci. 20, 327–339.

Baillet, S., Mosher, J.C., and Leahy, R.M. (2001). Electromagnetic brain mapping. IEEE Signal Process. Mag. 18, 14–30.

Baker, M. (2016). 1,500 scientists lift the lid on reproducibility. Nat. News 533, 452.

Balderston, N.L., Schultz, D.H., Baillet, S., and Helmstetter, F.J. (2014). Rapid Amygdala Responses during Trace Fear Conditioning without Awareness. PLOS ONE 9, e96803.

Barlow, H.B., Fitzhugh, R., and Kuffler, S.W. (1957). Change of organization in the receptive fields of the cat's retina during dark adaptation. J. Physiol. 137, 338–354.

Benbadis, S.R., Beran, R.G., Berg, A.T., Jr, J.E., Galanopoulou, A.S., Kaplan, P.W., Koutroumanidis, M., Moshe, S.L., Jr, D.R.N., Serratosa, J.M., et al. (2010). Atlas of Epilepsies (Springer Science & Business Media).

Bonaiuto, J.J., Afdideh, F., Ferez, M., Wagstyl, K., Mattout, J., Bonnefond, M., Barnes, G.R., and Bestmann, S. (2019). Estimates of cortical column orientation improve MEG source inversion. BioRxiv 810267.

Brodmann, K. (2006). Brodmann's: Localisation in the Cerebral Cortex (Springer US).

Brookes, M.J., Zumer, J.M., Stevenson, C.M., Hale, J.R., Barnes, G.R., Vrba, J., and Morris, P.G. (2010). Investigating spatial specificity and data averaging in MEG. NeuroImage 49, 525–538.

Buzsáki, G., Anastassiou, C.A., and Koch, C. (2012). The origin of extracellular fields and currents — EEG, ECoG, LFP and spikes. Nat. Rev. Neurosci. 13, 407–420.

Castelhano, M.S., Mack, M.L., and Henderson, J.M. (2009). Viewing task influences eye movement control during active scene perception. J. Vis. 9, 6–6.

Cavanagh, P., Hunt, A.R., Afraz, A., and Rolfs, M. (2010). Visual stability based on remapping of attention pointers. Trends Cogn. Sci. 14, 147–153.

Churan, J., Guitton, D., and Pack, C.C. (2011). Context dependence of receptive field remapping in superior colliculus. J. Neurophysiol. 106, 1862–1874.

Cichy, R.M., Ramirez, F.M., and Pantazis, D. (2015). Can visual information encoded in cortical columns be decoded from magnetoencephalography data in humans? NeuroImage 121, 193–204.

Coffey, E.B.J., Herholz, S.C., Chepesiuk, A.M.P., Baillet, S., and Zatorre, R.J. (2016). Cortical contributions to the auditory frequency-following response revealed by MEG. Nat. Commun. 7, 1–11.

Cohen, D. (1968). Magnetoencephalography: evidence of magnetic fields produced by alpharhythm currents. Science 161, 784–786.

Colby, C.L., and Goldberg, M.E. (1999). Space and Attention in Parietal Cortex. Annu. Rev. Neurosci. 22, 319–349.

Collaboration, O.S. (2015). Estimating the reproducibility of psychological science. Science 349.

Cornwell, B.R., Carver, F.W., Coppola, R., Johnson, L., Alvarez, R., and Grillon, C. (2008). Evoked amygdala responses to negative faces revealed by adaptive MEG beamformers. Brain Res. 1244, 103–112.

Cornwell, B.R., Arkin, N., Overstreet, C., Carver, F.W., and Grillon, C. (2012). Distinct contributions of human hippocampal theta to spatial cognition and anxiety. Hippocampus 22, 1848–1859.

Cottereau, B., Lorenceau, J., Gramfort, A., Clerc, M., Thirion, B., and Baillet, S. (2011). Phase delays within visual cortex shape the response to steady-state visual stimulation. NeuroImage 54, 1919–1929.

Darvas, F., Pantazis, D., Kucukaltun-Yildirim, E., and Leahy, R.M. (2004). Mapping human brain function with MEG and EEG: methods and validation. NeuroImage 23, Supplement 1, S289–S299.

Dassonville, P., Schlag, J., and Schlag-Rey, M. (1992). Oculomotor localization relies on a damped representation of saccadic eye displacement in human and nonhuman primates. Vis. Neurosci. 9, 261–269.

Deubel, H. (2008). The time course of presaccadic attention shifts. Psychol. Res. 72, 630-640.

Duhamel, J.R., Colby, C.L., and Goldberg, M.E. (1992). The updating of the representation of visual space in parietal cortex by intended eye movements. Science 255, 90–92.

Dumas, T., Dubal, S., Attal, Y., Chupin, M., Jouvent, R., Morel, S., and George, N. (2013). MEG evidence for dynamic amygdala modulations by gaze and facial emotions. PloS One 8, e74145.

Dumoulin, S.O., and Wandell, B.A. (2008). Population receptive field estimates in human visual cortex. NeuroImage 39, 647–660.

Duncan, J., and Humphreys, G. (1992). Beyond the search surface: visual search and attentional engagement. J. Exp. Psychol. Hum. Percept. Perform. 18, 578–588; discussion 589-593.

Duncan, J., and Humphreys, G.W. (1989). Visual search and stimulus similarity. Psychol. Rev. 96, 433–458.

Duncan, R.O., and Boynton, G.M. (2003). Cortical Magnification within Human Primary Visual Cortex Correlates with Acuity Thresholds. Neuron 38, 659–671.

Endo, S., Toyama, H., Kimura, Y., Ishii, K., Senda, M., Kiyosawa, M., and Uchiyama, A. (1997). Mapping visual field with positron emission tomography by mathematical modeling of the retinotopic organization in the calcarine cortex. IEEE Trans. Med. Imaging 16, 252–260.

Engel, S.A., Glover, G.H., and Wandell, B.A. (1997). Retinotopic organization in human visual cortex and the spatial precision of functional MRI. Cereb. Cortex 7, 181–192.

Fee, M.S., Mitra, P.P., and Kleinfeld, D. (1996). Automatic sorting of multiple unit neuronal signals in the presence of anisotropic and non-Gaussian variability. J. Neurosci. Methods 69, 175–188.

Felleman, D.J., and Van Essen, D.C. (1991). Distributed hierarchical processing in the primate cerebral cortex. Cereb. Cortex N. Y. N 1991 1, 1–47.

Fischer, T., Graupner, S.-T., Velichkovsky, B.M., and Pannasch, S. (2013). Attentional dynamics during free picture viewing: Evidence from oculomotor behavior and electrocortical activity. Front. Syst. Neurosci. 7.

Freeman, J., and Simoncelli, E.P. (2011). Metamers of the ventral stream. Nat. Neurosci. 14, 1195–1201.

Fries, P. (2005). A mechanism for cognitive dynamics: neuronal communication through neuronal coherence. Trends Cogn. Sci. 9, 474–480.

Fries, W. (1984). Cortical projections to the superior colliculus in the macaque monkey: a retrograde study using horseradish peroxidase. J. Comp. Neurol. 230, 55–76.

Goldenholz, D.M., Ahlfors, S.P., Hämäläinen, M.S., Sharon, D., Ishitobi, M., Vaina, L.M., and Stufflebeam, S.M. (2009). Mapping the signal-to-noise-ratios of cortical sources in magnetoencephalography and electroencephalography. Hum. Brain Mapp. 30, 1077–1086.

Gorgolewski, K.J., and Poldrack, R.A. (2016). A Practical Guide for Improving Transparency and Reproducibility in Neuroimaging Research. PLOS Biol. 14, e1002506.

Gorgolewski, K.J., Auer, T., Calhoun, V.D., Craddock, R.C., Das, S., Duff, E.P., Flandin, G., Ghosh, S.S., Glatard, T., Halchenko, Y.O., et al. (2016). The brain imaging data structure, a format for organizing and describing outputs of neuroimaging experiments. Sci. Data 3, 160044.

Gottlieb, J.P., Kusunoki, M., and Goldberg, M.E. (1998). The representation of visual salience in monkey parietal cortex. Nature 391, 481–484.

Gramfort, A., Strohmeier, D., Haueisen, J., Hämäläinen, M.S., and Kowalski, M. (2013). Time-frequency mixed-norm estimates: sparse M/EEG imaging with non-stationary source activations. NeuroImage 70, 410–422.

Gregory, R.L. (1966). Eye and brain: the psychology of seeing (New York, NY, US: McGraw-Hill).

Hagler, D.J., Halgren, E., Martinez, A., Huang, M., Hillyard, S.A., and Dale, A.M. (2009). Source estimates for MEG/EEG visual evoked responses constrained by multiple, retinotopically-mapped stimulus locations. Hum. Brain Mapp. 30, 1290–1309.

Hämäläinen, M.S., and Ilmoniemi, R.J. (1994). Interpreting magnetic fields of the brain: minimum norm estimates. Med. Biol. Eng. Comput. 32, 35–42.

Hämäläinen, M., Hari, R., Ilmoniemi, R.J., Knuutila, J., and Lounasmaa, O.V. (1993). Magnetoencephalography\char22{}theory, instrumentation, and applications to noninvasive studies of the working human brain. Rev. Mod. Phys. 65, 413–497.

Hartline, H.K. (1938). The response of single optic nerve fibers of the vertebrate eye to illumination of the retina. Am. J. Physiol. 121, 400–415.

Hartline, H.K. (1940). The receptive fields of optic nerve fibers. Am. J. Physiol.-Leg. Content 130, 690–699.

Hartmann, T.S., Bremmer, F., Albright, T.D., and Krekelberg, B. (2011). Receptive Field Positions in Area MT during Slow Eye Movements. J. Neurosci. 31, 10437–10444.

Hazan, L., Zugaro, M., and Buzsáki, G. (2006). Klusters, NeuroScope, NDManager: a free software suite for neurophysiological data processing and visualization. J. Neurosci. Methods 155, 207–216.

Helmholtz, H. von, and Southall, J.P.C. (2005). Treatise on Physiological Optics (Dover Publications).

Helo, A., Pannasch, S., Sirri, L., and Rämä, P. (2014). The maturation of eye movement behavior: Scene viewing characteristics in children and adults. Vision Res. 103, 83–91.

Hikosaka, O., Takikawa, Y., and Kawagoe, R. (2000). Role of the basal ganglia in the control of purposive saccadic eye movements. Physiol. Rev. 80, 953–978.

Hill, D.N., Mehta, S.B., and Kleinfeld, D. (2011). Quality metrics to accompany spike sorting of extracellular signals. J. Neurosci. Off. J. Soc. Neurosci. 31, 8699–8705.

Holmes, G. (1945). Ferrier Lecture: The Organization of the Visual Cortex in Man. Proc. R. Soc. Lond. B Biol. Sci. 132, 348–361.

Honda, H. (1989). Perceptual localization of visual stimuli flashed during saccades. Percept. Psychophys. 45, 162–174.

Horton JC, and Hoyt WF (1991). The representation of the visual field in human striate cortex: A revision of the classic holmes map. Arch. Ophthalmol. 109, 816–824.

Hubel, D.H., and Wiesel, T.N. (1959). Receptive fields of single neurones in the cat's striate cortex. J. Physiol. 148, 574–591.

Hubel, D.H., and Wiesel, T.N. (1962). Receptive fields, binocular interaction and functional architecture in the cat's visual cortex. J. Physiol. 160, 106-154.2.

Hubel, D.H., and Wiesel, T.N. (1968). Receptive fields and functional architecture of monkey striate cortex. J. Physiol. 195, 215–243.

Inaba, N., and Kawano, K. (2014). Neurons in cortical area MST remap the memory trace of visual motion across saccadic eye movements. Proc. Natl. Acad. Sci. 111, 7825–7830.

Itti, L., and Koch, C. (2000). A saliency-based search mechanism for overt and covert shifts of visual attention. Vision Res. 40, 1489–1506.

Jeffries, S.M., Kusunoki, M., Bisley, J.W., Cohen, I.S., and Goldberg, M.E. (2007). Rhesus monkeys mislocalize saccade targets flashed for 100ms around the time of a saccade. Vision Res. 47, 1924–1934.

Jonikaitis, D., and Theeuwes, J. (2013). Dissociating oculomotor contributions to spatial and feature-based selection. J. Neurophysiol. 110, 1525–1534.

Kuffler, S.W. (1953). Discharge patterns and functional organization of mammalian retina. J. Neurophysiol. 16, 37–68.

Kusunoki, M., and Goldberg, M.E. (2003). The Time Course of Perisaccadic Receptive Field Shifts in the Lateral Intraparietal Area of the Monkey. J. Neurophysiol. 89, 1519–1527.

Lee, C., Rohrer, W.H., and Sparks, D.L. (1988). Population coding of saccadic eye movements by neurons in the superior colliculus. Nature 332, 357–360.

Leigh, R.J., and Zee, D.S. (1991). The neurology of eye movements (F.A. Davis Co.).

Leuba, G., and Garey, L.J. (1989). Comparison of neuronal and glial numerical density in primary and secondary visual cortex of man. Exp. Brain Res. 77, 31–38.

Liu, Y., Yttri, E.A., and Snyder, L.H. (2010). Intention and attention: different functional roles for LIPd and LIPv. Nat. Neurosci. 13, 495–500.

Mack, S., Kandel, E.R., Jessell, T.M., Schwartz, J.H., Siegelbaum, S.A., and Hudspeth, A.J. (2013). Principles of Neural Science, Fifth Edition (McGraw Hill Professional).

Medendorp, W.P., Kramer, G.F.I., Jensen, O., Oostenveld, R., Schoffelen, J.-M., and Fries, P. (2007). Oscillatory Activity in Human Parietal and Occipital Cortex Shows Hemispheric Lateralization and Memory Effects in a Delayed Double-Step Saccade Task. Cereb. Cortex 17, 2364–2374.

Merriam, E.P., and Colby, C.L. (2005). Active Vision in Parietal and Extrastriate Cortex. The Neuroscientist 11, 484–493.

Merriam, E.P., Genovese, C.R., and Colby, C.L. (2007). Remapping in Human Visual Cortex. J. Neurophysiol. 97, 1738–1755.

Meyer, S.S., Bonaiuto, J., Lim, M., Rossiter, H., Waters, S., Bradbury, D., Bestmann, S., Brookes, M., Callaghan, M.F., Weiskopf, N., et al. (2017). Flexible head-casts for high spatial precision MEG. J. Neurosci. Methods 276, 38–45.

Mills, M., Hollingworth, A., Van der Stigchel, S., Hoffman, L., and Dodd, M.D. (2011). Examining the influence of task set on eye movements and fixations. J. Vis. 11, 17.

Mirpour, K., and Bisley, J.W. (2016). Remapping, Spatial Stability, and Temporal Continuity: From the Pre-Saccadic to Postsaccadic Representation of Visual Space in LIP. Cereb. Cortex N. Y. NY 26, 3183–3195.

Mitra, P., and Bokil, H. (2007). Observed Brain Dynamics (Oxford; New York: Oxford University Press).

Moon, S.Y., Barton, J.J.S., Mikulski, S., Polli, F.E., Cain, M.S., Vangel, M., Hämäläinen, M.S., and Manoach, D.S. (2007). Where left becomes right: a magnetoencephalographic study of sensorimotor transformation for antisaccades. NeuroImage 36, 1313–1323.

Moonesinghe, R., Khoury, M.J., and Janssens, A.C.J.W. (2007). Most Published Research Findings Are False—But a Little Replication Goes a Long Way. PLOS Med. 4, e28.

Moradi, F., Liu, L.C., Cheng, K., Waggoner, R.A., Tanaka, K., and Ioannides, A.A. (2003). Consistent and precise localization of brain activity in human primary visual cortex by MEG and fMRI. NeuroImage 18, 595–609.

Moschovakis, A.K. (1996). The superior colliculus and eye movement control. Curr. Opin. Neurobiol. 6, 811–816.

Murakami, S., and Okada, Y. (2006). Contributions of principal neocortical neurons to magnetoencephalography and electroencephalography signals. J. Physiol. 575, 925–936.

Nakamura, K., and Colby, C.L. (2002). Updating of the visual representation in monkey striate and extrastriate cortex during saccades. Proc. Natl. Acad. Sci. U. S. A. 99, 4026–4031.

Neupane, S., Guitton, D., and Pack, C.C. (2016a). Two distinct types of remapping in primate cortical area V4. Nat. Commun. 7, 10402.

Neupane, S., Guitton, D., and Pack, C.C. (2016b). Dissociation of forward and convergent remapping in primate visual cortex. Curr. Biol. CB 26, R491-492.

Neupane, S., Guitton, D., and Pack, C.C. (2017). Coherent alpha oscillations link current and future receptive fields during saccades. Proc. Natl. Acad. Sci. 114, E5979–E5985.

Nodine, C.F., Locher, P.J., and Krupinski, E.A. (1993). The Role of Formal Art Training on Perception and Aesthetic Judgment of Art Compositions. Leonardo 26, 219–227.

Ong, W.S., and Bisley, J.W. (2011). A lack of anticipatory remapping of retinotopic receptive fields in the middle temporal area. J. Neurosci. Off. J. Soc. Neurosci. 31, 10432–10436.

Oostenveld, R., Fries, P., Maris, E., and Schoffelen, J.-M. (2011). FieldTrip: Open Source Software for Advanced Analysis of MEG, EEG, and Invasive Electrophysiological Data.

Pachitariu, M., Steinmetz, N., Kadir, S., Carandini, M., and Harris, K.D. (2016). Kilosort: realtime spike-sorting for extracellular electrophysiology with hundreds of channels. BioRxiv 061481.

Parkkonen, L., Fujiki, N., and Mäkelä, J.P. (2009). Sources of auditory brainstem responses revisited: contribution by magnetoencephalography. Hum. Brain Mapp. 30, 1772–1782.

Pascual-Marqui, R.D., Michel, C.M., and Lehmann, D. (1994). Low resolution electromagnetic tomography: a new method for localizing electrical activity in the brain. Int. J. Psychophysiol. 18, 49–65.

Perry, G., Adjamian, P., Thai, N.J., Holliday, I.E., Hillebrand, A., and Barnes, G.R. (2011). Retinotopic mapping of the primary visual cortex – a challenge for MEG imaging of the human cortex. Eur. J. Neurosci. 34, 652–661.

Pienaar, R., FISCHL, B., CAVINESS, V., MAKRIS, N., and GRANT, P.E. (2008). A methodology for analyzing curvature in the developing brain from preterm to adult. Int. J. Imaging Syst. Technol. 18, 42–68.

Poghosyan, V., and Ioannides, A.A. (2007). Precise mapping of early visual responses in space and time. NeuroImage 35, 759–770.

Polyak, S.L. (1941). The retina: the anatomy and the histology of the retina in man, ape, and monkey, including the consideration of visual functions, the history of physiological optics, and the histological laboratory technique (University of Chicago Press: Chicago).

Potter, M.C., Wyble, B., Hagmann, C.E., and McCourt, E.S. (2014). Detecting meaning in RSVP at 13 ms per picture. Atten. Percept. Psychophys. 76, 270–279.

Qiu, A., Rosenau, B.J., Greenberg, A.S., Hurdal, M.K., Barta, P., Yantis, S., and Miller, M.I. (2006). Estimating linear cortical magnification in human primary visual cortex via dynamic programming. NeuroImage 31, 125–138.

Quiroga, R.Q., Nadasdy, Z., and Ben-Shaul, Y. (2004). Unsupervised Spike Detection and Sorting with Wavelets and Superparamagnetic Clustering. Neural Comput. 16, 1661–1687.

Rolfs, M., and Szinte, M. (2016). Remapping Attention Pointers: Linking Physiology and Behavior. Trends Cogn. Sci. 20, 399–401.

Rolfs, M., Jonikaitis, D., Deubel, H., and Cavanagh, P. (2011). Predictive remapping of attention across eye movements. Nat. Neurosci. 14, 252–256.

Ross, J., Morrone, M.C., and Burr, D.C. (1997). Compression of visual space before saccades. Nature 386, 598–601.

Rübel, O., Tritt, A., Dichter, B., Braun, T., Cain, N., Clack, N., Davidson, T.J., Dougherty, M., Fillion-Robin, J.-C., Graddis, N., et al. (2019). NWB:N 2.0: An Accessible Data Standard for Neurophysiology. BioRxiv 523035.

Sarvas, J. (1987). Basic mathematical and electromagnetic concepts of the biomagnetic inverse problem. Phys. Med. Biol. 32, 11.

Schall, J.D., Morel, A., King, D.J., and Bullier, J. (1995). Topography of visual cortex connections with frontal eye field in macaque: convergence and segregation of processing streams. J. Neurosci. 15, 4464–4487.

Scudder, C.A., Kaneko, C.S., and Fuchs, A.F. (2002). The brainstem burst generator for saccadic eye movements: a modern synthesis. Exp. Brain Res. 142, 439–462.

Sereno, M.I., Dale, A.M., Reppas, J.B., Kwong, K.K., Belliveau, J.W., Brady, T.J., Rosen, B.R., and Tootell, R.B. (1995). Borders of multiple visual areas in humans revealed by functional magnetic resonance imaging. Science 268, 889–893.

Sharon, D., Hämäläinen, M.S., Tootell, R.B.H., Halgren, E., and Belliveau, J.W. (2007). The advantage of combining MEG and EEG: Comparison to fMRI in focally stimulated visual cortex. NeuroImage 36, 1225–1235.

Shils, J.L., Litt, M., Skolnick, B.E., and Stecker, M.M. (1996). Bispectral analysis of visual interactions in humans. Electroencephalogr. Clin. Neurophysiol. 98, 113–125.

Siegle, J.H., López, A.C., Patel, Y.A., Abramov, K., Ohayon, S., and Voigts, J. (2017). Open Ephys: an open-source, plugin-based platform for multichannel electrophysiology. J. Neural Eng. 14, 045003.

Sommer, M.A., and Wurtz, R.H. (2002). A Pathway in Primate Brain for Internal Monitoring of Movements. Science 296, 1480–1482.

Sommer, M.A., and Wurtz, R.H. (2006). Influence of the thalamus on spatial visual processing in frontal cortex. Nature 444, 374–377.

Sperry, R.W. (1950). Neural basis of the spontaneous optokinetic response produced by visual inversion. J. Comp. Physiol. Psychol. 43, 482–489.

Stanton, G.B., Bruce, C.J., and Goldberg, M.E. (1995). Topography of projections to posterior cortical areas from the macaque frontal eye fields. J. Comp. Neurol. 353, 291–305.

Szinte, M., Jonikaitis, D., Rolfs, M., Cavanagh, P., and Deubel, H. (2016). Presaccadic motion integration between current and future retinotopic locations of attended objects. J. Neurophysiol. 116, 1592–1602.

Szinte, M., Jonikaitis, D., Rangelov, D., and Deubel, H. (2018). Pre-saccadic remapping relies on dynamics of spatial attention. ELife 7, e37598.

Tatler, B.W., and Vincent, B.T. (2008). Systematic tendencies in scene viewing. J. Eye Mov. Res. 2.

Tatler, B.W., Baddeley, R.J., and Gilchrist, I.D. (2005). Visual correlates of fixation selection: effects of scale and time. Vision Res. 45, 643–659.

Teeters, J.L., Godfrey, K., Young, R., Dang, C., Friedsam, C., Wark, B., Asari, H., Peron, S., Li, N., Peyrache, A., et al. (2015). Neurodata Without Borders: Creating a Common Data Format for Neurophysiology. Neuron 88, 629–634.

Tolias, A.S., Moore, T., Smirnakis, S.M., Tehovnik, E.J., Siapas, A.G., and Schiller, P.H. (2001a). Eye Movements Modulate Visual Receptive Fields of V4 Neurons. Neuron 29, 757–767.

Tolias, A.S., Moore, T., Smirnakis, S.M., Tehovnik, E.J., Siapas, A.G., and Schiller, P.H. (2001b). Eye Movements Modulate Visual Receptive Fields of V4 Neurons. Neuron 29, 757–767.

Treisman, A.M., and Gelade, G. (1980). A feature-integration theory of attention. Cognit. Psychol. 12, 97–136.

Troebinger, L., López, J.D., Lutti, A., Bestmann, S., and Barnes, G. (2014). Discrimination of cortical laminae using MEG. NeuroImage 102, Part 2, 885–893.

Umeno, M.M., and Goldberg, M.E. (1997). Spatial Processing in the Monkey Frontal Eye Field. I. Predictive Visual Responses. J. Neurophysiol. 78, 1373–1383.

Van Gisbergen, J.A.M., Van Opstal, A.J., and Tax, A.A.M. (1987). Collicular ensemble coding of saccades based on vector summation. Neuroscience 21, 541–555.

Walker, M.F., Fitzgibbon, E.J., and Goldberg, M.E. (1995). Neurons in the monkey superior colliculus predict the visual result of impending saccadic eye movements. J. Neurophysiol. 73, 1988–2003.

Wandell, B.A., Dumoulin, S.O., and Brewer, A.A. (2007). Visual field maps in human cortex. Neuron 56, 366–383.

Wang, X., Fung, C.C.A., Guan, S., Wu, S., Goldberg, M.E., and Zhang, M. (2016). Perisaccadic Receptive Field Expansion in the Lateral Intraparietal Area. Neuron 0.

Wardak, C., Olivier, E., and Duhamel, J.-R. (2004). A Deficit in Covert Attention after Parietal Cortex Inactivation in the Monkey. Neuron 42, 501–508.

Werf, J.V.D., Jensen, O., Fries, P., and Medendorp, W.P. (2008). Gamma-Band Activity in Human Posterior Parietal Cortex Encodes the Motor Goal during Delayed Prosaccades and Antisaccades. J. Neurosci. 28, 8397–8405.

Wolfe, J.M. (1998). What Can 1 Million Trials Tell Us About Visual Search? Psychol. Sci. 9, 33–39.

Wurtz, R.H., and Goldberg, M.E. (1989). The Neurobiology of Saccadic Eye Movements (Elsevier).

Yao, T., Treue, S., and Krishna, B.S. (2016). An Attention-Sensitive Memory Trace in Macaque MT Following Saccadic Eye Movements. PLOS Biol. 14, e1002390.

Zirnsak, M., and Moore, T. (2014). Saccades and shifting receptive fields: anticipating consequences or selecting targets? Trends Cogn. Sci. 18, 621–628.

(2004). The visual neurosciences, Vols. 1 & 2 (Cambridge, MA, US: MIT Press).